Master Thesis in Geographical Information Science nr 212

Compound Extreme Events in Hamburg, Germany: A Flood Risk Assessment

Iris Krohn

2026
Department of
Physical Geography and Ecosystem Science
Centre for Geographical Information Systems
Lund University
Sölvegatan 12
S-223 62 Lund
Sweden

Iris Krohn (2026). Compound Extreme Events in Hamburg, Germany: A Flood Risk Assessment

Master degree thesis, 30 credits in Geographical Information Science
Department of Earth and Environmental Sciences, Lund University

Compound Extreme Events in Hamburg, Germany: A Flood Risk Assessment

Iris Krohn
Master thesis, 30 credits, in Geographical Information Sciences

Supervisor: Marko Scholze
Department of Earth and Environmental Sciences (MGeo), Lund University

Abstract

Flooding can occur as a result of various events, including storm surges and heavy rainfall. Measures such as the construction of dykes and canal systems are implemented to protect people and property. However, compound flooding caused by storm surges and heavy rainfall occurring simultaneously is usually overlooked. This is also the case in the German city of Hamburg, which is used as the study area for this thesis. The aim of this study is to determine the risk of compound flooding caused by heavy rainfall and storm surges and to compare it with the risk of individual extreme events. For this purpose, a flood frequency analysis is first carried out to determine storm surge and heavy rainfall levels of extreme events with a return period of 100 years. These values are then used as input for a hydrodynamic model with which the flooding scenarios are simulated. The results show that the extent of flooding in the compound event is significantly greater than in the individual extreme events. Extensive flooding can be seen along the Elbe and in low-lying areas of the city. This is due to the phenomenon that the high water level of the river during the storm surge prevents rainwater from draining away, causing it to accumulate in certain areas according to the topography. The results of this study underscore the need to integrate compound flooding into flood management in Hamburg and comparable cities worldwide.

Keywords: Geography, Geographical Information Systems, Physical Geography, Flood Frequency Analysis, Hydrodynamic Model, Compound Flood, Storm Surge, Heavy Rainfall

Zusammenfassung

Überflutungen können als Resultat verschiedener Ereignisse, unter anderem Sturmfluten und Starkregen, auftreten. Um Menschen und Sachgüter zu schützen, werden Maßnahmen wie die Errichtung von Deichen und Kanalsystemen umgesetzt. Gekoppelte Überflutungen aus gemeinsam auftretender Sturmflut und Starkregen werden dabei jedoch für gewöhnlich missachtet. So auch in der deutschen Metropole Hamburg, welche für diese Arbeit als Untersuchungsgebiet verwendet wird. Das Ziel dieser Studie ist es, das Risiko einer gekoppelten Überflutung aus Starkregen und Sturmflut zu ermitteln und dem Risiko der individuellen Extremereignisse gegenüberzustellen. Dafür wird zunächst eine statistische Analyse durchgeführt, um Sturmflut- und Starkregenhöhen von Extremereignissen mit einer Widerkehrzeit von 100 Jahren zu bestimmen. Diese Werte werden anschließend als Eingabe für ein hydrodynamisches Modell verwendet, mit welchem die Überflutungsszenarien simuliert werden. Die Ergebnisse zeigen auf, dass das Ausmaß der Überflutung bei dem gekoppelten Extremereignis deutlich höher ausfällt als bei den einzelnen Extremereignissen. Es zeigen sich weitreichende Überflutungen entlang der Elbe sowie in niedrig-gelegenen Bereichen der Stadt. Dieses ist auf das Phänomen zurückzuführen, dass aufgrund des hohen Wasserstandes des Flusses während der Sturmflut, das anfallende Regenwasser nicht abfließen kann und sich daher der Topographie folgend in bestimmten Gebieten ansammelt. Die Ergebnisse dieser Studie untermauern die Notwendigkeit, gekoppelte Überflutungen in das Hochwassermanagement Hamburgs und vergleichbarer Städte weltweit zu integrieren.

Schlüsselwörter: Geographie, Geographische Informationssysteme, Physische Geographie, Hochwasserfrequenzanalyse, Hydrodynamisches Modell, Gekoppelte Überflutung, Sturmflut, Starkregen

Table of Contents

Abstract iv
Zusammenfassung v
Table of Contents vii
List of Tables ix
List of Figures ix
List of Abbreviations x
1. Introduction 1
2. Background 3
2.1 Flood Frequency Analysis 3
2.2 Flood Simulation 5
3. Study Area 7
3.1 Topography 7
3.2 Climatic Conditions 9
3.3 Flood Risk Management 10
3.3.1 Storm Surges and Heavy Rainfall Events in Hamburg 10
3.3.2 Protection against Coastal Flooding 11
3.3.3 Protection Against Heavy Rainfall 12
3.4 Delimitation of the Study Area 12
4. Materials 15
4.1 Flood Frequency Analysis 15
4.2 Flood Simulation 17
5. Methodology 21
5.1 Structure 21
5.2 Sampling of Extreme Values 23
5.2.1 Event Sampling Methods 23
5.2.2 Peaks over Threshold 24
5.2.2.1 Threshold Selection 24
5.2.2.2 Independence Criterion 25
5.3 Fitting of Probability Distributions 26
5.4 Formation of Value Pairs 27
5.4.1 Determination of the Priority Variable 27
5.4.2 Assignment of the Secondary Variable 27
5.5 Correlation Analysis 28
5.6 Fitting of the Copula 29
5.7 Determination of Design Values 29
5.8 Flood Simulation – Model Selection 31
5.9 Model Calibration 32

5.9.1 DEM ... 32
5.9.2 Surface Roughness ... 35
5.10 Model Validation ... 35
5.10.1 DEM ... 36
5.10.2 Boundary Conditions ... 38
5.11 Simulation of Flood Events ... 39
5.11.1 Storm Surge ... 39
5.11.2 Heavy Rainfall ... 40
5.11.3 Compound Event ... 40
6. Results ... 41
6.1 Flood Frequency Analysis ... 41
6.1.1 Sampling of Extreme Values ... 41
6.1.2 Fitting of Probability Distributions ... 42
6.1.3 Formation of Value Pairs & Correlation Analysis ... 43
6.1.4 Fitting of the Copula ... 44
6.1.5 Determination of Design Values ... 45
6.2 Flood Simulation ... 46
6.2.1 Model Validation ... 46
6.2.2 Simulation of Flood Events ... 49
6.2.2.1 Univariate Scenario ... 49
6.2.2.2 Bivariate Scenario ... 53
6.2.2.3 Comparison of the Univariate Events with the Bivariate Event ... 56
7. Discussion ... 59
7.1 Sampling of Extreme Values ... 59
7.2 Characterisation of the Statistical Correlation ... 61
7.3 Flood Risk of the Univariate and Bivariate Events ... 62
7.4 Outlook ... 63
8. Conclusion ... 67
References ... 69
Appendix ... 91

List of Tables

Table 1 - Materials used for this thesis 18
Table 2 - Input files needed to run the flood simulations using LISFLOOD-FP. 32
Table 3 - Manning's Roughness Coefficient for the different land use classes in the study area 35
Table 4 - Probability distributions, which were fitted to the extreme value series. The parameter values were determined using the maximum likelihood methodology. 43
Table 5 - Results of the correlation analysis 44
Table 6 - Determined design values of the compound and univariate events 45
Table A1 - Pairs of extreme rainfall and associated maximum TWL of the same day used for the bivariate analysis 91

List of Figures

Figure 1 - Topography of Hamburg, Germany 8
Figure 2 - Characterisation of the study area 14
Figure 3 - Flow chart of the methodology used. In the flood frequency analysis, the amount of rainfall and the total water level (TWL) of events with a return period of 100 years are determined. These values are then used as input for the flood simulation. 22
Figure 4 - DEM, which was used to calibrate the model. To ensure a realistic simulation at the boundaries, the study area was extended to include areas from the neighbouring federal states. In addition, information on the topography of the Elbe and the height of the flood defences was incorporated. 34
Figure 5 - Adjustments made to the flood defence structures to recreate the flooding of 1962 37
Figure 6 - Comparison between the observed hydrograph of the storm surge of 6 December 2013 and the corresponding design hydrograph of the storm surge of 1962 39
Figure 7 - Time series with their determined thresholds. Events above the thresholds were extracted and used to create the extreme value series. 42
Figure 8 - Scatter plot of the generated value pairs 43
Figure 9 - Contour of those pairs of values from TWL and rainfall that have a return period of 100 years. The pair of values selected according to the EFC methodology is marked in red. 45
Figure 10 - Comparison between the modelled and actual extent of the 1962 flood. Red areas show the flooding according to the reference layer. Areas marked in blue are those that were marked as flooded in both cases. Green areas were only designated as flooded in the model. 48

Figure 11 - Results of the simulation of a univariate storm surge with a return period of 100 years 50
Figure 12 - Results of the simulation of a univariate heavy rainfall event with a return period of 100 years 51
Figure 13 - Comparison of the observed hydrograph of the 2013 storm surge with the constructed univariate and bivariate hydrographs 52
Figure 14 - Comparison of the observed hyetograph of the 2024 heavy rainfall event with the constructed univariate and bivariate hyetographs 52
Figure 15 - Temporal coordination of the two variables. To represent a worst-case scenario, the 53
Figure 16 - Results of the simulation of a compound event consisting of a storm surge and heavy rainfall with a return period of 100 years 55
Figure 17 - Comparison of water depths for the univariate storm surge and the compound event. Areas marked in red are those in which the water depth is higher in the univariate event. Areas marked in blue show a higher water depth in the compound event. 57
Figure 18 - Comparison of water depths for the univariate heavy rainfall and the compound event. Areas marked in red are those in which the water depth is higher in the univariate event. Areas marked in blue show a higher water depth in the compound event. 58

List of Abbreviations

Abbreviation	Definition
AM	Annual Maximum
DEM	Digital Elevation Model
EFC	Equivalent Frequency Combination
FFA	Flood Frequency Analysis
GPD	Generalised Pareto Distribution
MvCAT	Multivariate Copula Analysis Toolbox
POT	Peaks-Over-Threshold
SFA	Same Frequency Amplification
SLR	Sea Level Rise
TWL	Total Water Level

1. Introduction

According to the Centre for Research on the Epidemiology of Disasters (2023), between 2003 and 2022, floods accounted for the majority (170 out of 369) of disasters caused by natural hazards worldwide. Climate change and increasing urbanisation are causing flooding in urban areas to become an ever-greater problem, increasingly jeopardising the safety of residents and socioeconomic development (Xu et al., 2022). Coastal cities are the most severely affected, where flooding can be triggered not only by heavy rainfall but also by storm surges (Chen et al., 2023). When these two types of flooding occur together, the severity of the flooding is amplified, threatening great economic losses and casualties (Lai et al., 2021). This is mainly due to coastal backwater effects, in which the drainage of rainwater is slowed down or even completely blocked by a simultaneous storm surge (Wahl et al., 2015; Xu et al., 2024). Flood events caused by the interaction of several drivers are referred to as compound flood events (Couasnon et al., 2020). Examples include the flash flood in Lisbon in 1967 (Trigo et al., 2016), the Ravenna flood in 2015 (Bevacqua et al., 2017) and the floods in the Bouregreg estuary in Morocco in 2017 (Zellou & Rahali, 2019). Quantifying compound flood risk, defined by frequency and potential impact in terms of flood extent and depth, is essential for policymaking, disaster risk reduction and engineering practices such as the construction of flood defence structures (Bevacqua et al., 2019). Despite this, coastal flooding risk analyses usually do not take compound events into account but instead perform independent risk assessments for coastal flooding and pluvial flooding (Wahl et al., 2015). This is based on the assumption that different types of flooding occur independently of each other, making an extreme compound flood event very unlikely (Wahl et al., 2015). However, recent studies have found that storm surges and heavy rainfall exhibit a significant positive correlation in many regions, meaning that the probability of them occurring together is higher than would appear to be the case if they were independent. Ignoring compound events therefore results in a significant underestimation of flood risk (Chen et al., 2023; Dubois et al., 2024; Jalili Pirani & Najafi, 2023; Zhu et al., 2024).

This thesis conducts a flood risk assessment for the German metropolis of Hamburg. The city is located in the estuary of the Elbe River, which exposes it to various types of flooding. Flood risk assessments for coastal flooding and heavy rainfall have been established by the city, however compound events are not taken into account. To close this research gap, this thesis determines the compound flood risk by simulating an event with a return period of 100 years. The return period is a statistical measure that represents the estimated interval between two events of the same magnitude (Zellou & Rahali, 2019). Extreme events with a return period of 100 years are commonly analysed in flood risk assessments and used for the dimensioning of flood defence structures, for example (Milly et al., 2002).

The aim of this study is to quantify the flood risk posed by a compound flood from heavy rainfall and storm surge in Hamburg, Germany, and to characterise the divergence of separately occurring heavy rainfall and storm surge events with the same return period. The purpose of this is to enhance the understanding and assessment of compound flood risk in Hamburg, Germany, and to demonstrate the added value of a compound analysis compared to the traditional independent approach. To this end, the following research questions will be answered and the associated hypotheses tested:

1. How can the statistical correlation between storm surges and heavy rainfall in Hamburg be characterised?

Hypothesis 1:

Storm surges and heavy rainfall show a significant positive correlation. As a result, the probability and intensity of a compound event is higher than it would appear if the two factors were assumed to be independent.

2. Which areas of Hamburg are at risk from a compound flood caused by storm surge and heavy rainfall with a return period of 100 years?

2.1 Which areas of Hamburg are at risk from a compound flood caused by storm surge and heavy rainfall with a return period of 100 years?

Hypothesis 2:

Areas bordering the Elbe and its tributaries, as well as low-lying areas in general, show a high risk of flooding. Due to the coastal backwater effect, the flood risk of the compound event will be higher than that of the individual extreme events.

The remainder of this thesis is divided into the following sections: Chapter 2 presents background information and a literature review on the methodology used. In Chapter 3, a description of the study area follows. Chapter 4 presents the materials used. Chapter 5 introduces the methodology used to produce the results in Chapter 6. The results are discussed in Chapter 7. The thesis wraps up with a conclusion in Chapter 8.

2. Background

2.1 Flood Frequency Analysis

The habitation of coastal areas has a long tradition and is justified by numerous advantages in terms of agriculture, fishing, transportation and access to water (Naghettini, 2017). At the same time, however, there is also a major risk: Lamb (1995) notes that the number of deaths due to flooding in the North Sea region reached 1.3 million in the late Middle Ages. In response to this, the construction of protective structures such as dykes, dams and reservoirs was initiated (Knottnerus, 2005). Reliable estimates of flood characteristics are necessary for the construction of these structures (Naghettini, 2017). The analysis and prediction of water levels and rainfall intensities is therefore a long-standing and ongoing task in water resources engineering (Naghettini, 2017). The methodology of flood frequency analysis (FFA) is based on using observed data to determine the probability that a defined threshold value will be reached or exceeded (Kidson & Richards, 2005). Similarly, the severity of an event with a specified return period can be determined (Mathias, 2023).

To create flood risk assessments, a univariate FFA is traditionally performed, in which a single type of flooding (pluvial, fluvial or coastal) is considered (Chen et al., 2023). This involves fitting a probability distribution to an extreme-value series consisting of the maximum values within a given period (Naghettini, 2017). For example, Milly et al. (2002) perform a univariate FFA to determine changes in the occurrence of extreme river floods in the context of climate change. Another study examines coastal flood hazard in New York City through univariate analysis of flood height (Garner et al., 2017). Over the years, new probability distribution models and statistical approaches have been developed to produce more accurate estimates for extreme events (Naghettini, 2017).

However, various studies have found that different types of flooding often exhibit statistical dependence, as they occur as a result of the same weather system (Lai et al., 2021). For example, during Hurricane Harvey in 2017, pluvial and coastal flooding occurred simultaneously in Houston, USA (Emanuel, 2017; Zhang et al., 2018). Loganathan et al. (1987) find a significant correlation between high tides and high river water levels in Chesapeake Bay, USA, in an analysis of 628 pairs of tide and river water levels. They also show that the probability of a joint occurrence is underestimated under the assumption of independence (Loganathan et al., 1987). A study in south-west England shows a statistical correlation between rainfall and wave surge levels (Coles et al., 1999). Svensson & Jones (2004) find a significant dependence between river flow and daily maximum sea surge for most catchments along the southern and western coasts of Britain. The strength of the dependence varies based on meteorological and orographic conditions as well as soil moisture and lag time (Svenson & Jones, 2004).

Based on these findings, the univariate FFA has recently been extended by a bivariate FFA in order to enable a more realistic assessment of flood risk (Chen et al., 2023). A bivariate FFA allows the analysis of compound scenarios in which two types of flooding occur together (Maity, 2018). Joint distribution functions are used to describe the probability of a compound event. In recent years, a wide variety of methods have been used to form these, but they have a number of drawbacks (Chen & Guo, 2019). For example, the probability distributions of the two variables must belong to the same family, and the dependency structure is not modelled separately but by adjusting the parameters of the probability distributions (Favre et al., 2004). Furthermore, many models assume a linear dependence between the variables, which leads to difficulties when a non-linear or asymmetric dependence structure is present (Chen et al., 2023). Copula functions are the most recent and promising mathematical tool used for bivariate analyses (Xiao et al., 2008). Copulas can capture various dependence structures between two variables described by different probability distributions and then integrate them into a joint distribution function (Serinaldi et al., 2009). They were described by Sklar (1973) and first proposed for a bivariate FFA by Favre et al. (2004). Since then, copulas have been used in numerous studies to investigate compound flooding. This includes studies on the combination of different types of flooding, such as fluvial-coastal flooding (e.g. Dubois et al., 2024; Ganguli et al., 2020; Paprotny et al., 2018; Sadegh et al., 2018) and fluvial-pluvial floods (e.g. Jalili Pirani & Najafi, 2023; Zhong et al., 2020). Furthermore, bivariate analyses are also used to investigate the dependence between different components of the same flood type. For coastal floods, this includes, for example, wave activity and water level (Mazas & Hamm, 2017) or wave height and storm surge height (Wahl et al., 2012). In fluvial analyses, for example, the relationship between river discharge and volume has been characterised (Favre et al., 2004; Salvadori et al., 2013).

The combination of pluvial and coastal flooding used in this study has also been examined recently in various studies. In their study of a compound event involving heavy precipitation and high tidal levels in Shenzhen, China, Tu et al. (2018) show that a bivariate analysis using copula functions is very effective in characterising the joint probability of occurrence. Similarly, Xu et al. (2019) describe that a bivariate FFA allows for a more adequate assessment of flood risk than a univariate analysis. Chen et al. (2023) find a significant positive correlation between heavy rainfall and storm surge in a river basin in China. They also show that the probability of co-occurrence is underestimated if this dependence is ignored (Chen et al., 2023). A study of the entire Canadian coast shows that in 80% of locations there is a significant correlation between extreme precipitation and high-water levels (Jalili Pirani & Najafi, 2023). A global analysis by Lai et al. (2021) confirms that there is a significant positive correlation between the two variables in most regions, meaning that the return period of an extreme compound event is on average about two years shorter than a univariate analysis would suggest (Lai et al., 2021). Furthermore, Wahl et al. (2015) show that the number of compound events involving extreme rainfall and storm surges has risen sharply in the United States over the last century. Similarly, Lian et al. (2013) find that the probability of such compound events in Fuzhou, China has increased by more than 300% since 1984.

2.2 Flood Simulation

Statistical values from the FFA provide information about the magnitude of the two variables for the defined return period, but they do not reveal the practical implications of such an event. Statistical modelling is therefore combined with hydrological or hydrodynamic models (Candela & Aronica, 2017; Lian et al., 2013; Ming et al., 2022; Xu et al., 2024). These models are capable of simulating the extent and depth of flooding and are therefore used extensively in flood risk assessments (Li et al., 2025). When choosing a suitable model, a balance must be struck between the level of detail in the simulation and computational efficiency. Hydrological models can simulate the movement, storage and transformation of water in the hydrological cycle, such as precipitation, evapotranspiration and surface runoff of rainwater (Green et al., 2025). They require less computational time, but as a result, they are less able to represent physical processes in detail (Shen & Jiang, 2023). Hydrodynamic models can accurately model the flow behaviour of water on the surface as well as in rivers and oceans due to the use of governing equations, e.g. shallow-water equations (Green et al., 2025). They are therefore usually able to simulate the flooding process accurately but encounter computational limitations in large-scale applications (Shen & Jiang, 2023). For realistic modelling of flood dynamics in compound floods, such as the interaction between rivers and the sea in estuaries or the influence of flood protection structures on surface runoff, the latter are usually preferred in the current literature (Green et al., 2025). For example, Kumbier et al. (2018) use a hydrodynamic model to simulate a compound flood consisting of river flooding and storm surge in an estuary in Australia. They show that not including river flooding results in an underestimation of the flood depth and extent (Kumbier et al., 2018). Zhong et al. (2024) use a model based on Delft3D-FLOW and HEC-RAS to simulate various extreme compound flooding events. Zellou & Rahali (2019) combine a bivariate FFA based on copulas with the CAESAR-LISFLOOD model to simulate compound flooding from extreme rainfall and storm surge in an estuary in Morocco. As a result, they produce inundation maps that show that a bivariate simulation can depict real flood events more accurately than a univariate one (Zellou & Rahali, 2019).

As can be seen from the studies presented, there is a wide range of hydrodynamic models that can be used. Additionally, in the wake of technological advancements, the number of models developed is steadily increasing (Bates et al., 2021; Chen & Liu, 2014; Lee et al., 2019). The choice of a specific model is based on the application at hand, modelling requirements and computational efficiency (Bulti & Abebe, 2020). Basically, five types of models can be distinguished based on their underlying approach: rapid flood spreading, one-dimensional sewer, one-dimensional surface, two-dimensional surface and coupled sewer-surface models (Bulti & Abebe, 2020). The order of the types listed reflects the complexity of the models. Models based on the rapid flood spreading approach offer low accuracy, making them suitable only for large-scale applications but with lower computational costs, while coupled sewer-surface models have high accuracy and are suitable for small-scale applications but have high computational costs (Bulti & Abebe, 2020). A review based on 279 studies dealing with compound flooding in coastal-estuarine regions shows that in recent years, the use of two-dimensional surface and coupled sewer-surface models has dominated (Green et al., 2025).

Two-dimensional surface models are based on a grid of cells covering the entire study area (Kim et al., 2014). In each cell, rainfall and catchment parameters such as terrain elevation are homogeneous (RainGain, 2015). Surface runoff can spread from one cell to the four orthogonally adjacent cells and is calculated using two-dimensional shallow water equations (Bulti & Abebe, 2020). In addition to determining the maximum inundation extent, water depth and velocity, two-dimensional surface models are capable of simulating flow around small-scale topographic features, making them suitable for use in urban areas (Liu et al., 2012; Nkwunonwo et al., 2020). However, one disadvantage is that they do not take into account the effect of sewer systems (Bulti & Abebe, 2020).

Coupled sewer-surface models are characterised by the combination of a 1D sewer model with a 2D surface model (Bulti & Abebe, 2020). This enables them to simulate not only the flow behaviour in both systems, but also interactions, for example via gullies and manholes (Jahanbazi & Egger, 2014). The flood simulations of such models are characterised by high accuracy (Rangari et al., 2018), but they also have high computational costs and data requirements (Kourtis et al., 2017; Schlauß & Grottker, 2016). They are therefore suitable for in-depth analyses that require detailed modelling of complex drainage systems (Bulti & Abebe, 2020).

3. Study Area

The study area for this thesis covers most of the city of Hamburg. With a population of 1.86 million, Hamburg is Germany's second-largest city (Federal Statistical Office of Germany, 2025). It is home to Europe's third-largest container port and is therefore the most important trade and economic centre in Northern Europe (Hamburg Ministry of Economics and Innovation, n.d.). It is connected to the North Sea via the river Elbe. Despite being more than 100 km from the open coast, the city is strongly exposed to the forces of the tides. The entire area of the Elbe within the city borders is affected by the tides, which means that the water level in Hamburg is almost independent of the water level upstream (FGG Elbe, 2021). Even inland flooding in upstream areas contributes little to an increase in the water level in Hamburg (Environment, Climate, Energy and Agriculture Authority [BUKEA], 2015a). The water level conditions in tidal areas of rivers depend on sea level development as well as morphological and anthropogenic changes (FGG Elbe, 2021). The entire city area belongs to the Elbe river basin, which means that all precipitation either drains directly into the Elbe or via one of seven tributaries (FGG Elbe, 2021).

3.1 Topography

Figure 1 shows the topography of Hamburg. The city can be divided into two types of landscape, which have a significant impact on the elevation of the terrain. The higher-lying geest, a landform found in northern Germany, Denmark and the Netherlands that was formed on sand deposits from the last ice age, and the lower-lying marshland, which was formed on alluvial sediments (BUKEA, 2015a). The latter stretches in a band from west to east through the southern part of the city. It encompasses the entire course of the Elbe River, as well as the areas bordering it to the west and southeast. In many areas, the terrain elevation is just above 0 m. The transition from the marsh to the geest is clearly marked by an abrupt, sharp rise in terrain elevation.

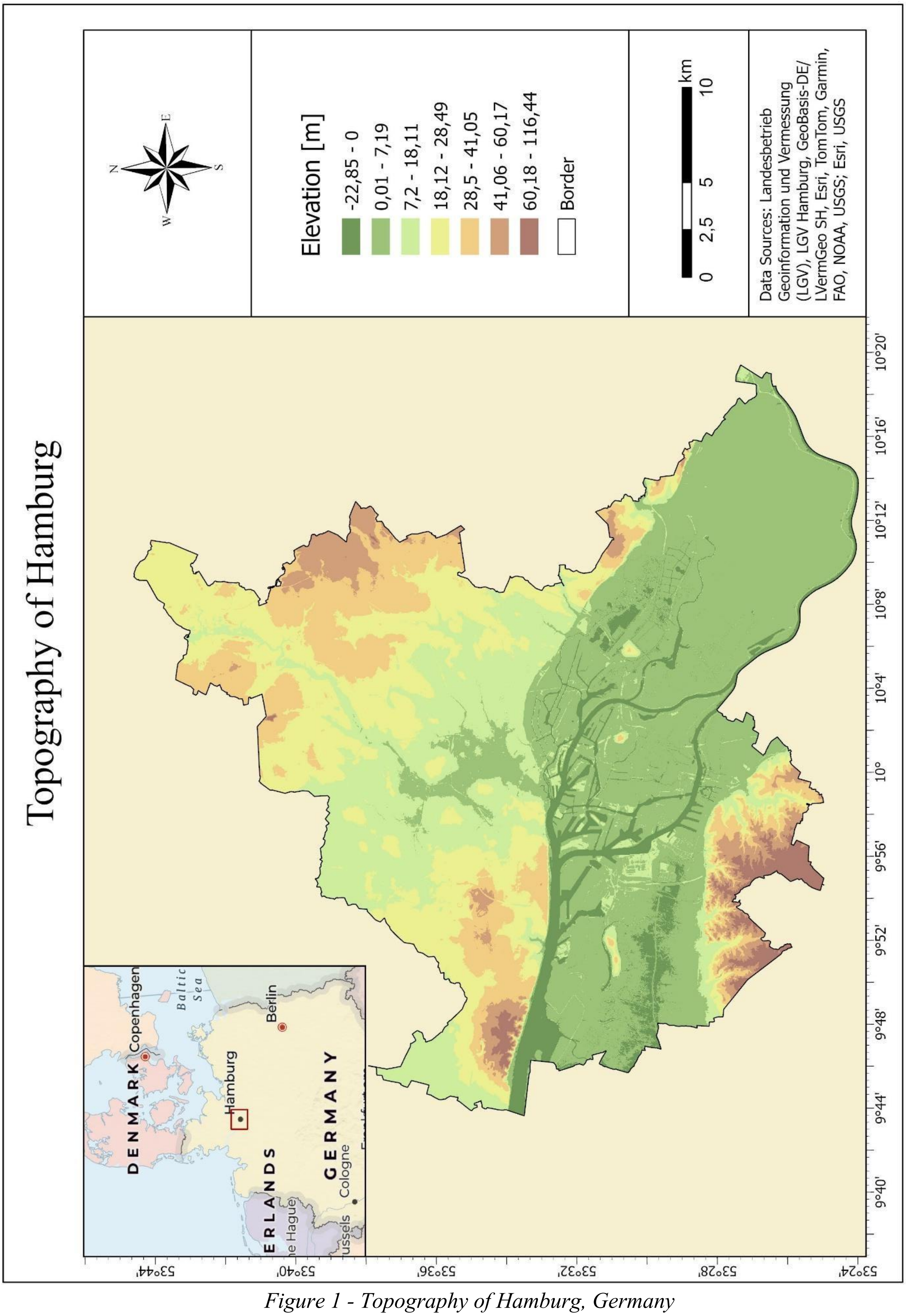

Figure 1 - Topography of Hamburg, Germany

3.2 Climatic Conditions

Storm surges are caused by various factors, such as wind pushing water towards the coast or the barometric pressure effect, when the water level rises due to low-pressure weather systems (Dubois et al., 2024). In Hamburg, storm surges are mainly caused by storms from the northwest, which push water masses from the North Sea into the Elbe estuary (FGG Elbe, 2021). Other influencing factors include long-distance waves from the Atlantic and the spring-neap cycle, which describes an intensification of the tide during full and new moon (BUKEA, 2015b). The storm surge season in Hamburg runs from September to March (Hamburg Wasser, 2024). Heavy rainfall events can occur under various meteorological conditions, such as intense cyclonic activity and convective weather conditions, which can occur in conjunction with the conditions that cause storm surges (Dubois et al., 2024).

An analysis of storm activity in the North Sea between 1912 and 2012 shows high variability without a clear long-term trend (Weisse et al., 2012). This result is supported by a study by Germany's National Meteorological Service (DWD, 2021), which found no significant trend in the number of storm days in Hamburg between 1981 and 2010. An evaluation of a series of climate projections shows that there is no significant trend in the frequency and intensity of storms for the period 2071 - 2100 either (Storch et al., 2018). Based on this finding, it is therefore not expected that storm activity in Hamburg will change significantly (Storch et al., 2018). The greatest influence on extreme water levels therefore comes from sea level rise (SLR). In the report of the Intergovernmental Panel on Climate Change (IPCC, 2021), the global mean sea level rise under the SSP5 8.5 scenario is estimated at 63 - 101 cm by the end of the century. It is assumed that values within this range also apply to the German North Sea coast (BUKEA, 2021). This is confirmed by a study conducted by the Royal Netherlands Meteorological Institute, which, using the same emissions scenario, projects a SLR in a similar range—between 59 and 124 cm by the year 2100—for the Netherlands (KNMI, 2024). Storm surge water levels on the North Sea coast are therefore expected to increase at the same rate as the mean sea level (Klein et al., 2018).

In terms of precipitation, there has been an increase in annual precipitation totals in Hamburg of 112 mm for the period from 1881 to 2020 (BUKEA, 2021). The largest increase is in winter (DWD, 2021). Heavy rainfall events are also showing a positive trend. The number of days per year on which heavy rainfall occurred increased by 3.4 between 1951 and 2021 (DWD, 2021). By 2100, Hamburg is expected to see a 3% increase in total precipitation, with an increase in winter and a decrease in summer (BUKEA, 2021). Heavy rainfall events are also expected to increase (DWD, 2021). The evaluation of a simulation under RCP8.5 shows an increase in heavy rainfall events of 15 - 45% in the period 2071 - 2100 relative to the period 1976 - 2005

(Climate Change and Consequences for Water Management [KLIWA], 2019). This is based on the phenomenon that rising temperatures lead to a higher amount of water vapour in the atmosphere, which in turn leads to more intense rainfall events (BUKEA, 2021). The intensity increases by 14% per degree Celsius of warming (BUKEA, 2021).

With regard to compound events involving storm surges and heavy rainfall, climate change is expected to cause a significant increase in Northern Europe (Rutgersson et al., 2021). Bevacqua et al. (2019) conclude that an event in the North Sea region with a current return period of 60 years will occur statistically every 10 years in 2100. This is due to SLR and more frequent heavy rainfall events (Bevacqua et al., 2019). Ganguli et al. (2020) show that the compound flood hazard in north-western Europe is strongly influenced by SLR.

3.3 Flood Risk Management

3.3.1 Storm Surges and Heavy Rainfall Events in Hamburg

Hamburg is repeatedly hit by severe storm surges. The highest water levels were recorded in 1976, 1994 and 2013 (Hamburg Port Authority [HPA], 2019). The highest water level ever measured is 6.45 m above sea level (HPA, 2019). However, storm surges have also occurred in more recent years. The River Basin Community Elbe (FGG Elbe, 2024) reports three severe storm surges (higher than 4.6 m above sea level) and one very severe storm surge (5.84 m above sea level) in Hamburg since 2018. However, these storm surges did not have any significant impact (FGG Elbe, 2024).

In contrast, local heavy rainfall events have repeatedly caused major damage in the past (BUKEA & RISA, 2024). Over 180 heavy rainfall events were recorded in Hamburg between 2012 and 2022 (Agency of Roads, Bridges and Waters [LSBG], 2022). On 10 May 2018, for example, major flooding resulted from a heavy rainfall event in the east of the city, causing considerable damage due to undercutting and erosion (BUKEA, 2025a). Similar events occurred on 18 June 2020 in the south-west of Hamburg (BUKEA, 2025a) and on 27 June 2024 in the entire city (North German Public Radio & TV [NDR], 2024).

3.3.2 Protection against Coastal Flooding

Those areas of Hamburg that lie on marshland are particularly vulnerable to storm surges due to their low elevation. This comprises one-third of the entire city (BUKEA, 2015a). To protect these areas, dykes were built as early as the 12th century, which were repeatedly raised and renewed in response to storm surges (BUKEA, 2015a). The storm surge in 1962 marked a turning point in flood protection. The dykes at that time were dilapidated in many areas and not designed to withstand the height of this storm surge (LSBG, 2012). This resulted in numerous dyke breaches, flooding an area of 125 km², roughly 1/6 of the city, and killing 315 people (BUKEA, 2015a).

This storm surge goes down as the most devastating in Hamburg's history (NDR, 2025). This was followed by a massive expansion of the protective structures, as a result of which none of the storm surges that have occurred since then have caused serious damage (BUKEA, n.d.a). Today, the city is protected by flood defences with a total length of 103 km, of which 78 km are dykes and 25 km are flood barriers (BUKEA, n.d.b). There are also flood barriers at the mouths of tributaries (FGG Elbe, 2021). Every year, Hamburg invests 20 - 30 million euros in flood protection (BUKEA, n.d.a). The level of protection is continuously reviewed and adapted to climate change projections, in particular SLR (BUKEA, n.d.a). The current height of the structures is between 7.5 m and 9.25 m and takes into account SLR until 2050 (BUKEA, n.d.a). However, there are also areas that lie in front of the public flood protection line. These include the port facilities and the Speicherstadt, a UNESCO World Heritage Site (BUKEA, 2024a). Despite the potential dangers, urban development is progressing in these low-lying areas (BUKEA, n.d.a). One example of this is HafenCity, which is the largest inner-city urban development project in Europe and covers an area of 157 hectares (HafenCity Hamburg GmbH, n.d.). Alternative protection concepts such as mound construction and flood protection polders are being used to protect these structures (BUKEA, 2015a).

In 2007, the EU introduced the Flood Risk Management Directive in response to several catastrophic floods around the turn of the millennium (FGG Elbe, 2024). This provides a framework for the assessment and management of flood risks and pursues the primary goal of protecting people from flooding, reducing flood risk and preventing damage to the environment, culture and economy (BUKEA, 2015b). These guidelines have been implemented in Germany since 2010 (BUKEA, 2015b). Every six years, flood hazard maps and flood risk maps are created and a risk management plan is developed (FGG Elbe, 2024). Based on the flood events that have occurred since the last report, risk areas for coastal flooding are identified (FGG Elbe, 2024). As of 2024, 45% of Hamburg's total area is classified as a risk area (FGG Elbe, 2024). This encompasses the entire marshlands as well as the low-lying areas bordering them to the north. The hazard maps and risk maps depict three flood scenarios with return periods of 10, 100 and 200 years (BUKEA, 2020). Based on these maps, a catalogue of measures is being developed to reduce the extent of possible flood damage. This includes adapted land use and construction methods, as well as educating and warning the population (BUKEA, 2015b).

3.3.3 Protection Against Heavy Rainfall

Hamburg has several structures in place to prevent large-scale flooding during heavy rainfall. These include retention basins and a 1,840-kilometre-long sewer network that drains rainwater into the Elbe or one of its tributaries (Hamburg Wasser, 2025). The dimensions of these facilities are based on the probability of rainfall events, which are characterised by the recurrence interval, duration and amount of rainfall (Bremen University [HSB], 2017). Despite the existence of these facilities, flooding often occurs during heavy rainfall. The reason for this is that the sewer network, retention basins and water bodies become overloaded and cannot drain the accumulated water (Hamburg Wasser, 2020). A lack of infiltration areas and a high degree of sealing, which has continuously increased in the past, are cited as the causes of this (Hamburg Wasser, 2020). To counter this problem, a plan has been presented to transform Hamburg into a ‘sponge city’. The concept behind this is to store, infiltrate, evaporate or use as much water as possible in order to relieve the sewer network, reduce flooding and protect infrastructure and water bodies (BUKEA, n.d.c). To implement this, programmes have been initiated to promote unsealing and the construction of rainwater cisterns, infiltration systems and green roofs (BUKEA, n.d.c).

Although heavy rainfall is not classified as a significant risk under the Water Resources Act, the current risk management plan from 2021 addresses the dangers for the first time (FGG Elbe, 2021). Hazard maps for heavy rainfall were developed, showing the extent of flooding and the maximum water depth for a 30-, 100- and 1000-year heavy rainfall event (BUKEA, 2024b).

3.4 Delimitation of the Study Area

The boundaries of the study area and its characteristics are shown in Figure 2. The study area is defined in the west, south and east by the official borders of the city. The northern boundary is defined by the boundary of the coastal flood risk area, which was established in the city's current risk management plan. As coastal flooding has no impact on the areas north of this boundary, the flood risk posed by compound flooding is also classified as very low. These areas were therefore excluded from this flood risk assessment. The study area is traversed by the river

Elbe, which enters the city of Hamburg in the south-east, in the district of Bergedorf. The river is approximately 400 m wide at this point (BUKEA, 2015a). The Elbe flows through Hamburg for a length of 51 km (BUKEA, 2015a). It splits into the Norderelbe and Süderelbe at the Elbe island of Wilhelmsburg and rejoins further downstream before leaving the city in the west. The area north of the Norderelbe represents the inner-city area, which has a mixed use of industrial and residential space. This type of use is also predominant in Wilhelmsburg (BUKEA, 2015a). To the west of Wilhelmsburg, in the Waltershof district, are the port facilities, which are located in front of the public flood protection line. The districts of Harburg and Bergedorf in the south and south-east of Hamburg are characterised by agricultural use (BUKEA, 2015a).

Figure 2 also shows the locations of the Schulau gauging station and the Fuhlsbüttel weather station, whose significance for this study is described in Section 4.1.

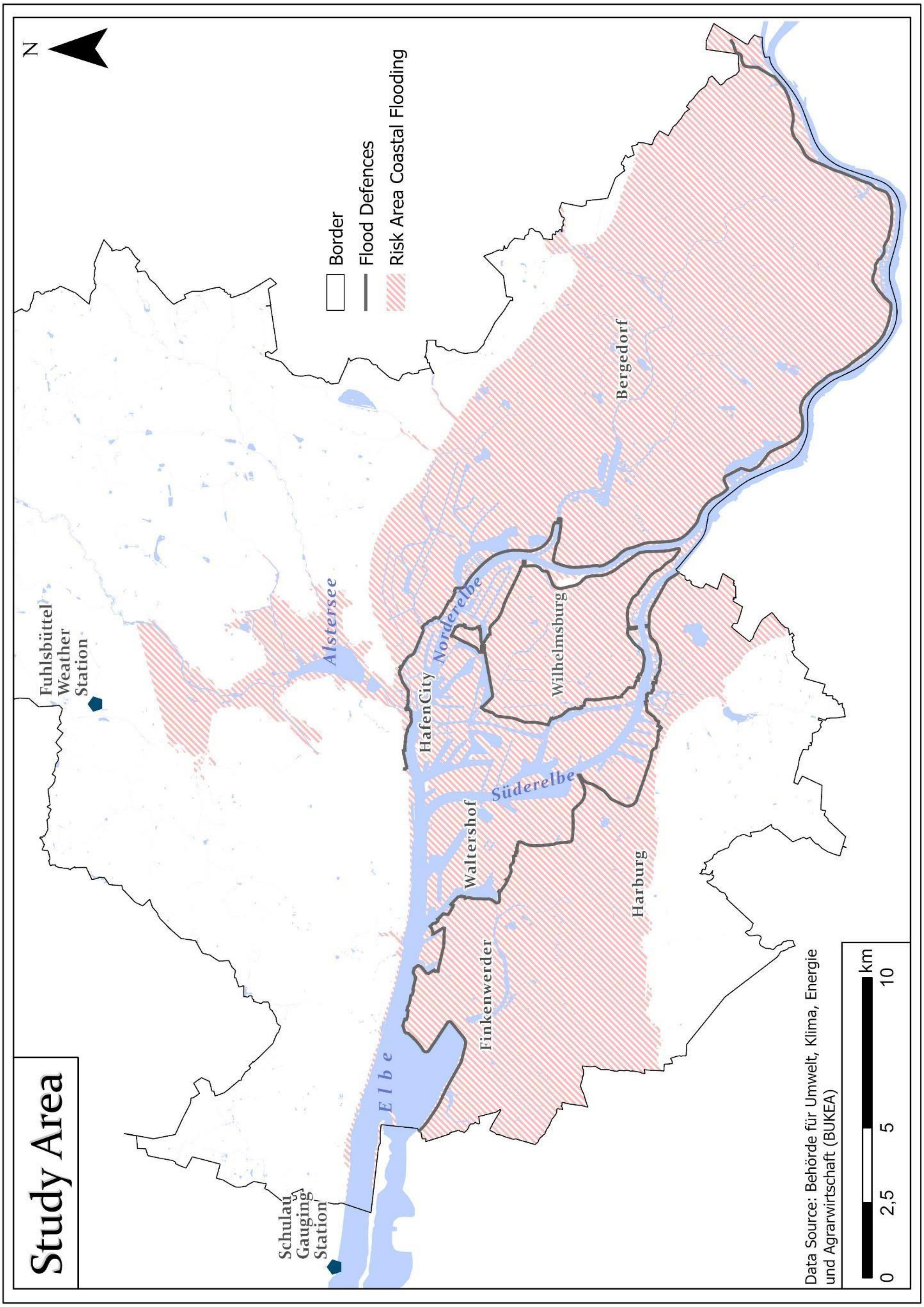

Figure 2 - Characterisation of the study area

4. Materials

4.1 Flood Frequency Analysis

Two time series were required for the flood frequency analysis. The first contained the total water level (TWL) of the Elbe in the west of the city. According to the definition of the United States Geological Survey (n.d.), the TWL represents the combination of tides, surge and wave run-up. It therefore describes the actual water level measured at the gauge.

A key feature of the time series is its length, as this has a direct impact on the estimates of the probability distributions and joint distributions in flood frequency analysis (Lucey & Gallien, 2024). Although there is no suggested minimum record length for coastal flooding events (Lucey & Gallien, 2024), inaccuracies can be introduced by time series that are too short. For example, a random accumulation of extreme events may occur in the selected time window, resulting in the adjusted distribution overestimating the probability of occurrence (Schulte, 2015). Similarly, a very low or even absent occurrence of extreme events leads to an underestimation of the probability of occurrence of extreme events (Schulte, 2015). In their analysis of a compound flooding event caused by rainfall, storm surge and waves, Lucey and Gallien (2024) find that uncertainties are greatly reduced when the time series covers at least 70 years. However, as a review of TWL time series shows, only about 60 gauging stations worldwide have such long records (Lai et al., 2021). Upon enquiry to the Hamburg Port Authority, which operates various gauging stations in Hamburg, it was stated that continuous water level time series for all gauges in the tidally influenced sections of the Elbe are only available from the year 2000 onwards (U. Ferk, personal communication, 27 August 2025).

To circumvent the problem of short observed time series, many studies use modelled data (Xu et al., 2023; Dubois et al., 2024; Lai et al., 2021). One example of this is the Global Tide and Surge Reanalysis dataset. This dataset contains global surge and extreme sea level time series based on hydrodynamic modelling (Muis et al., 2016). Another example is a global sea level change time series, which contains 10-minute TWL data from 1950 onwards and is made available free of charge by the Copernicus Climate Change Service (Copernicus Climate Change Service, 2022). However, the limitation of these modelled datasets lies in their low spatial resolution, which makes it impossible to accurately reconstruct the TWL in topographically complex areas such as estuaries (Yan et al., 2024).

Despite the inaccuracies introduced by the short length of the time series, it was decided for this work that the observed data is preferable to the imprecise, reconstructed data. Therefore, TWL data from the Schulau gauge station located to the west of the city was used for flood modelling of Hamburg (Figure 2). Minute-by-minute water level data is available for download on the Pegel Online website of the Federal Waterways and Shipping Administration and covers the period from 1 January 2000 to 31 December 2024 (Federal Waterways and Shipping Administration [WSV], n.d.). It is raw data (WSV, n.d.).

The second time series required for the flood frequency analysis contained rainfall data. As is customary in similar studies analysing compound flooding caused by rainfall, daily rainfall values (24-hour cumulative rainfall) were also used for this study (Chen et al., 2023; Jalili Pirani & Najafi, 2023; Lai et al., 2021; Lucey & Gallien, 2024; Xu et al., 2023).

An analysis comparing the rainfall time series from five weather stations in the city shows that there are spatial variations in rainfall patterns for Hamburg (Verworn Langenhagen & Kuchenbecker, n.d.). The authors find that, using daily precipitation totals, the precipitation amount of an extreme event with a return period of 100 years differs by up to 15 mm. The values in the south-east of the city are rather low (approx. 74 mm), while the highest values were determined north of Finkenwerder, directly adjacent to the Elbe (approx. 89 mm) (Verworn Langenhagen & Kuchenbecker, n.d.). However, since small-scale modelling exceeds the scope of this work and long time series from many measuring stations are not available, it was decided to use data from a single measuring station as representative for the entire city. Germany's National Meteorological Service operates two measuring stations in Hamburg, which record rainfall time series that continue to this day (DWD, n.d.). Due to the lower number of downtimes during the study period, the Fuhlsbüttel weather station, in the north of the city, was selected (Figure 2). The data is freely available and can be downloaded from Germany's National Meteorological Service's Climate Data Centre (n.d.a). The rainfall time series covers the same period as the TWL data. The rainfall data has been verified by the operator (DWD, 2024). In addition, a time series of hourly rainfall totals was required to create a design hyetograph, which was used as input for the hydrodynamic model. This data is also freely available for the Fuhlsbüttel weather station in the Climate Centre of Germany's National Meteorological Service (DWD, n.d.b).

The location of the selected weather station can be used to classify the inaccuracies that arise from the use of a single time series. The generalised precipitation total for an event with a return period of 100 years, as determined in this study, deviates from the local values to varying degrees. Based on the study by Verworn Langenhagen & Kuchenbecker (n.d.), it can be assumed that the flood risk from heavy rainfall in the western areas of the city, along the Elbe, is rather underestimated, while it is slightly overestimated in the south-east.

4.2 Flood Simulation

To perform the flood simulation, several input data sets are required in addition to the design hydrograph and design hyetograph, which are created using the results of the FFA. Topographical information is provided in the form of a digital elevation model (DEM) with a spatial resolution of 1 m by the State Office for Geoinformation and Surveying of the City of Hamburg (2022). For realistic modelling of flood dynamics at the city borders, the simulation area was extended to include areas from the neighbouring federal states of Lower Saxony and Schleswig-Holstein. DEMs with a spatial resolution of 1 m are available for both federal states (State Office for Geoinformation and Cadastre Lower Saxony, 2025; State Office for Surveying and Geoinformation Schleswig-Holstein, 2023). In order to correctly model the water flow within the Elbe and adjacent water areas, topographical data of the waterbed was used in addition to the surface DEMs. The data is provided free of charge by the WSV in raster format with a spatial resolution of 1 m (WSV, 2022).

Land use data was used to consider different roughness values for different land uses. The feature layer distinguishes between 24 land use classes based on Hamburg's land use plan. The data is freely available on Esri Germany's Open Data Portal (Free and Hanseatic City of Hamburg, Ministry of Urban Development and Housing, 2022).

A feature layer was considered for the accurate representation of flood defence structures. The layer provided by the Hamburg State Agency for Roads, Bridges and Waterways contains information on the location of protective structures as well as their height and date of construction (State Agency for Roads, Bridges and Waterways, 2020).

A feature layer depicting the extent of the actual flooding was used to validate the simulation of the 1962 storm surge. The layer, created by the Ministry of the Environment, Climate, Energy and Agriculture, is freely available on the Hamburg Geoportal (BUKEA, 2014).

A summary of all the materials used is provided in Table 1.

Table 1 - Materials used for this thesis

Data	Characteristics	Source	Purpose
DEM	Topographical data of Hamburg Spatial resolution: 1 m Format: TIF	State Office for Geoinformation and Surveying of the City of Hamburg Accessed via Geoportal-Hamburg URL: https://geoportal-hamburg.de Date of Access: 2025-09-26	Construction of DEM for Model Calibration
DEM	Topographical data of Schleswig-Holstein Spatial resolution: 1 m Format: TIF	State Office for Surveying and Geoinformation Schleswig-Holstein URL: https://www.schleswig-holstein.de Date of Access: 2025-09-26	Construction of DEM for Model Calibration
DEM	Topographical data of Lower Saxony Spatial resolution: 1 m Format: TIF	State Office for Geoinformation and Cadastre Lower Saxony Accessed via GDI-NI URL: https://ni-harvest-prod.geocat.live Date of Access: 2025-09-26	Construction of DEM for Model Calibration
Extent of the Storm Surge 1962	Format: CSV	BUKEA Accessed via Geoportal-Hamburg URL: https://geoportal-hamburg.de Date of Access: 2025-10-08	Model Validation
Flood Defence Structures	Position of flood defence structures, attribute information about height & date of construction Format: CSV	State Agency for Roads, Bridges and Waterways Accessed via Geoportal-Hamburg URL: https://geoportal-hamburg.de Date of Access: 2025-10-01	Construction of DEM for Model Calibration & Model Validation

Table 1 – Continued

Data	Characteristics	Source	Purpose
Land Use	Distinction between 24 land use classes Format: Shapefile	Land Use Plan Hamburg 2022 Ministry of Urban Development and Housing Accessed via Esri Deutschland – Open Data Portal URL: https://opendata-esridech.hub.arcgis.com Date of Access: 2025-10-06	Construction of Manning's file for Model Calibration
Time Series Rainfall	Daily observed values (24-hour cumulative rainfall) Period: 2000-01-01 to 2024-12-31 Verified Data	Measuring station Hamburg-Fuhlsbüttel DWD URL: https://opendata.dwd.de Date of Access: 2025-09-04	FFA
Time Series Rainfall	Hourly observed values (60-minute cumulative rainfall) Period: 2000-01-01 to 2024-12-31 Verified Data	Measuring station Hamburg-Fuhlsbüttel DWD URL: https://opendata.dwd.de Date of Access: 2025-07-29	Construction of Design Hyetograph for Flood Simulation
Time Series TWL	Minute-by-minute observed values Period: 2000-01-01 to 2024-12-31 Raw Data	Schulau gauge station Accessed via the WSV's Pegel Online website URL: https://www.pegelonline.wsv.de Date of Access: 2025-10-03	FFA & Construction of Design Hydrograph for Flood Simulation
Topography of Elbe Riverbed	Topographical data of the Elbe riverbed Spatial resolution: 1m Format: TIF	WSV URL: https://www.kuestendaten.de Date of Access: 2025-09-25	Construction of DEM for Model Calibration

5. Methodology

5.1 Structure

The structure of the methodology used in this study is depicted in a flow chart (Figure 3). The methodology is divided into two sections.

The first section consists of the FFA, in which the time series of the TWL and rainfall were used as input. The aim of this analysis is to determine the intensity of an event with a defined return period (Mathias, 2023). Depending on the choice of a univariate or bivariate scenario, different methodological steps are followed to determine the design values, which are the calculated rainfall and TWL values, for an event with a return period of 100 years. First, for both cases, events that can be classified as extreme are extracted from the time series (Chen & Guo, 2019). An event is defined here as a continuous physical phenomenon that lies outside the mean range of the environmental variable (Bernardara et al., 2014). Subsequently, probability distributions are adjusted for these extreme events of both variables. In the case of a univariate analysis, the design values can be determined directly using the adjusted distributions (Coles, 2001). For the bivariate analysis, the relationship between the variables must additionally be characterised (Coles, 2001). For this purpose, value pairs are formed, which are then examined in a correlation analysis (Xu et al., 2023). Based on the results of this analysis, a copula can be fitted (Zhu et al., 2024). Using the fitted distributions and the copula, a joint distribution function is constructed, which can be used to determine the bivariate design values (Xu et al., 2023).

In the second section, univariate and compound flooding is simulated. The model is calibrated to the study area using various input data (Zellou & Rahali, 2019). To validate that the model produces realistic results, a historical event is reproduced, and the result is compared with the actual extent of the flooding (Ming et al., 2022). After successful validation, the compound and univariate floods are simulated using the previously calculated design values (Zellou & Rahali, 2019).

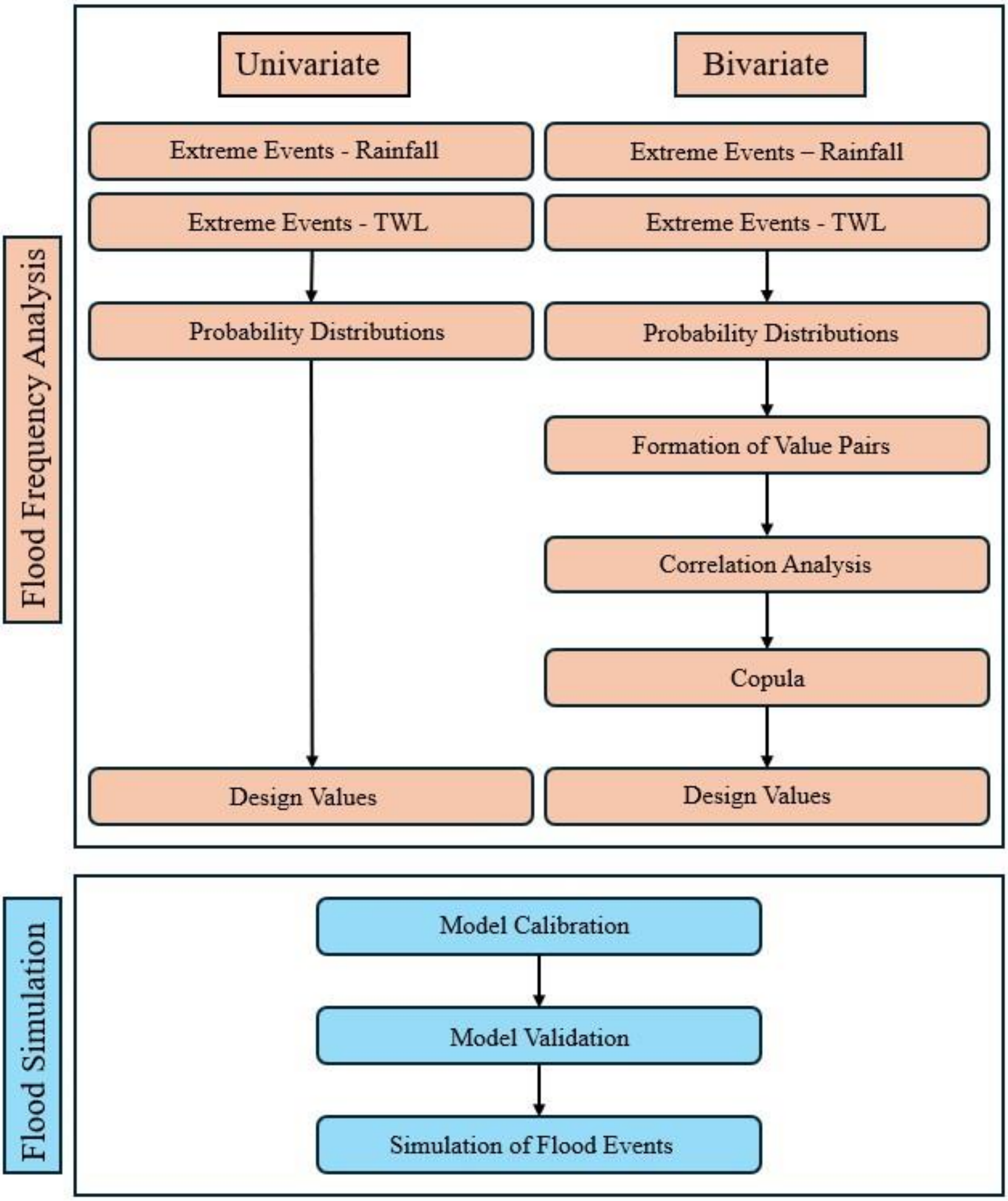

Figure 3 - Flow chart of the methodology used. In the flood frequency analysis, the amount of rainfall and the total water level (TWL) of events with a return period of 100 years are determined. These values are then used as input for the flood simulation.

5.2 Sampling of Extreme Values

5.2.1 Event Sampling Methods

To determine the design values of a defined return period, the first step is to fit a probability distribution to an extreme series (Li & Zheng, 2016). This extreme series is created by extracting extreme values from the observed time series using an event sampling method (Chen et al., 2023). Mazas & Hamm (2017) note that the choice of sampling method probably has the greatest influence on the result of the extreme value analysis. At the same time, they emphasise that there is no universal answer as to which methodology is preferable to the other, but that this decision must be made individually for each application (Mazas & Hamm, 2017). In hydrological frequency analysis, there are two methods that are usually used to extract extreme values from time series (Chen & Guo, 2019). In the annual maximum (AM) method, the event with the highest value is extracted for each year in the time series (Eslamian & Eslamian, 2022). In the peaks-over-threshold (POT) method, all events that exceed a specified threshold are extracted (Ben-Zvi, 2009).

Due to its simplicity, the traditional AM methodology is still the most commonly used in most countries (Bezak et al., 2014). For example, it is explicitly recommended by the Federal Emergency Management Agency, the US authority for disaster control, for the evaluation of coastal hazards (Federal Emergency Management Agency, 2016). It is also considered better and safer than POT for the construction of structures such as dykes or other flood protection facilities (Chen et al., 2023). However, a key disadvantage is the limitation to one sample per year. For applications where only short time series are available, the number of samples is insufficient for statistical analysis (Chen et al., 2023). Furthermore, additional TWL or rainfall extremes may occur in a given year, which are lost using the AM methodology (Zhou et al., 2016). Regarding compound floods in particular, this may include events with a lower value for one variable but a higher value for the other, which are essential for statistical analysis (Chen et al., 2023). Despite the choice of the maximum value per year, the AM methodology does not guarantee that only extreme events are selected. Thus, very low values can also be included in the selection if no extreme event has occurred in a given year (Bezak et al., 2014).

In addition to AM, the POT methodology is increasingly being used in FFAs (Zhu et al., 2024). It enables a more physically sound recording of extreme events, as it considers both the frequency and magnitude of extreme events (Önöz & Bayazit, 2001). The higher number of samples allows more information about extreme events to be extracted than with the AM methodology (Bezak et al., 2014). The consensus is that the POT methodology delivers more robust results, provided that certain conditions are met with regard to the choice of threshold and the independence of events (Ngongondo et al., 2013). For example, Bezak et al. (2014) note that the POT methodology allows for a more precise determination of the return periods of river floods, as it provides a better fit to the observed data compared to AM.

Due to its greater suitability for FFAs and the fact that the available data only covers a period of 25 years, the POT methodology was selected for this thesis.

5.2.2 Peaks over Threshold

When using the POT methodology to extract the extreme values from the time series, two criteria must be considered: selecting a suitable threshold and ensuring the independence of events (Zhou et al., 2016).

5.2.2.1 Threshold Selection

The POT methodology is based on Pickands' theorem, which states that the distribution of data exceeding a given threshold converges towards a generalised Pareto distribution (GPD) (Pickands, 1975). The selected threshold must therefore be high enough that the distribution of events approximates a GPD (Beirlant et al., 1996). However, the higher the threshold, the lower the amount of data that can be used to calibrate the parameters of the distribution. This increases the variance and thus the inaccuracy (Beirlant et al., 1996). The selected threshold must therefore be adjusted so that it is as high as necessary to maintain the smallest possible deviation from the GPD, but at the same time as low as possible to ensure the largest possible amount of data (Bernardara et al., 2014). A frequently chosen approach to solving this problem is to set an average number of events per year and adjust the threshold accordingly (Lang et al., 1999). The specified number of events is based on expert knowledge of the physics and dynamics of the variable under consideration (Bernardara et al., 2014). A literature review shows that a range of three to seven events per year is used for both TWL and rainfall (Camus et al., 2021; Floris et al., 2010; Marcos et al., 2019; Lowe & Gregory, 2005; Tawn & Vassie, 1989; Vousdoukas et al., 2016; Walton, 2000). For this study, the thresholds for both variables were therefore approximated at an average of five events per year.

The basic assumption of FFA is usually that flooding caused by extreme TWL or extreme rainfall occurs evenly over the time window under consideration (Lima et al., 2015). In reality, however, anthropogenic influences such as land use changes or climate change cause hydrological properties to change over time (Vogel et al., 2011). Such a time series is referred to as non-stationary (Zhou et al., 2016). An evaluation of annual flood discharges shows that these processes are also relevant in Hamburg. A sharp upward trend has been observed, which is attributed to increasing soil sealing and climate change (BUKEA, 2015a). In order to take this factor into account in the POT methodology, Zhou et al. (2016) argue that different thresholds should be defined for different sections of non-stationary time series. The first step in this process is to perform a Mann-Kendall test (Zhou et al., 2016). This test is used to determine a linear and / or non-linear trend in the time series (Eslamian & Eslamian, 2022). A trend in hydrology is defined as a steady and regular movement through which values either increase or decrease over time (Kottegoda, 1980). For more detailed specifications of the Mann-Kendall test, see Salas (1993). In this study, Burkey's (2025) MATLAB function was used to perform the test. If no significant trend is detected, a single threshold is used for the entire time series (Zhou et al., 2016). If the Mann-Kendall test shows a positive result, the next step is to perform a test to determine change points (Zhou et al., 2016). In this study, the Pettitt test was used for this purpose, performed using the MATLAB function by Dey (2025). For further specifications on the Pettitt test, see Pettitt (1979). Assuming that λ change points are detected, the time series is divided into $\lambda + 1$ sections. A threshold is then set for each section, which approximates an average of five events per year (Zhou et al., 2016).

5.2.2.2 Independence Criterion

A rainfall or TWL event has a duration that exceeds the temporal resolution of the time series used (Bernardara et al., 2014). For example, an extra-tropical storm can repeatedly trigger heavy rainfall or extreme TWLs over several days (Weisse et al., 2012). In the time series, this phenomenon is represented by extreme values occurring in quick succession. Since the values can be attributed to the same storm event, they are dependent (Koscielny-Bunde et al., 2006). However, a central condition in Pickands' theorem is that the extracted events must be independent of each other (Pickands, 1975). In practice, this condition is usually met by specifying a minimum time lag between two events (Camus et al., 2021). The concept here is that two events can be classified as independent of each other if a certain amount of time has elapsed (Bernardara et al., 2014). The length of the minimum time lag depends on the physical properties of the locally prevailing meteorological conditions and should slightly exceed the average length of these conditions (Bernardara et al., 2014). As was the case for setting the threshold, expert knowledge was therefore also drawn upon here.

A review of the literature has shown that minimum time lags of between 12 and 72 hours are used for rainfall events in Central and Western Europe, while between 72 and 96 hours are usually specified for TWLs (Camus et al., 2021; Hendry et al., 2019; Marcos et al., 2011; Jalili Pirani & Najafi, 2023; Vousdoukas et al., 2016; Willems, 2000; Xu et al., 2023). Since a common minimum time lag must be used for the compound event, a value of 72 hours was selected for both variables in this study. As a result, for those events in which the threshold was exceeded multiple times within the 72-hour window, only the maximum value was adopted (Bernardara et al., 2014).

A statistical test was used to verify that the use of the minimum time lag in combination with the selected threshold actually fulfils the requirement of independent, evenly distributed extreme events. The Poisson distribution describes the probability that a given number of evenly distributed, independent events will occur within a defined period of time (Haight, 1967). From this context, it can be deduced that the extracted events are independent if they follow a Poisson distribution (Lang et al., 1999). The test proposed by Cunnane (1979) is usually used for this verification, which compares how much the mean number of annual events deviates from the Poisson distribution. For further specifications on the Cunnane test, see Naghettini (2017). If the test failed, the threshold was increased iteratively until the test was successful.

5.3 Fitting of Probability Distributions

The next step was to fit a probability distribution to the data. For this purpose, the Multivariate Copula Analysis Toolbox (MvCAT) version 2.0 by Sadegh et al. (2018) was used. In the POT methodology, extreme events are selected in such a way that they approximate a GPD. This distribution is therefore also used to model the probability structure of the extreme series (Pickands, 1975). The parameters defining the distribution were determined using the maximum likelihood method. This method adjusts the values so that there is as little deviation as possible between the observed and modelled probabilities (Sadegh et al., 2018). For further information on this method, see Coles (2001). Various goodness-of-fit tests, including chi-square and quantile-quantile plots, ensure that the adjusted GPD accurately reflects the observed distribution of extreme events (Sadegh et al., 2018).

5.4 Formation of Value Pairs

5.4.1 Determination of the Priority Variable

For the bivariate analysis, value pairs had to be formed next. There are two methods for doing this: Either the extreme events of the rainfall time series are used and each event is assigned the corresponding TWL value (= priority of rainfall), or the extreme events of the TWL time series are used and each event is assigned the corresponding rainfall value (= priority of TWL) (Chen et al., 2023). The choice of methodology can have a decisive influence on the correlation analysis. For example, in their analysis of a compound flood in southern Sweden, Dubois et al. (2024) find a significant positive correlation when rainfall (represented as river water level) is the priority variable, whereas no significant correlation is found when TWL is the priority variable. A similar result is found in a study of compound floods along the Canadian coast. Here, too, a higher correlation is found when using the priority of rainfall than when using the priority of TWL (Jalili Pirani & Najafi, 2023).

One limitation to consider arises when TWL is selected as the priority variable. It is often the case that there is no rainfall during the period when extreme water levels occur, meaning that the corresponding value pair does not represent a compound event (Chen et al., 2023). In this case, the corresponding value pairs must be removed from the sample, which reduces the amount of input data for the correlation analysis and adjustment of the copula (Jalili Pirani & Najafi, 2023). This can lead to less accurate results, especially for short time series (Lucey & Gallien, 2024).

Based on this reasoning, rainfall was selected as the priority variable for this study.

5.4.2 Assignment of the Secondary Variable

The next step was to determine how the values of the secondary variable would be assigned to the extreme events of the priority variable (Camus et al., 2021). A commonly used methodology for this is to define a time window around the extreme event (Wahl et al., 2015; Ward et al., 2018; Couasnon et al., 2020). The maximum value within the time window is then adopted as the value of the secondary variable (Camus et al., 2021). The time windows most commonly used in the literature are 0 days (assignment of the value on the same day) (Chen et al., 2023; Lian et al., 2013; Zellou & Rahali, 2019) and a lag of ± 1 day (Jalili Pirani & Najafi, 2023; Ward et al., 2018). However, some studies also use time windows of up to ± 5 days (Couasnon et al., 2020; Ward et al., 2018). Xu et al. (2023) investigate the correlation of rainfall and surge pairs using time windows between zero and seven days in a total of 26 estuary regions. They find that in most estuary regions, the correlation is highest when using the value on the same day (Xu et al., 2023). Hendry et al. (2019) reach the same conclusion in their study on compound flooding along the UK coast. They also note that the time lag varies depending on the characteristics of the catchment. For example, in large catchments, the highest correlation occurs with a time lag of several days, while in smaller catchments, the correlation is highest on the same day (Hendry et al., 2019).

The study area in this thesis is characterised by short flow paths, as the Elbe and its tributaries extend throughout the entire study area. All rainfall therefore drains directly into the tide-influenced Elbe. Due to these characteristics and the small size of the study area, it can be assumed that a short time lag is most suitable for the creation of the compound event. Based on this consideration and the evaluations by Xu et al. (2023) and Hendry et al. (2019), a time window of zero days was chosen for this study. Accordingly, each extreme rainfall event was assigned the maximum TWL value for the same day.

5.5 Correlation Analysis

To determine whether there is a statistical dependence between rainfall and TWL, a correlation analysis was performed. Correlation coefficients can be used to determine the direction and strength of the correlation between the two variables (Naghettini, 2017). The coefficient can take values in the range from -1 to 1. Positive values indicate a positive correlation, which means that as the value of one variable increases, the other also increases, while negative values indicate that as the value of one variable increases, the other decreases (Naghettini, 2017). The standard significance level of 5% was used to reject the null hypothesis H0, which states that the two variables are independent. If the value p output by the test is < 0.05, H0 is rejected and a significant correlation between the variables exists. Similarly, a p-value of > 0.05 indicates that H0 is accepted and the variables are independent (Dubois et al., 2024). In this study, the three correlation coefficients Kendall's tau, Spearman's rho and Pearson correlation coefficient were used. The latter is suitable for expressing a linear dependence between the variables (Naghettini, 2017). Kendall's tau and Spearman's rho are suitable for capturing dependencies in non-normally distributed distributions, for which the Pearson correlation coefficient is unsuitable (Chen & Guo, 2019). For further information on the three correlation coefficients, see Naghettini (2017) and Chen & Guo (2019).

MvCAT was used to perform the correlation analysis and subsequent copula fitting.

5.6 Fitting of the Copula

Based on the results of the correlation analysis, a copula was then selected and adjusted. MvCAT contains 26 different copula families, from which the most suitable one is selected (Sadegh et al., 2017). For specifications of the tool and the process of selecting the copula, see Sadegh et al. (2018). Various tests are performed to verify the suitability and fit of the adjusted copula (Sadegh et al., 2017). This includes maximum likelihood, root-mean-square error and the Bayesian Information Criterion, which is a measure that compares the accuracy of the fit to the data with the complexity of the model (Naghettini, 2017). For further information on the latter, see Brockwell & Davis (1991).

5.7 Determination of Design Values

Finally, the design values for the bivariate and univariate events with a return period of 100 years were determined.

The following equation was used to calculate the univariate design values:

$$Z_N = \mu + \frac{\sigma}{\xi}\left[(N n_y \zeta_u)^{\xi} - 1\right] \quad (1)$$

Here, the GPD with its adjusted parameters σ and ξ is used to determine the design value Z of an event with a return period of N years (Coles, 2001). ζ corresponds to the probability that a single observation exceeds the threshold value μ defined within the POT methodology (Coles, 2001). In practice, this is calculated using the mean annual exceedance rate, which corresponds to the quotient of the observed number of exceedances of μ and the number of years in the time series n_y (Coles, 2001).

Unlike the univariate event, the bivariate event does not have a single design value, but rather an infinite number of combinations of rainfall and TWL that correspond to an event with a return period of 100 years (Salvadori et al., 2011). Depending on the characteristics of the study area, severe flooding can be triggered if at least one of the two variables exceeds a critical threshold (OR scenario) or if both variables exceed their respective critical thresholds simultaneously (AND scenario) (Chen et al., 2023). Jalili Pirani and Najafi (2023) emphasise that the choice of scenario should be based on the aim of the study and historical flood events. The OR scenario shows the total flood hazard, regardless of whether it is primarily defined by extreme rainfall or extreme TWL (Dubois et al., 2024). To maintain a 100-year joint return period in this case, the value of each variable must exceed a very high critical threshold as either one could cause the system to fail independently. In contrast, the AND scenario is used for situations in which critical flooding occurs solely due to the simultaneous occurrence of both variables (Xu et al., 2023). As this is very rare, the values of the two variables are less extreme.

As described in Chapter 3, critical flooding based solely on the occurrence of a storm surge is prevented by the extensive flood protection measures in Hamburg. Similarly, during normal or low TWL conditions, the water resulting from an extreme rainfall event can be drained into the Elbe, thereby preventing widespread flooding. Accordingly, a high risk of flooding only occurs when a simultaneous high TWL prevents drainage. Due to this dynamic, the AND scenario was selected for this study.

The joint probability distribution for the AND scenario is calculated using the following equation:

$$E_{AND} = P\big((R > r) \cap (T > t)\big) = 1 - F_r(r) - F_t(t) + F_c(r,t) \tag{2}$$

Where $F_r(r)$ and $F_t(t)$ are the probability distributions of rainfall and TWL, and $F_c(r,t)$ is the copula (Chen et al., 2023). The contour, which contains all possible value pairs corresponding to an event with a return period of 100 years, can then be created using the following equation:

$$T_{AND} = \frac{1}{\zeta E_{AND}} \tag{3}$$

Here, T_{AND} represents the joint return period and ζ the mean annual exceedance rate of the priority variable (Chen et al., 2023). The equivalent frequency combination (EFC) method was used to select the pair of values on the contour. This is a frequently used approach, which has been established as the standard for determining design values in China, for example (Xiao et al., 2008, 2009; Chen et al., 2010). This methodology selects the combination in which both variables have the same probability of occurrence (Chen & Guo, 2019). An analysis by Chen & Guo (2019), in which various methodologies such as conditional expectation combination, component-wise excess realisation and most-likely realisation are compared, has shown that the EFC method delivers reliable results and is therefore highly suitable for selecting the pair of values.

5.8 Flood Simulation – Model Selection

In the second section of the methodology, a numerical model was used to simulate the extent of flooding for the univariate and bivariate events. Following the current literature on modelling compound floods, two-dimensional surface models and coupled sewer-surface models were considered for this study. Due to the high computational cost of coupled sewer-surface models, it was not possible to use them within the scope of this thesis. In addition, it was assumed that a two-dimensional surface model would be suitable for the purpose of this study, which primarily requires a comparison between univariate and compound events.

The hydrodynamic model LISFLOOD-FP was used for this thesis. This model was developed specifically for coastal flooding simulations and strikes a balance between accurate capture of the dominant physical processes and substantially reduced computational effort (Bates et al., 2005). This configuration allows fine spatial resolution simulations to be performed on a regional scale within a few hours on a normal PC (Bates et al., 2005). LISFLOOD-FP is a grid-based model designed by Bates & De Roo (2000) and has been continuously developed since then. Version 8.2 from 2025 was used for this study. For further information on the function and characteristics of the model, see Bates et al. (2005, 2013) and Chowdhury & Kesserwani (2024). The model has been used in various studies to simulate flood events and has been confirmed as suitable for realistic modelling of flood dynamics (Liu et al., 2019; O'Loughlin et al., 2020; Shustikova et al., 2019; Wing et al., 2020). A description of the input files required to run the simulation is provided in Table 2.

Table 2 - Input files needed to run the flood simulations using LISFLOOD-FP.

File Name	Purpose	Format
Boundary Condition File	Specification of the properties of the simulation area boundaries (e.g. constant or time-varying sea level, inflow or outflow of water)	Text file
DEM File	Topographical information for realistic simulation of runoff characteristics; definition of the extent and spatial resolution of the simulation area	Raster
Manning's Coefficient File	Definition of spatially varying surface friction	Raster
Parameter File	Names of the files used for the simulation; definition of the solver; specifications for executing the model (e.g. simulation duration)	Text file
Rainfall Data File	Definition of spatially uniform, time-varying rainfall	Text file
Start File	Definition of the water depth of areas that are covered with water at the start of the simulation (e.g. rivers, lakes)	Raster

5.9 Model Calibration

To calibrate the model to the study area, a number of input files must be created.

5.9.1 DEM

The central element of the model is a DEM. This must be structured in such a way that, in addition to the topography of the terrain surface, it also includes the characteristics of the Elbe riverbed in order to simulate realistic flow behaviour (Zellou & Rahali, 2019). To this end, the three DEMs of the federal states of Hamburg, Schleswig-Holstein and Lower Saxony were first merged into a single DEM (Figure 4). Since the DEM lacks information about the ground beneath water bodies, it was combined with topographical data on the riverbed of the Elbe (Figure 4).

A key factor in modelling is cell size. Smaller cell sizes allow for more detailed simulations of flow behaviour, which leads to more accurate results (Altenau et al., 2017). At the same time, however, a finer grid also leads to higher computational effort, which is reflected in longer computing times (Nwogwu et al., 2025). Therefore, a balance had to be struck between accuracy and computational efficiency. Since the choice of cell size depends on the selected model, the study area and the objective of the study, there is no central guidance on which cell size should be chosen, which means that a subjective decision must be made (Nwogwu et al., 2025). Similar studies have shown that grid scales of 50 m or less are often required for accurate flood simulation in urban areas (Bates et al., 2005). To ensure the feasibility of this study within the defined time frame, a maximum computing time of 24 hours was set. Several grid resolutions between 10 and 50 m were tested, with a resolution of 25 m ultimately being selected. At this resolution, all simulations could be completed within 15 - 20 hours. Bilinear interpolation was used to convert the original 1 m DEM.

For a realistic simulation of a flood event in a city such as Hamburg, it is essential that the position and height of flood defence structures are represented in the DEM (Ming et al., 2022). Since the values in the DEM were interpolated, the heights of the protective structures were changed. Furthermore, flood barriers in particular were not captured at all in many areas due to their narrow width. Therefore, a feature layer of the flood defence structures was used to determine the position of the protective structures in the DEM and to adjust the values of the corresponding cells to the correct height (Figure 4).

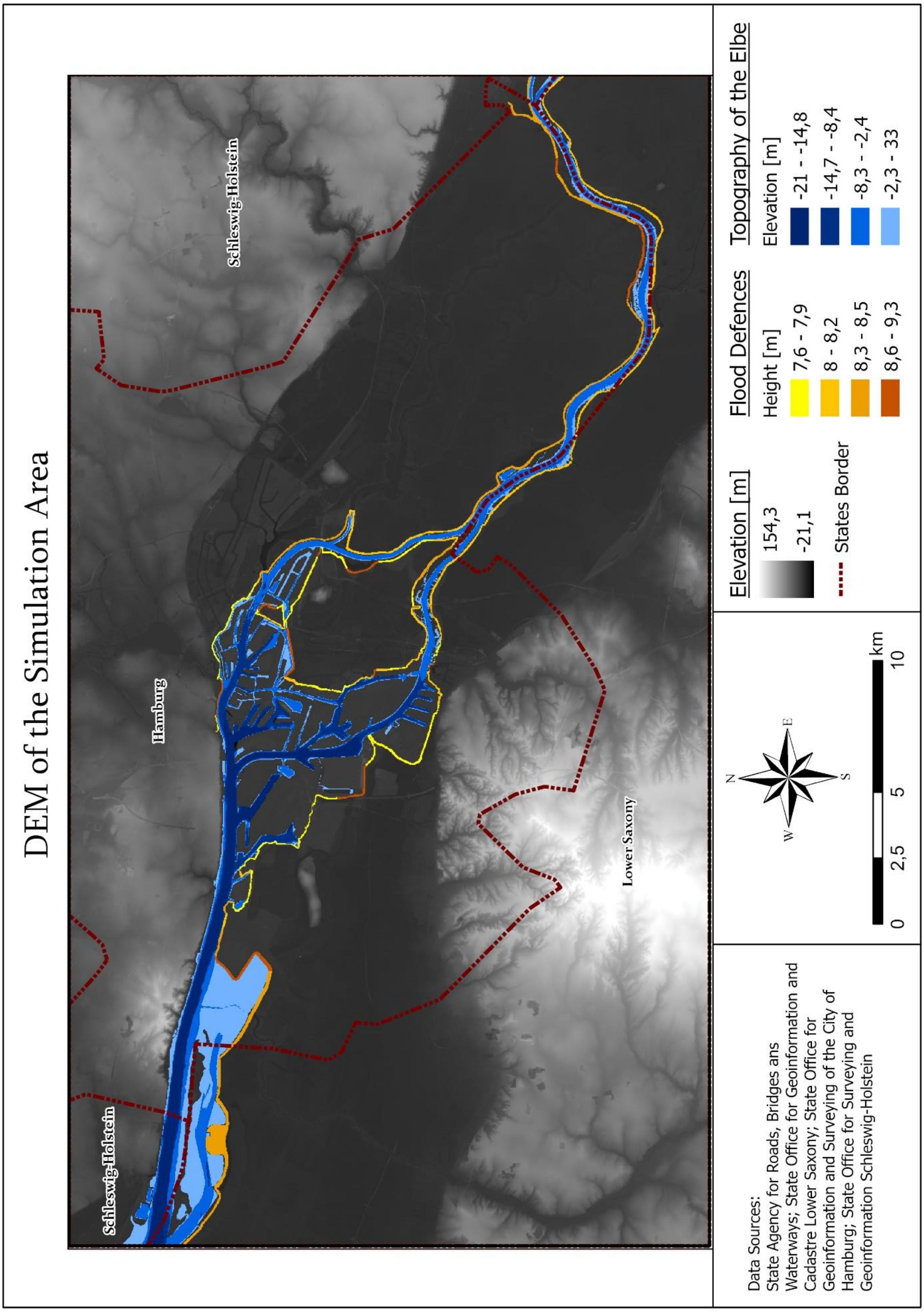

Figure 4 - DEM, which was used to calibrate the model. To ensure a realistic simulation at the boundaries, the study area was extended to include areas from the neighbouring federal states. In addition, information on the topography of the Elbe and the height of the flood defences was incorporated.

5.9.2 Surface Roughness

The roughness of different surfaces affects flow behaviour and thus directly influences the extent of flooding, water depth and flow velocity (Gallegos et al., 2009). In order to realistically reproduce this behaviour, a land use layer of the study area is used, and a Manning's roughness coefficient is assigned to each land use class (Zellou & Rahali, 2019). This coefficient reflects the resistance to flow of the surface, which is influenced by factors such as particle size or vegetation (Marcus et al., 1992). For this work, values proposed by Strahler & Chow (1964) and Van der Sande et al. (2003) were used.

A feature layer of land use in Hamburg was used to construct the layer. The original 24 land use classes were grouped into seven super classes. Table 3 shows the classes used and the assigned Manning's roughness coefficients. The layer was converted into a raster with the same format as the DEM.

Table 3 - Manning's Roughness Coefficient for the different land use classes in the study area

Land Use	Manning's Roughness Coefficient
Agriculture	0.04
Forest	0.2
Green Spaces	0.1
Industrial	0.15
Residential	0.15
Roads	0.015
Water	0.03

5.10 Model Validation

In order to validate that the model produces realistic results, a historical flood event was recreated (Ming et al., 2022). As already described in Chapter 3, the storm surge of 1962 is considered the most devastating in Hamburg's history. As a result, it has been the subject of numerous reports, studies and analyses, from which the necessary information about the impact on flood protection structures, the height of the TWL and the extent of the flooding could be obtained.

5.10.1 DEM

Because massive expansion of flood protection structures took place after the storm surge of 1962 in order to better protect the city from future flooding events, the current DEM did not accurately reflect the situation in 1962. An adjustment was therefore necessary, which consisted of four steps: reducing the height of existing protection structures, removing protection structures that did not exist at the time, adding structures that existed at that time but do not exist today and taking dyke breaches into account. In the first step, the height was reduced to a universal value of 5.70 m, which corresponds to the reported dyke height in 1962 (BUKEA, n.d.a). In the second step, based on the map by Laubitz-Bertram (2012) and the information on the date of construction from the layer provided by the Hamburg State Agency for Roads, Bridges and Waterways (2020), those protective structures that did not exist at the time were removed by adjusting the terrain height in the DEM to the value of the area behind them. Thirdly, protective structures that were in place at the time were manually added and their height was also set at 5.70 m. To take dyke breaches into account, gaps with a width of at least 2 cells (50 m) were integrated into the protective structures based on the map from the State Office for Geoinformation and Surveying of the City of Hamburg (1962). The elevation in these gaps was adjusted to the level of the area behind them to allow water to flow in. Figure 5 shows an overview of the adjustments to the protective structures.

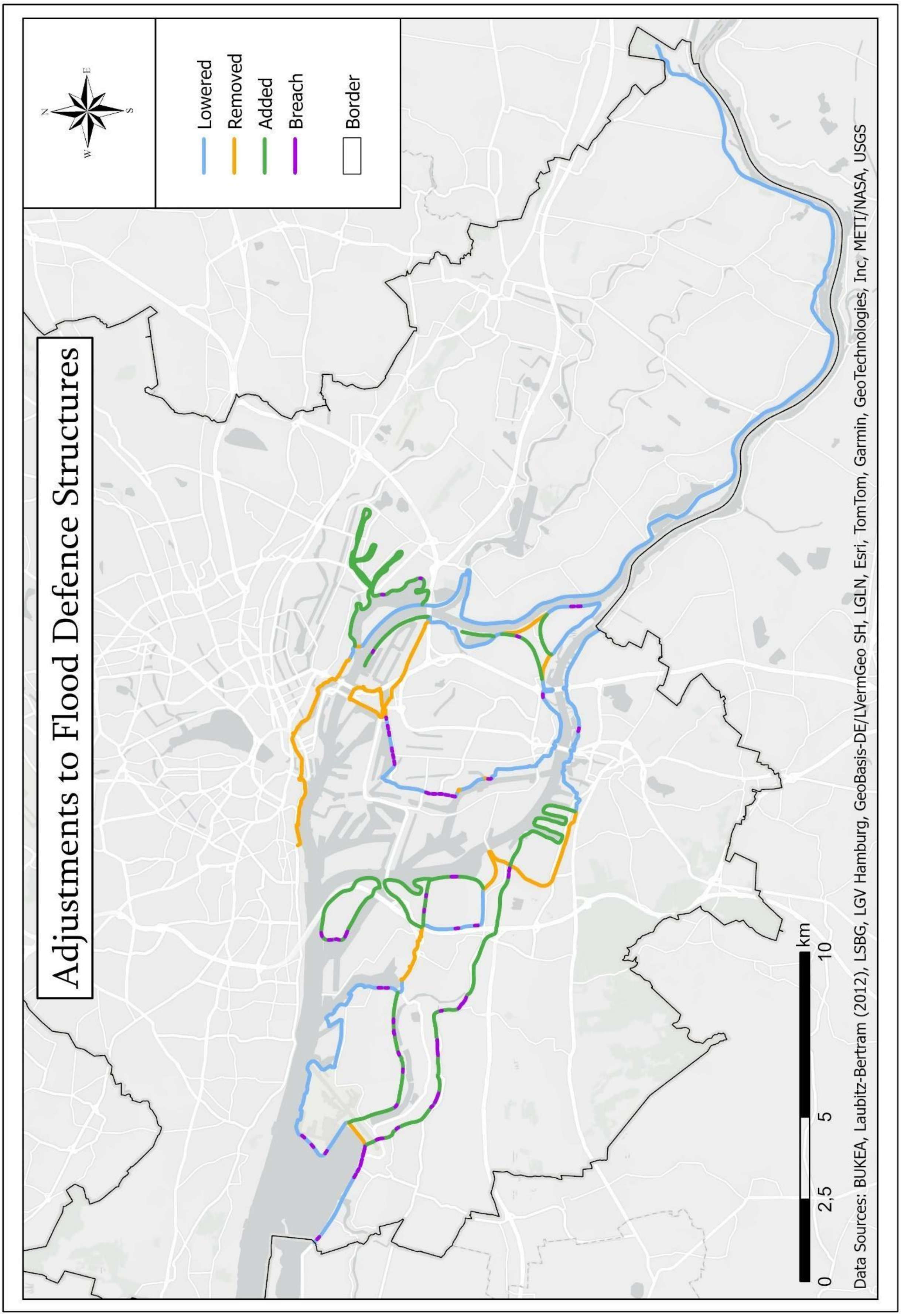

Figure 5 - Adjustments made to the flood defence structures to recreate the flooding of 1962

5.10.2 Boundary Conditions

In order to reproduce the course of the storm surge of 1962, a hydrograph of the event at the Schulau gauge station was required. However, as this data was not available, a design hydrograph was created using the same frequency amplification (SFA) method (Xiao et al., 2009). This methodology amplifies observed events using a constant amplification factor to reflect a defined design event (Xu et al., 2024). For this work, the SFA methodology was used to adjust an observed hydrograph from the Schulau gauge station so that it contained the known maximum TWL of the 1962 storm surge at its peak. To map a realistic storm surge progression, the event of 6 December 2013 was used. This day marks the highest storm surge in the available TWL time series. A time window of 72 hours was selected for the simulation period, from two days before the peak to one day after the peak (Ming et al., 2022). The peak of the 2013 event was 576.92 cm above sea level, while the peak of the 1962 storm surge was 586 cm above sea level (Ministry of Food, Agriculture and Forestry, State Office for Water Management, Schleswig-Holstein, 1962). The amplification factor, which represents the ratio between the design value and the observed value of the 2013 storm surge (Xu et al., 2024), was 1.0157. Figure 6 shows the design hydrograph that was created. This hydrograph was defined as a boundary condition at the western border, where the Elbe exits the simulation area.

To create the start file, the water level of the Elbe was set to the start value of the hydrograph (182.02 cm).

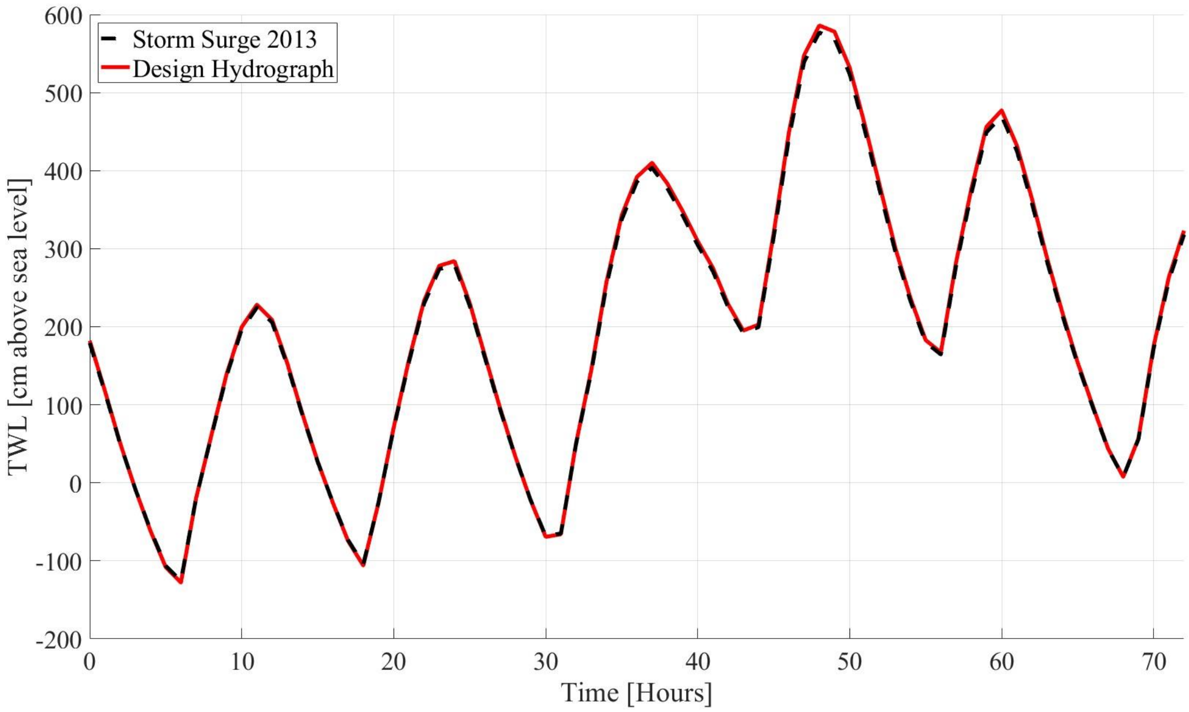

Figure 6 - Comparison between the observed hydrograph of the storm surge of 6 December 2013 and the corresponding design hydrograph of the storm surge of 1962

5.11 Simulation of Flood Events

To analyse the flood risk of a compound event compared to univariate events, three scenarios were simulated, all with a return period of 100 years: a storm surge, a heavy rainfall event and a compound event.

5.11.1 Storm Surge

A design hydrograph was created as the boundary condition for the storm surge. As for the reconstruction of the 1962 storm surge, the storm surge of 6 December 2013 was used as the reference hydrograph. The SFA methodology was also used here. To do this, the amplification factor was first calculated from the ratio between the peak of the reference hydrograph and the design value determined from the univariate FFA. The amplification factor was then used to determine the remaining values of the design hydrograph. To create the start file, the water level of the Elbe was set to the start value of the design hydrograph.

5.11.2 Heavy Rainfall

A design hyetograph was created to simulate the heavy rainfall event. As with the creation of the design hydrograph, an extreme event from the rainfall time series was selected. The selected heavy rainfall event took place on 27 June 2024 and caused widespread flooding in Hamburg (NDR, 2024). For the application of the SFA methodology, the amplification factor was determined from the ratio between the rainfall sum of the reference hyetograph and the design value from the univariate FFA. The hourly rainfall sums were then determined by applying the amplification factor to the reference hyetograph. The resulting design hyetograph was then stored in the rainfall data file. The water level of the Elbe was set at mean sea level for the entire duration of the simulation in order to simulate a scenario in which the accumulated rainwater can drain freely.

5.11.3 Compound Event

A design hydrograph and design hyetograph were also used to simulate the compound event. The creation process was similar to the methodology used for the univariate simulations, with the sole difference being that the design values from the bivariate FFA were used.

The aim of this simulation is to depict a worst-case scenario to show the maximum extent of the flood risk of such a compound event. Due to the characteristics of the study area, it was assumed that the greatest flooding would occur when maximum TWL and maximum rainfall coincided. The simultaneous occurrence of the two extremes was therefore defined such that the maximum rainfall would be reached one hour before the maximum TWL value. The one-hour time lag was intended to ensure that the rainwater accumulating in the entire study area would have time to reach the river.

6. Results

6.1 Flood Frequency Analysis

6.1.1 Sampling of Extreme Values

Since the TWL time series contains raw data, the first step was to check for erroneous values. Since the maximum values of the time series are used to adjust the GPD, it was ensured that there were no outliers in this range. To this end, the recorded maximum values were compared with various lists of all severe storm surges recorded at the Schulau gauge or nearby stations (Federal Maritime and Hydrographic Agency, 2011, 2018; Jensen, 2019). Three extreme events from the time series were not mentioned in any of the official lists, which is why it was assumed that these were measurement errors. The corresponding values were therefore removed from the time series.

The POT methodology was applied to both time series to extract the extreme values. For the rainfall time series, a Mann-Kendall test was performed first. The result is a p-value of 0.6169, which is well above the significance level of 0.05. Accordingly, the null hypothesis H0, which states that there is no trend, is accepted. According to the methodology of Zhou et al. (2016), a single threshold is therefore appropriate. To determine the threshold, a value was approximated that is as close as possible to an average of five events per year. For this time series, this value is 18 mm, which corresponds to exactly five events per year. All events above this threshold were extracted from the time series. The independence of the events was ensured by applying a minimum time lag of 72 hours. However, the extreme value series failed the test by Cunnane (1979), which is why the threshold was increased iteratively in 0.5 mm increments. At a value of 20 mm, the test was positive, thus fulfilling the requirement that the extreme value series follows a Poisson distribution. The threshold of 20 mm corresponds to the 98.63rd percentile, meaning that the events extracted correspond to the upper 1.37% (Figure 7). This corresponds to 91 extreme events in the given time series.

For the TWL time series, the Mann-Kendall test showed a significant positive trend averaging 0.0019 cm per year. To determine whether the use of multiple thresholds is appropriate based on this result, the Pettitt test was performed. This showed no change points in the time series. Based on this result and the fact that the determined trend was extremely small, with a total increase in TWL of only 0.048 cm over the period under consideration, a single threshold was used for this time series. Here, too, a value was approximated that is close to an average of five events per year. The determined threshold is 336 cm, which corresponds to an average of 4.96 events per year. This threshold corresponds to the 98.64th percentile (Figure 7). All events above this threshold were extracted from the time series, and the independence was ensured by applying the minimum time lag. The test according to Cunnane (1979) was positive, confirming the suitability of the extreme value series created. A total of 94 extreme events were identified in the 25-year period under review.

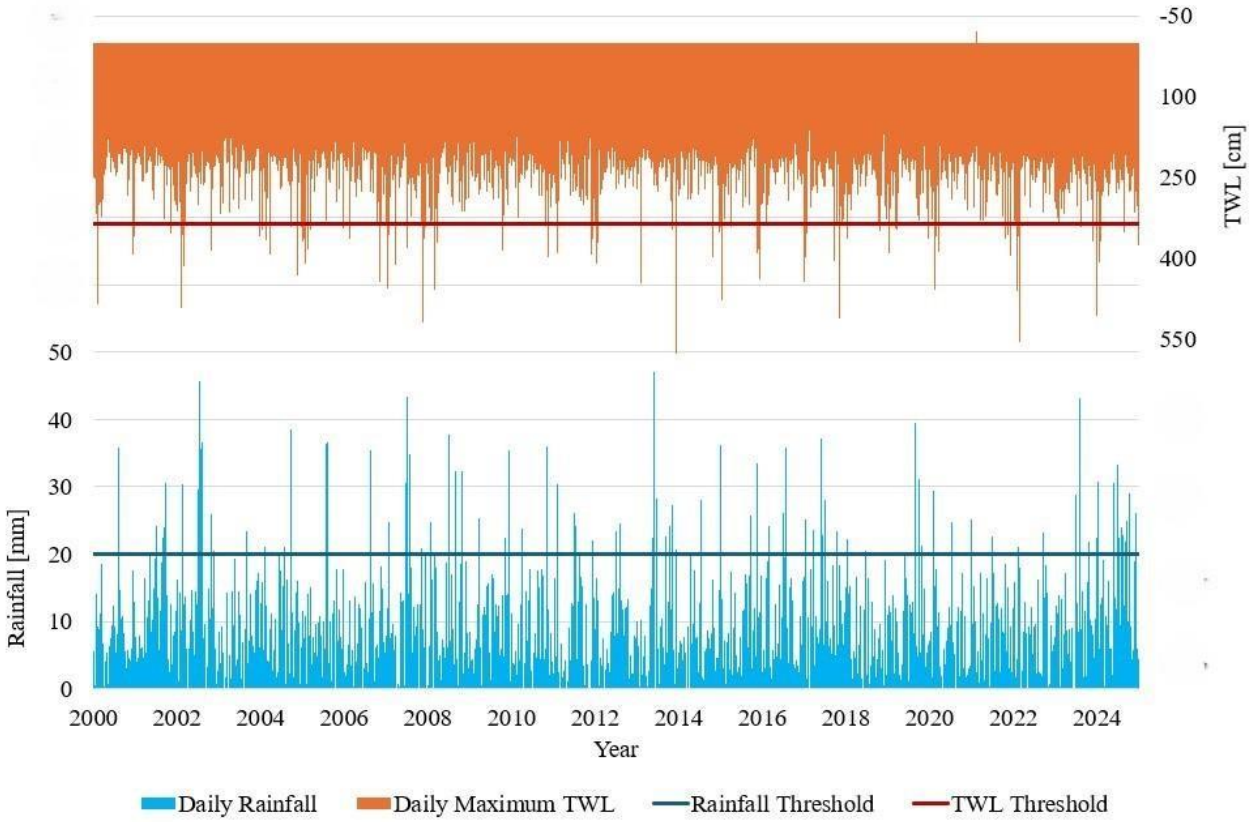

Figure 7 - Time series with their determined thresholds. Events above the thresholds were extracted and used to create the extreme value series.

6.1.2 Fitting of Probability Distributions

Next, probability distributions were fitted to the extreme value series of rainfall and TWL. Since the extreme value series were created using the POT methodology, the GPD is the distribution that is best suited for modelling the data (Pickands, 1975). The distribution equation and the parameters adjusted using the maximum likelihood method are shown in Table 4. Positive test results confirmed the goodness of fit of the adjusted distributions.

Table 4 - Probability distributions, which were fitted to the extreme value series. The parameter values were determined using the maximum likelihood methodology.

Variable	Probability Distribution	Equation	Parameters
Rainfall	GPD	$F(y) = 1 - [1 + \xi\left(\frac{y-\mu}{\sigma}\right)]^{-\frac{1}{\xi}}$	Location μ = 20.0 Scale σ = 9.88 Shape ξ = -0.28
TWL	GPD		Location μ = 336.0 Scale σ = 40.76 Shape ξ = -0.04

6.1.3 Formation of Value Pairs & Correlation Analysis

To form the value pairs for the bivariate analysis, each rainfall event was assigned the maximum TWL value of the same day (Table A1). Figure 8 displays the generated pairs of values in a scatter plot.

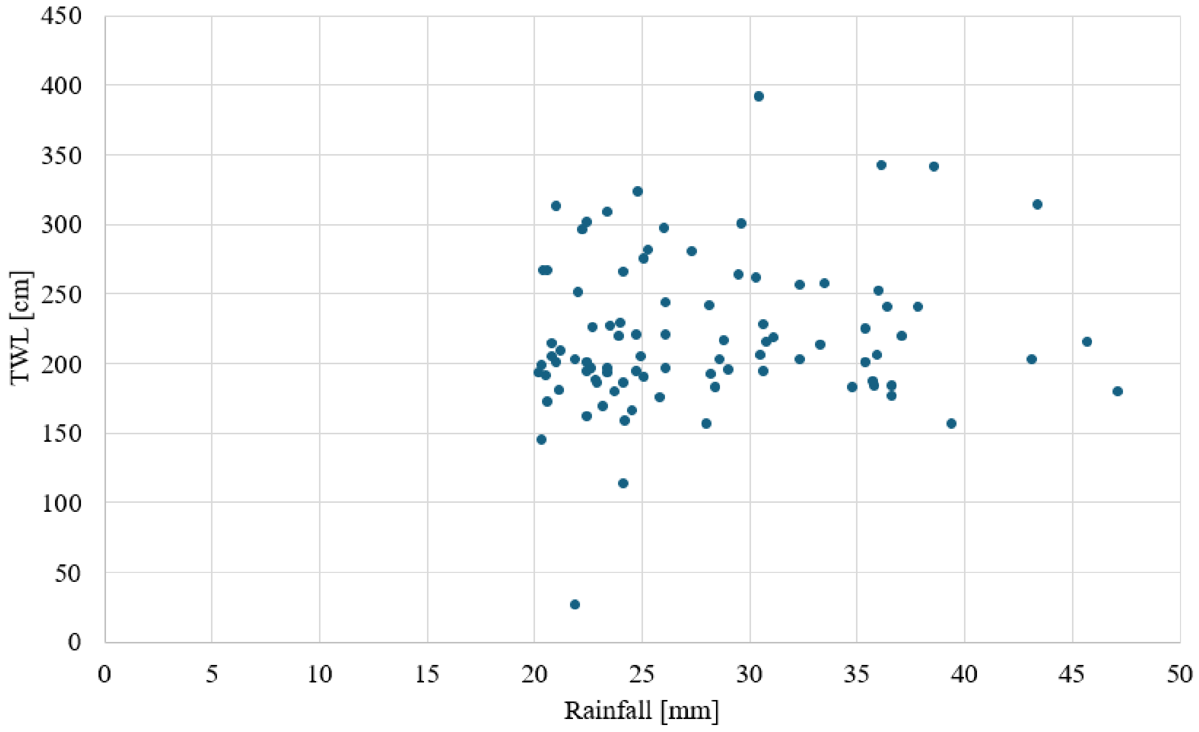

Figure 8 - Scatter plot of the generated value pairs

The value pairs were subsequently used for the correlation analysis. The three correlation coefficients Kendall's tau, Spearman's rho and Pearson correlation coefficient were used for this purpose. The values of the coefficients and the associated p-values are depicted in Table 5. All three coefficients show that there is a slight positive correlation between the two variables. However, the p-values of all three coefficients are above the significance level of 0.05, which means that H0 is accepted and the positive correlation is classified as insignificant.

Table 5 - Results of the correlation analysis

Correlation Coefficient	Coefficient Value	p-Value
Kendall's tau	0.0869	0.2278
Spearman's rho	0.1392	0.1906
Pearson correlation coefficient	0.1286	0.2271

6.1.4 Fitting of the Copula

Since the correlation analysis showed that there is no significant correlation between the variables, the process of selecting a suitable copula family could be dispensed with. This is justified by the fact that in the case of independence, the independence copula is used (Brunner et al., 2016; Dubois et al., 2024). This copula is defined by the following equation by Nelsen (2003):

$$C(u, v) = uv \tag{4}$$

Here, u and v represent the fitted probability distributions. The unique feature of this copula is therefore that the joint probability is obtained purely by multiplying the individual probabilities (Dubois et al., 2024).

6.1.5 Determination of Design Values

The univariate design values of an event with a return period of 100 years were calculated using equation (1) (Table 6). For the compound scenario, the joint probability distribution was calculated from equation (2) and then the contour of the value pairs for a return period of 100 years was created using equation (3) (Figure 9). The EFC methodology was then used to select the value pair on the contour (Figure 9). Under the given use of the independence copula, this corresponds to the univariate events with a return period of 10 years. The bivariate design values are listed in Table 6.

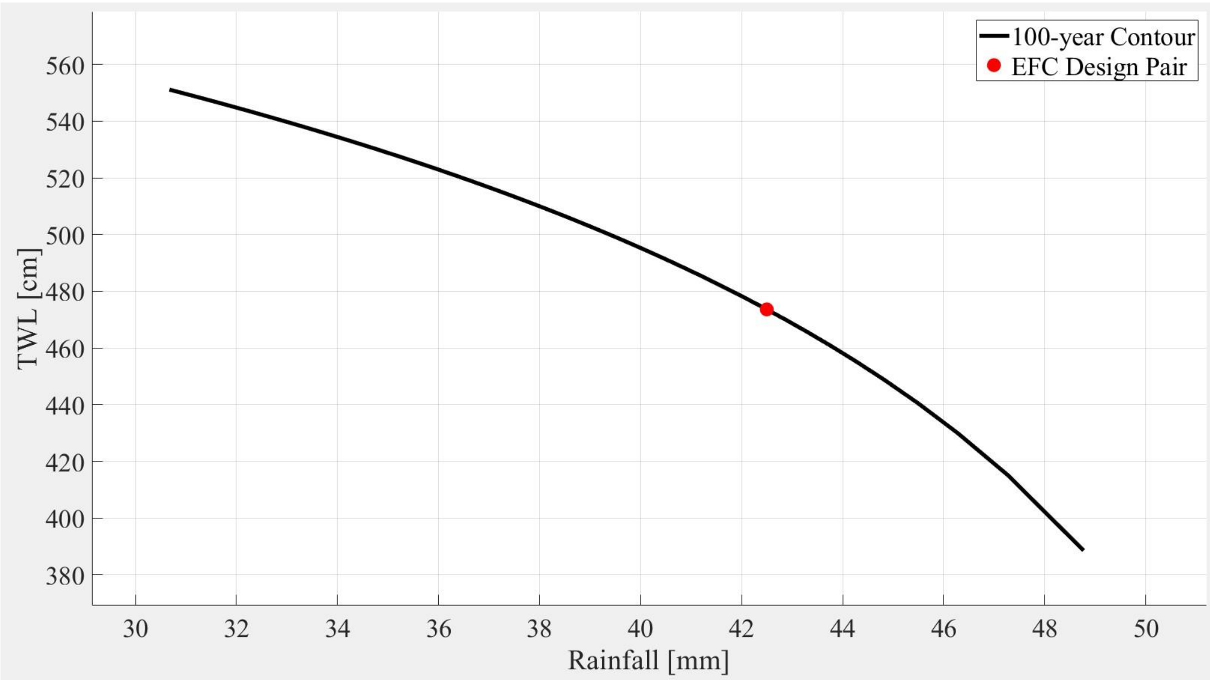

Figure 9 - Contour of those pairs of values from TWL and rainfall that have a return period of 100 years. The pair of values selected according to the EFC methodology is marked in red.

Table 6 - Determined design values of the compound and univariate events

Scenario	Design Value Rain [mm]	Design Value TWL [cm]
Univariate Rain	48.8	-
Univariate TWL	-	549
Compound Event	42.5	473

6.2 Flood Simulation

6.2.1 Model Validation

In order to validate that the calibration of the LISFLOOD-FP model for the study area was successful and that realistic simulations of flood events can be generated; the storm surge of 1962 was reproduced. In addition to the Manning's Coefficient File, the adjusted DEM (Figure 5) and the design hydrograph (Figure 6) were used for this purpose.

Figure 10 shows the comparison between the simulated and actual extent of flooding. It is immediately apparent that the areas correctly identified as flooded by the model (marked in blue on the map) are smaller than those in the reference layer. This can be attributed to the following two factors: Firstly, when analysing the areas in the reference layer, it is apparent that these are always contiguous sub-areas. However, due to small-scale differences in terrain elevation, it is likely that there were isolated sections within these large areas that were not flooded. This can be seen in a comparison with the model results, which show a significantly smaller-scale structure with fewer large, contiguous areas. Upon enquiry, the BUKEA confirmed that the layer, which was created by digitising old maps, is a generalised representation of the extent of the 1962 flooding. It shows the spread of the flood without taking small-scale structures into account (F. Nohme, personal communication, 15 January 2026). Due to this generalisation, the reference layer contains inaccuracies. The second factor relates to changes in the topography that have taken place since 1962. This includes, in particular, artificial terrain elevations, which have been carried out in almost all affected areas, such as Wilhelmsburg, Harburg and Bergedorf (BUKEA, 2025b). A reduced extent of flooding also results from the implementation of alternative protection concepts, such as the construction of polders in the harbour area from 1976 onwards (LSBG, 2012) and the construction of the HafenCity on artificial mounds (Ministry of Urban Development and Housing, 2025).

The areas depicted in green are those that were identified as flooded by the model but were not flooded according to the reference layer. It is noticeable that the proportion of these areas is very small. The identified flooding in Finkenwerder and Waltershof, for example, can be attributed to the fact that these areas were not developed until after 1962. There is an Airbus production plant in Finkenwerder, which already existed at that time but has been steadily expanded over the years (Link, n.d.). The western section was completed in 2002 (BUKEA, 2025b).

The evaluation of Figure 10 shows that the calibration of the model was successful. There is a high degree of agreement in the designation of areas that were flooded during the storm surge of 1962, with a very low proportion of areas incorrectly designated as flooded. Deviations, in particular the lower extent of flooding, are largely due to topographical changes. The suitability of the model for simulating present-day univariate and bivariate flood scenarios has therefore been validated.

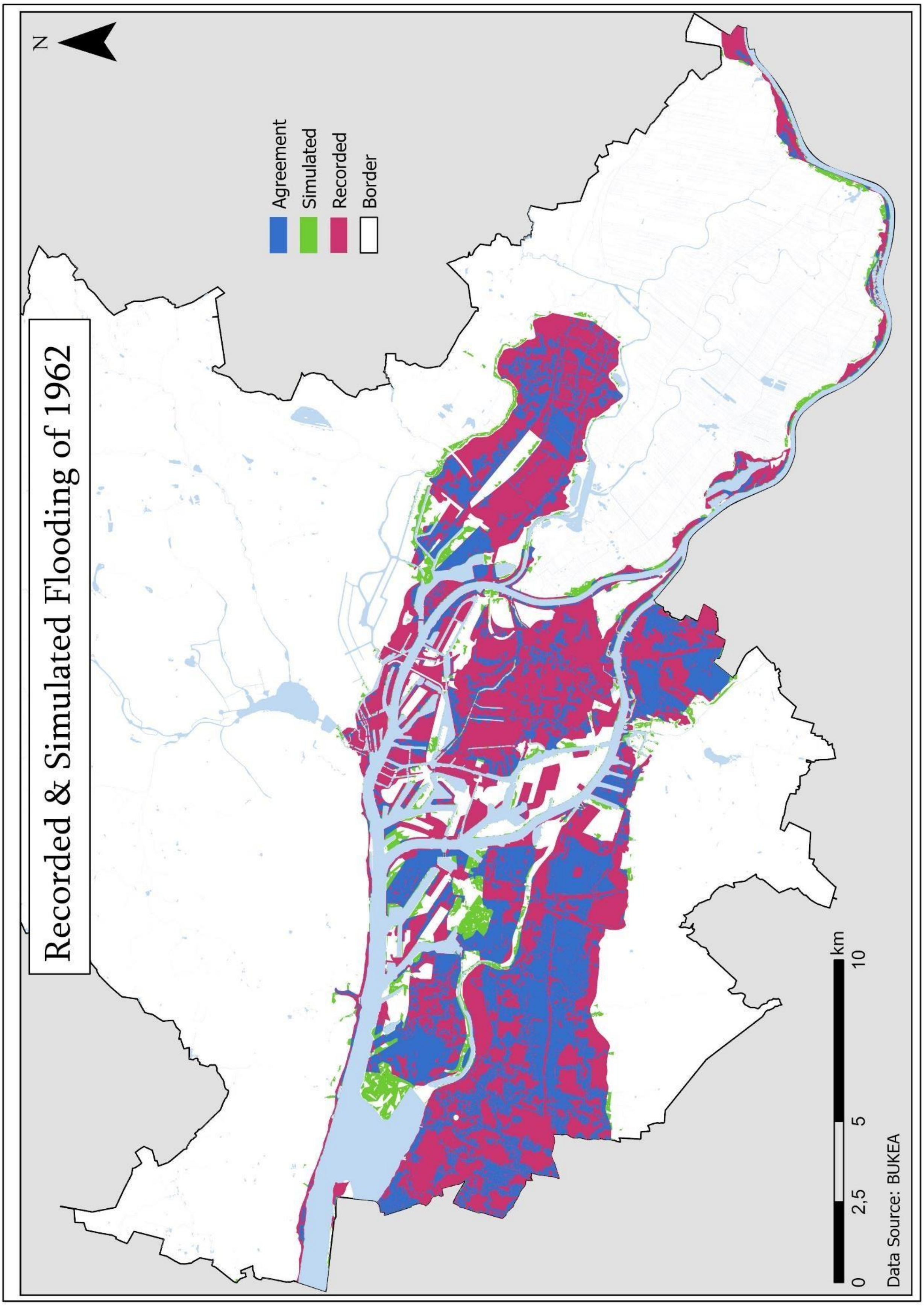

Figure 10 - Comparison between the modelled and actual extent of the 1962 flood. Red areas show the flooding according to the reference layer. Areas marked in blue are those that were marked as flooded in both cases. Green areas were only designated as flooded in the model.

6.2.2 Simulation of Flood Events

6.2.2.1 Univariate Scenario

To simulate the univariate storm surge event, a design hydrograph was created based on the observed hydrograph of the 2013 storm surge and adjusted to the determined peak value of 549 cm (Table 6) using the SFA methodology (Figure 13). This was then defined as the boundary condition at the western edge of the study area, across the entire width of the Elbe. To create the start file, the water level of the Elbe at the beginning of the simulation was set to a value of 170 cm.

Figure 11 shows the results of a simulation of a storm surge event with a return period of 100 years. The resulting flooding occurs exclusively along the Elbe; there is no spread of the flood wave or water masses to more distant areas. In principle, minor flooding occurs in many sections immediately adjacent to the Elbe, but this is usually limited to a width of less than 100 metres. Exceptions to this can be seen in the harbour area in the west of the city, for example in eastern and northern Finkenwerder, where flooding occurs in areas that are in some cases more than 250 metres away from the Elbe.

To simulate the univariate heavy rainfall event, a design hyetograph was created based on the hyetograph of the observed heavy rainfall event on 27 June 2024 (Figure 14). For this purpose, the total rainfall amount was adjusted to the calculated value of 48.8 mm (Table 6) using the SFA methodology. The design hyetograph was then entered into the rainfall data file.

Figure 12 shows the results of the simulation. Outside the Elbe itself and some canals and tributaries, the maximum flood depth is approximately 1.5 m. These values are reached in isolated areas of Harburg, in the south-west of the study area and in the northern parts of Bergedorf in the east of the city. In the north, these higher water depths are mainly limited to the Alstersee. However, the majority of the study area, approximately 90%, exhibits very shallow water depths of no more than 8 centimetres. One factor worth noting is that the water depths along the Elbe are no greater than in the rest of the study area.

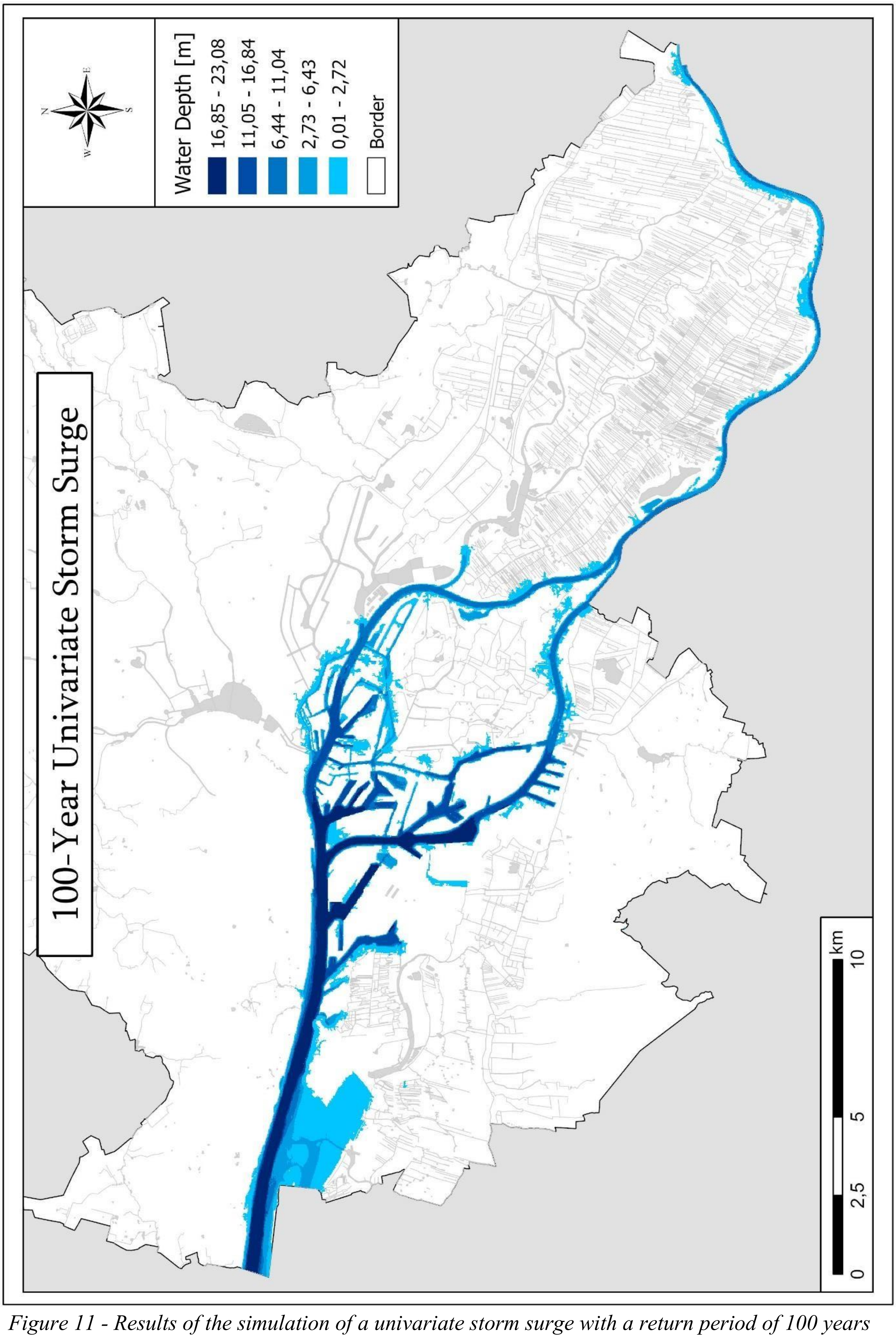

Figure 11 - Results of the simulation of a univariate storm surge with a return period of 100 years

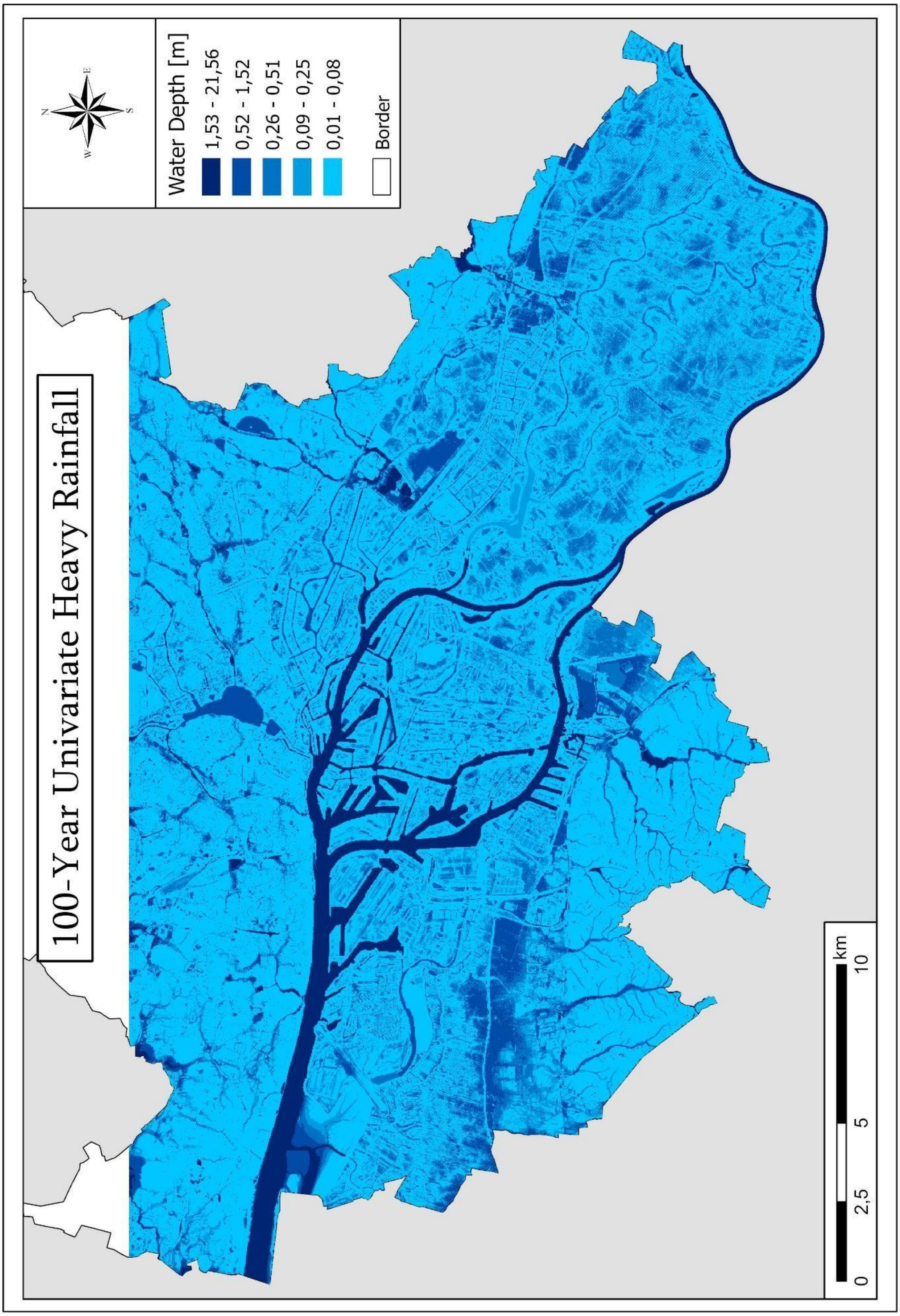

Figure 12 - Results of the simulation of a univariate heavy rainfall event with a return period of 100 years

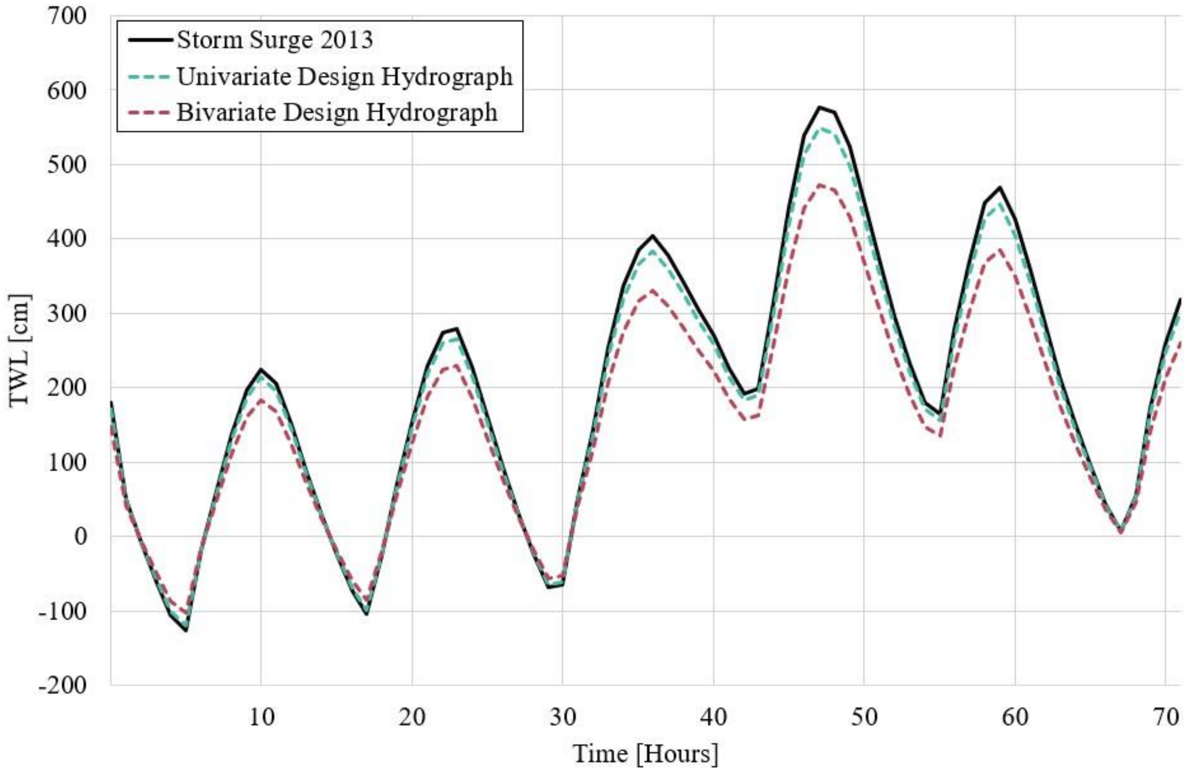

Figure 13 - Comparison of the observed hydrograph of the 2013 storm surge with the constructed univariate and bivariate hydrographs

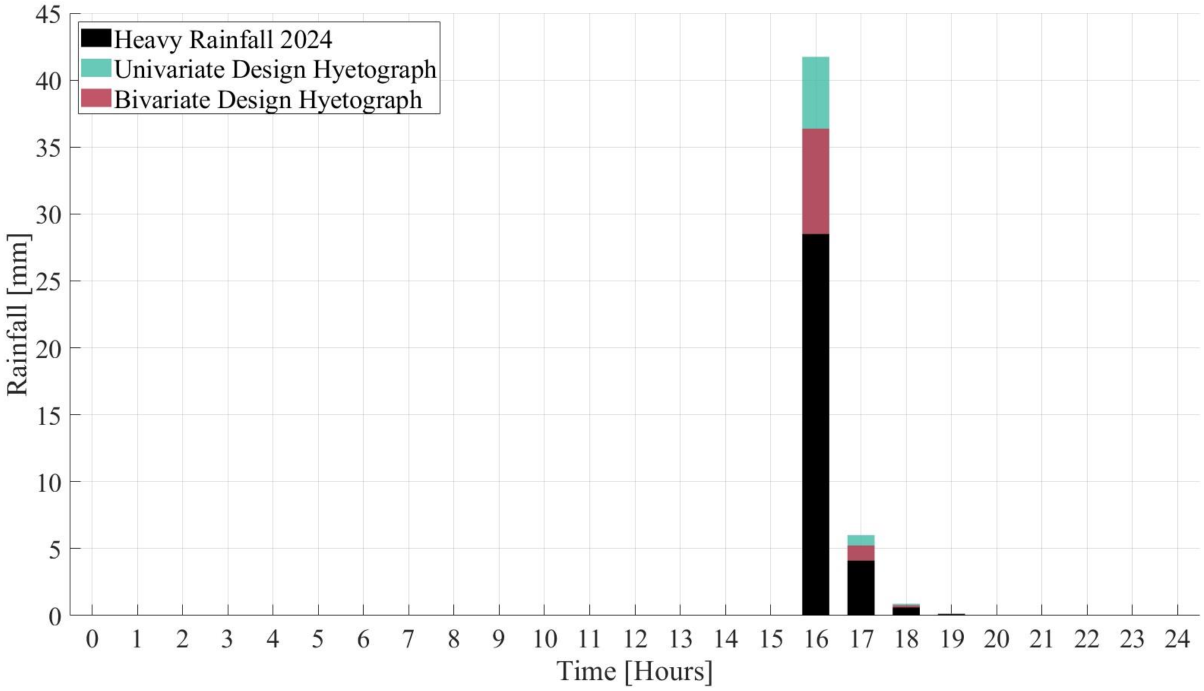

Figure 14 - Comparison of the observed hyetograph of the 2024 heavy rainfall event with the constructed univariate and bivariate hyetographs

6.2.2.2 Bivariate Scenario

To simulate the bivariate scenario, a design hydrograph with a peak value of 473 cm (Table 6) and a design hyetograph with a total rainfall amount of 42.5 mm (Table 6) were created (Figure 13, 14). To create the start file, the water level of the Elbe was set to the start value of the hydrograph of 147 cm above sea level. For the convergence of the two extremes, the peak of the heavy rainfall event was set to hour 47, while the peak of the TWL occurred one hour later (Figure 15).

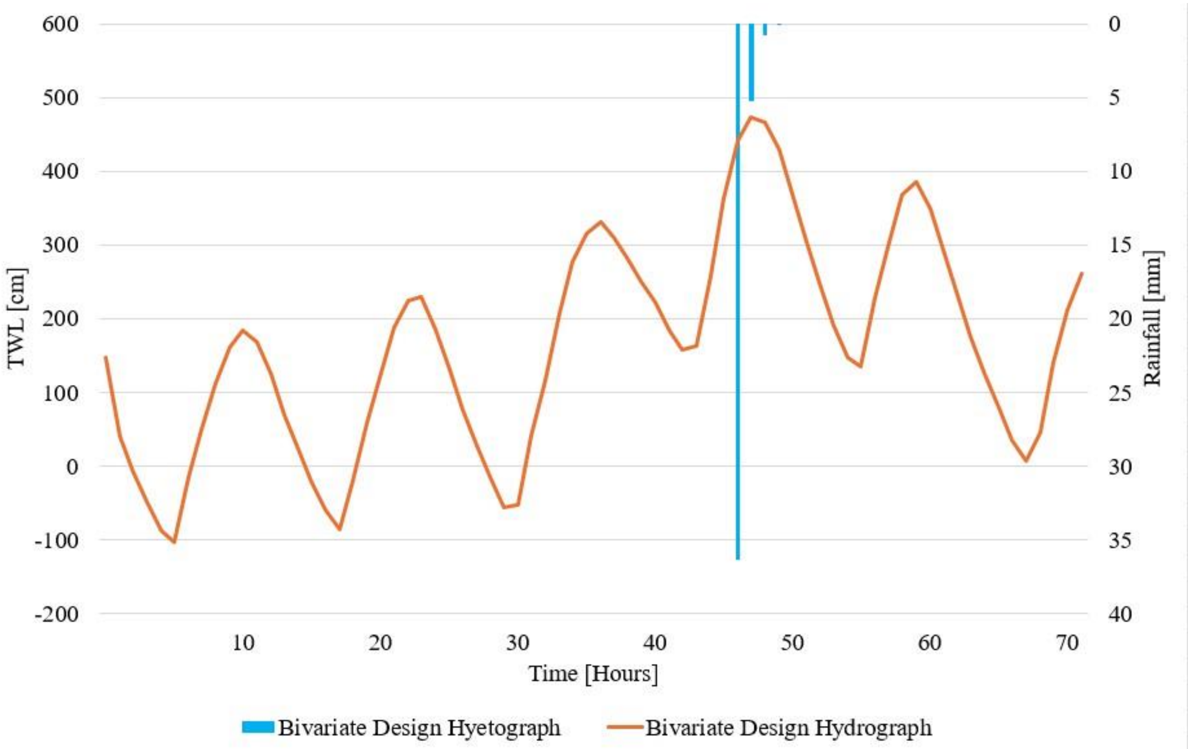

Figure 15 - Temporal coordination of the two variables. To represent a worst-case scenario, the maximum rainfall occurs one hour before the TWL peak.

Figure 16 shows the resulting extent of flooding from the compound event. As can be seen, the majority of the study area is dominated by two categories: areas with low water depths (< 1.4 m) and areas with medium water depths (1.4 - 5 m). Areas with high water depths (> 11 m) are found in the western part of the Elbe, while slightly lower water depths occur in the eastern section. Medium water depths can be found both in small areas distributed throughout the study area and in large, contiguous areas. The latter can be found in Harburg, for example, but especially in Bergedorf. Here, it is also particularly clear that the areas with medium water depths border almost directly on the Elbe. Also noteworthy is the Alstersee, which has a water depth of approximately 5.4 m and is surrounded by areas with medium water depths.

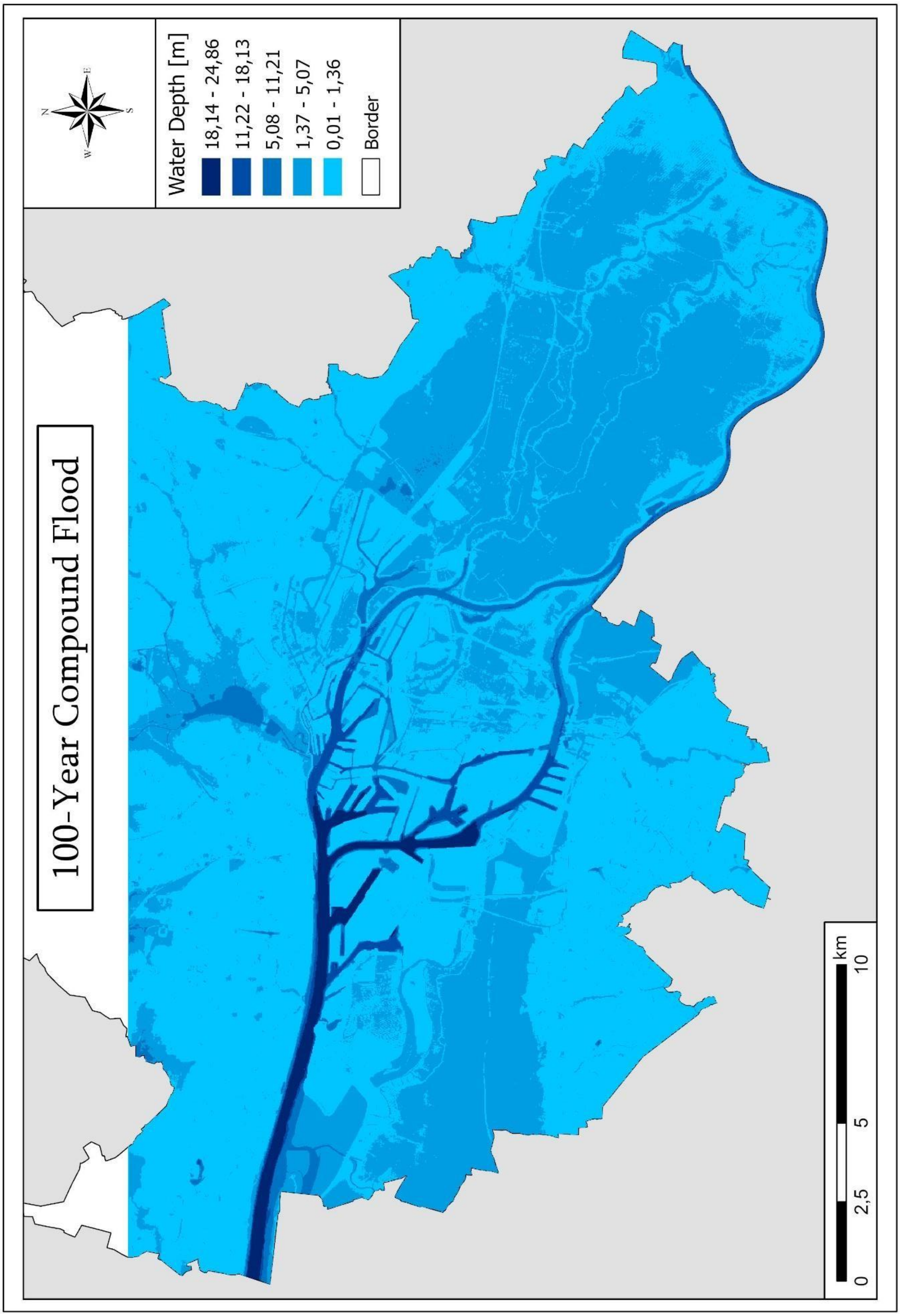

Figure 16 - Results of the simulation of a compound event consisting of a storm surge and heavy rainfall with a return period of 100 years

6.2.2.3 Comparison of the Univariate Events with the Bivariate Event

Comparison maps were created to examine the differences in flood risk between the univariate and bivariate events.

Figure 17 shows the comparison between the univariate storm surge and the bivariate event. It is noticeable that the areas with higher water depths in the univariate event are relatively small. These cells represent only 0.0002% of the total study area. The affected areas are almost exclusively located in the 50 m wide strip directly adjacent to the Elbe. Individual exceptions to this can be found in the areas north and west of Wilhelmsburg, in the centre of the study area. Large parts of the areas in the north and south have similar water depths in both scenarios. A moderately higher water depth occurs in the Alstersee and in the north of Bergedorf, while the greatest differences occur north of the Norderelbe and in the canals north of HafenCity, which connect the lake to the Elbe. On average, the water depth per cell in the bivariate event is 1.1 m higher than in the univariate event. It is also noteworthy that the water depth within the Elbe is slightly higher in the bivariate scenario than in the univariate scenario, despite a lower storm surge height.

Figure 18 compares the univariate heavy rainfall event with the bivariate event. It is apparent that the proportion of areas with higher water depths in the univariate scenario is significantly higher than in Figure 17. These areas are concentrated north and south of the coastal flood risk area and along the flood defences. The water depths in the harbour areas and around Wilhelmsburg in particular are similar in both scenarios. As in Figure 17, it should be emphasised again that the majority of the study area exhibits a higher water depth in the bivariate scenario, despite a lower amount of rainfall. In this context, it should be noted that the pure storm surge effect, as can be seen in Figure 11, is limited to the few areas in front of the flood protection line. Areas with moderately and much higher water depths in the bivariate event show a similar distribution to that in Figure 17. On average, the water depth in the bivariate scenario is 1.1 m higher, although it should be noted that a large part of this can be explained by the up to 473 cm higher water level of the Elbe. Accordingly, the actual difference in terms of heavy rainfall is significantly smaller.

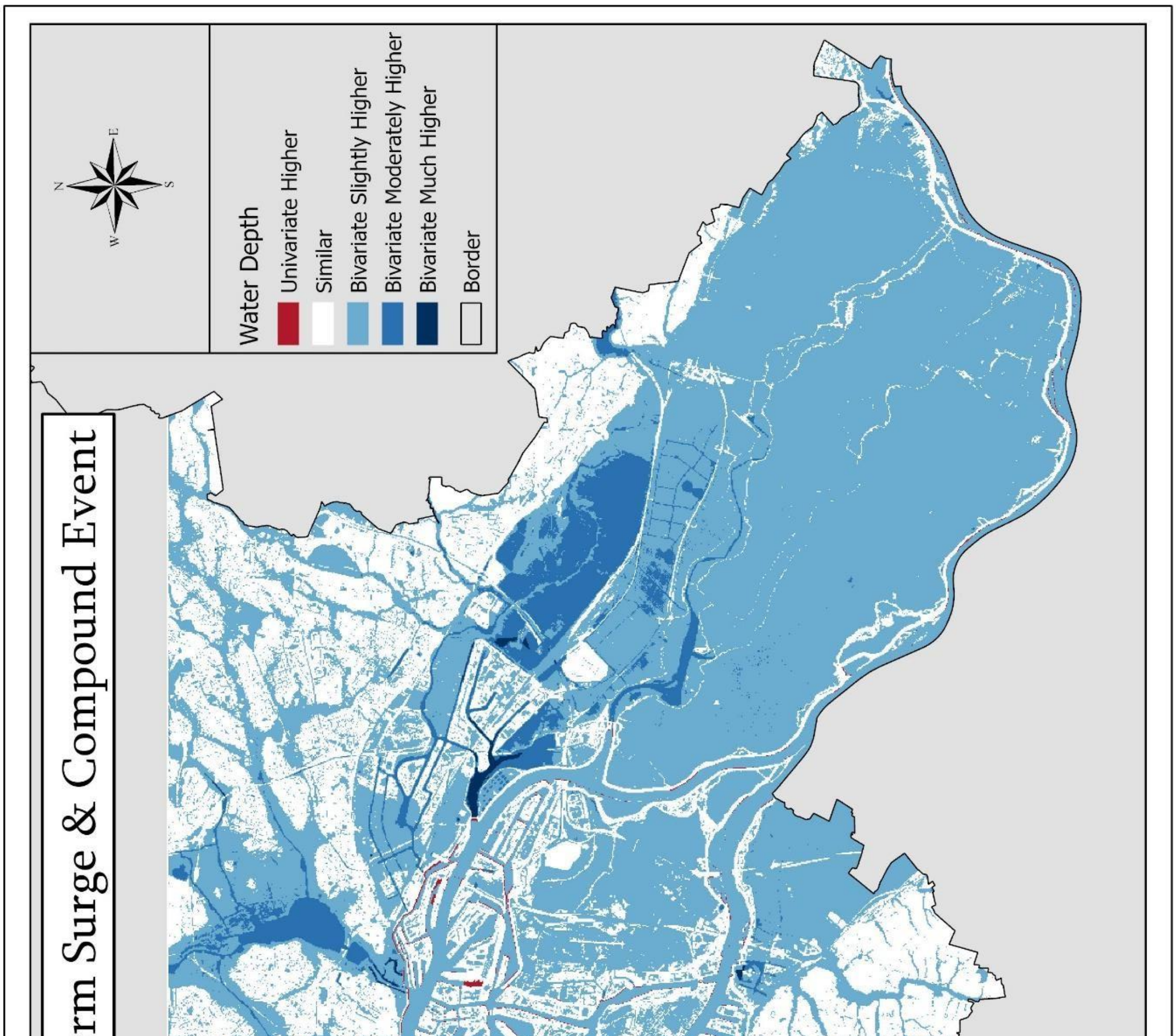

Figure 17 - Comparison of water depths for the univariate storm surge and the compound event. Areas marked in red are those in which the water depth is higher in the univariate event. Areas marked in blue show a higher water depth in the compound event.

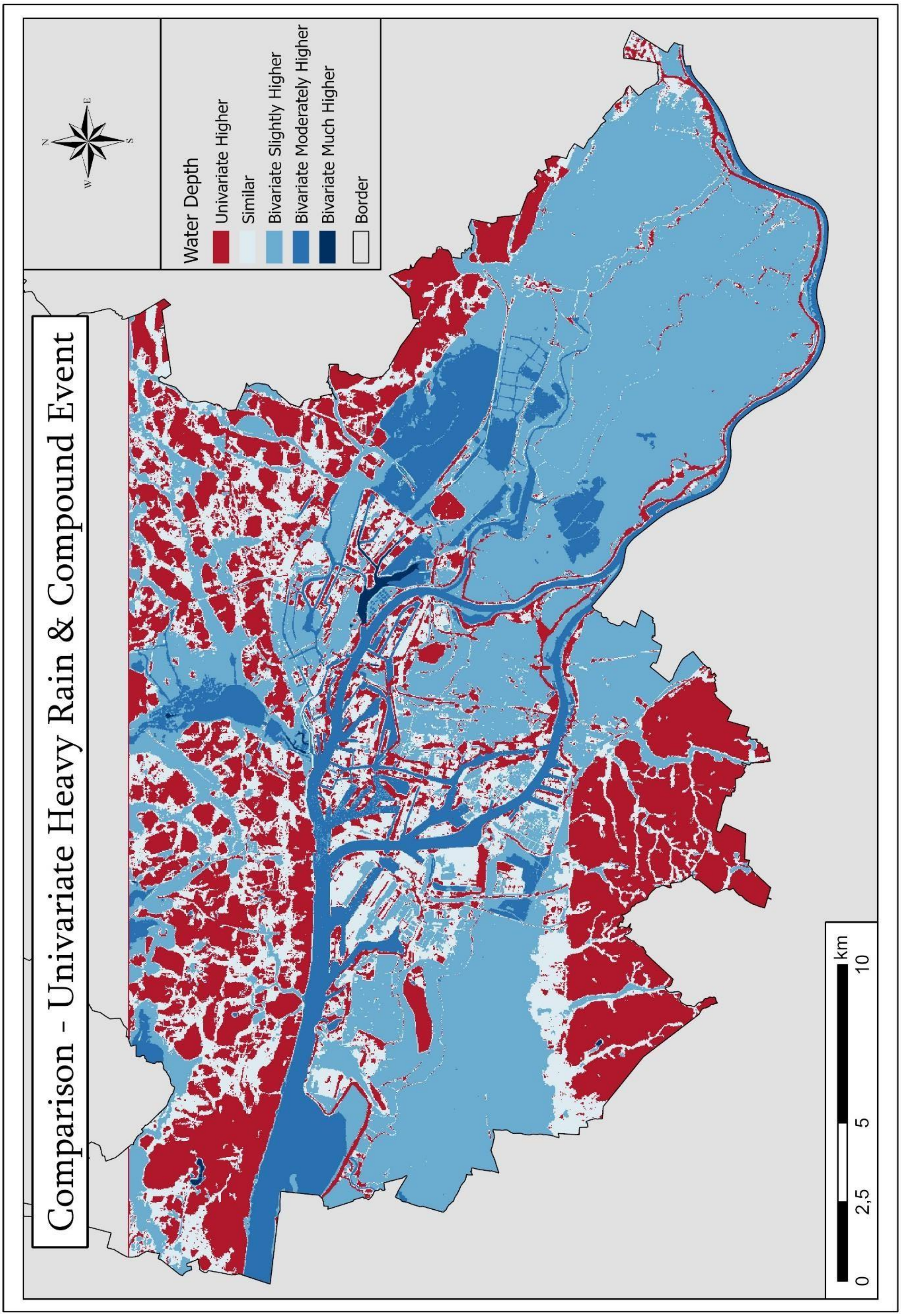

Figure 18 - Comparison of water depths for the univariate heavy rainfall and the compound event. Areas marked in red are those in which the water depth is higher in the univariate event. Areas marked in blue show a higher water depth in the compound event.

7. Discussion

7.1 Sampling of Extreme Values

The Mann-Kendall test did not identify any significant trend in the rainfall series. This contrasts with the analysis by the BUKEA (2021), which identified an increase in annual precipitation totals in Hamburg between 1881 and 2020. These results are supported by studies conducted by the DWD (2021) and KLIWA (2019). The reason for the lack of a trend in the present analysis is based on two factors: the length of the time series used and the strength of the trend. The studies point to an increase of 112 mm over a period of 139 years (BUKEA, 2021). Assuming a linear trend, this suggests an increase in annual precipitation totals of approximately 20 mm for the 25-year period under review. In relation to an average annual precipitation total of 775 mm (DWD, 2021), this increase can be classified as minor. It can therefore be assumed that although there is a trend in the given time series, it is so small that it is classified as insignificant by the Mann-Kendall test, which operates with a significance level of 5%. Furthermore, natural variations in rainfall can also cause deviations from the actual trend in this short time series (Schulte, 2015). Assuming a stationary time series, despite the knowledge that a trend is very likely, introduces inaccuracies that affect the further course of the analysis, such as the creation of the extreme value series, the adjustment of the probability distributions and the determination of the design values.

Unlike the rainfall series, a significant positive trend has been observed for the maximum daily water level series. This result is consistent with the analyses by the BUKEA (2021) and Klein et al. (2018), who found an increase in extreme water levels parallel to SLR for the German North Sea coast. Analyses by Copernicus (2025) identify a global mean SLR of 3.7 mm per year for the period from 1999 to 2024, resulting in a total increase of 9.38 cm. The Mann-Kendall test determined an average increase of 0.019 mm per year for the time series, which corresponds to a total increase of 0.475 mm over the 25-year period under consideration. The trend determined is therefore significantly lower than would be expected. On the one hand, the deviations can be explained by the influence of the short time series described in the previous section. On the other hand, changes in water levels can be caused by anthropogenic changes (FGG Elbe, 2021). A study on the hydrodynamic development of the tide-influenced sections of the Elbe shows that the estuary has been strongly influenced by anthropogenic factors for centuries (Fickert & Strotmann, 2007). The development of water levels shows clear deviations from the mean SLR, which can be explained by a superimposition of external natural influences with various anthropogenic interventions in the tidal system of the Elbe (Fickert & Strotmann, 2007). For example, continuous deepening of the Elbe led to a reduction in the mean low tide level of in some cases several centimetres per year (Fickert & Strotmann, 2007). The last adjustment was made in 2022, which included a deepening of 1 m (Hafen Hamburg Marketing e.V., 2022). At the same time, the width of the Elbe was increased by up to 20 m in some sections (Hafen Hamburg Marketing e.V., 2022). Furthermore, the introduction and continuous adaptation of flood protection measures led to a change in the tidal regime (Fickert & Strotmann, 2007). The significantly weaker trend can be considered a result of these factors.

As a result of applying the POT methodology according to Zhou et al. (2016), the thresholds were determined to correspond to the 98.63rd percentile for the rainfall series and the 98.64th percentile for the TWL series. The extreme value series created therefore contained the highest 1.37% and 1.36% of rainfall and TWL events, respectively. In addition to the approach used in this study, various alternative methodologies for threshold selection are used in the literature. One of these methodologies is the use of mean residual life plots. Xu et al. (2023), for example, use these to determine the thresholds of surge time series for several estuaries. The thresholds determined in this way range from the 99th to the 99.4th percentile (Xu et al., 2023). Other studies do not adjust individual thresholds and instead use more general reference values. This introduces inaccuracies into the subsequent statistical analysis, as the extracted extreme events do not converge to a GPD if the threshold is set too low (Beirlant et al., 1996). Due to the poor fit of the probability distribution, the design values determined cannot be considered accurate (Sadegh et al., 2018). Despite this, such methods are used, particularly in global studies, in order to limit the computational effort. An example of this is to set the threshold based on a defined return period. Bevacqua et al. (2019) choose a 1-year return period for the analysis of a compound event consisting of precipitation and storm surge; the corresponding threshold corresponds to the 99.7th percentile. They also apply the restriction that the threshold is lowered to the 95th percentile if fewer than 20 value pairs emerge from the original extreme value series (Bevacqua et al., 2019). The most commonly used alternative methodology is simply to set a percentile. For example, Chen et al. (2023) and Jalili Pirani & Najafi (2023), who investigate compound flooding from storm surges and heavy rainfall, use a threshold corresponding to the 95th percentile. Ming et al. (2022) use the 90th percentile for the analysis of a trivariate compound flood, and Ruggiero et al. (2010) set the 99.5th percentile in their study on wave heights. Despite the use of different methodologies, there is a consensus that the selected threshold should be in the range from the 90th to approximately the 99.5th percentile. The thresholds determined in this study therefore show good agreement.

7.2 Characterisation of the Statistical Correlation

The results of the correlation analysis between heavy rainfall and storm surge in Hamburg showed a slightly positive but not significant correlation. This contradicts the results of most previous studies in which a statistical dependence between different types of flooding was established. For the combination of storm surge and heavy rainfall considered in this paper, significant positive correlations were found for study areas in various parts of the world, including China (Chen et al., 2023; Lian et al., 2013; Tu et al., 2017; Xu et al., 2019), Canada (Jalili Pirani & Najafi, 2023) and the USA (Wahl et al., 2015).

Although there is a consensus that in most regions there is a significant positive correlation between the variables and that this affects the probability and intensity of compound events, some studies show that certain study areas are exempt from this. For example, Jalili Pirani & Najafi (2023) find that six of the 41 study areas analysed along the Canadian coast show no significant correlation between heavy rainfall and storm surge. In their analysis of compound events involving storm surges, precipitation and waves, Lucey & Gallien (2024) find no significant correlation in 33% of the scenarios examined. They attribute this to the choice of event sampling method and different climate conditions (Lucey & Gallien, 2024).

Studies on the occurrence of compound flooding have found that the probability of weather systems that can trigger heavy rainfall and storm surges varies depending on latitude, local topography and the shape of the coastline (Chang et al., 2013; Hawcroft et al., 2012; Khouakhi et al., 2017). Weather systems characterised by strong winds, low pressure and abundant moisture transportation are cyclones (Khouakhi et al., 2017; Walsh et al., 2016). Tropical cyclones are responsible for over 80% of compound floods in East Asia and over 50% of compound floods in Central America and northern Australia (Lai et al., 2021). In mid and high latitudes, over 60% of heavy rainfall and extreme storm surges are triggered by extratropical cyclones (Lai et al., 2021). Lai et al. (2021) find a strong positive correlation between extreme precipitation and extreme storm surges in Asia, Australia, North America and Southern Europe, as these regions are most affected by cyclones. This result is consistent with the studies presented, which find a predominantly significant positive correlation in these regions. At the same time, Lai et al. (2021) note that in many regions of Europe, a nonsignificant correlation between the two variables dominates. The reason for this lies primarily in the seasonality of extreme precipitation and extreme storm surges (Ward et al., 2018). These extremes occur in different seasons in large parts of Europe (Lai et al., 2021). This behaviour is also evident in Hamburg, where storm surges occur mainly between September and March, while heavy rainfall events occur mainly between June and August (Hamburg Wasser, 2024). Although compound floods are also triggered by extratropical cyclones in Europe, this seasonal separation ensures that extreme storm surges and heavy rainfall events occur less frequently at the same time. The non-significant correlation found in this study reflects this effect.

The nature and strength of the correlation between storm surges and heavy rainfall has a direct impact on the level of the bivariate design values. In regions with a significant positive correlation, the probability of such compound events is increased, which means that the design values for a specified return period are higher than would be expected from an independent consideration of the variables (Chen et al., 2023). This results in a smaller discrepancy between the design values of the univariate events and the bivariate event. In the present case, the design values correspond to the values obtained from an independent consideration of the variables. As a result, the bivariate design values are significantly lower than the univariate values.

7.3 Flood Risk of the Univariate and Bivariate Events

As part of flood risk management, flood hazard maps for storm surges and heavy rainfall events were produced for the city of Hamburg. A comparison between the official coastal flood hazard map for an event with a return period of 100 years and the univariate TWL map created in this study shows a high degree of consistency. This validates that the FFA, in combination with the hydrodynamic model used, has produced realistic results.

The official heavy rainfall map is not directly comparable with the univariate heavy rainfall map created in this study due to a different scenario and deviating modelling. In the official map, a 1-hour extreme event with a return period of 100 years is depicted (BUKEA, 2020), while the univariate map depicts an extreme event based on 24 hours. Furthermore, the official map is created using a coupled 1D-2D model that takes into account not only the topography but also the sewer network, infiltration and interception (BUKEA & RISA, 2024). Although the univariate map is based on simplified modelling, there are similarities in the general spatial distribution of areas with a higher flood risk.

To assess the flood risk of a compound event compared to single-driver floods in Hamburg, the created maps (Figures 11, 12 and 16 – 18) are interpreted. First, the differences between the univariate storm surge and the compound event are analysed. The univariate storm surge event has a peak water level that is 76 cm higher than the bivariate event. Despite this, the flood risk is only minimally higher and is limited to individual areas along the Elbe and in the harbour. This result demonstrates the effectiveness of the flood protection structures. With a current height of between 7.5 m and 9.25 m, they are designed to withstand a storm surge with a return period of 200 years (BUKEA, n.d.a). The flood protection structures are therefore capable of withstanding both the lower, bivariate storm surge with a peak of 473 cm and the higher univariate storm surge with a peak of 549 cm. The flood risk posed by storm surges in Hamburg can therefore be classified as low and is limited to those areas in front of the flood protection structures.

An analysis of Figures 12 and 18 shows that rainwater accumulates in hollows, depressions, lakes and canals if it cannot drain directly into the Elbe. This effect is much more pronounced in the compound scenario than in the univariate heavy rainfall scenario, even though the total rainfall in the former is 6.3 mm lower. The observed result that the flood risk is higher in the compound scenario than in the univariate scenario is consistent with the findings of previous studies (Xu et al., 2024; Zellou & Rahali, 2019). The reason for this lies in the most significant difference between the two scenarios, namely the higher water level of the Elbe in the compound event. The backwater effect is therefore responsible for the higher flood risk. This describes how rainwater cannot drain away due to the high-water level in the river, causing it to collect in low-lying areas and tributaries and trigger flooding there (Wahl et al., 2015). Evidence for this behaviour can be found in the comparison maps (Figures 17 and 18). For example, it can be seen that the water depth of the Elbe in the bivariate scenario is slightly higher than in the univariate storm surge event, despite a lower storm surge height. This can be attributed to the fact that rainwater from the entire city drains into the Elbe. In the univariate heavy rainfall event, this is evident from the lower extent of flooding, as the rainwater can drain into the Elbe, which has a low water depth of mean sea level in this simulation. Furthermore, both comparison maps show that the water depth in some areas directly adjacent to the Elbe is much higher in the compound scenario than in the univariate scenarios. These are central tributaries that drain the rainwater from a large area into the Elbe. The high water depth in the bivariate scenario results from the fact that the outflow is blocked due to the storm surge.

The results of these analyses show that those areas of Hamburg that are at risk of compound flooding are, on the one hand, those with low elevations. This specifically includes northern Harburg, parts of Wilhelmsburg, Bergedorf and those areas bordering the Alstersee. On the other hand, those areas along the central tributaries to the Elbe, especially east of the Norderelbe and along the canals connecting the Alstersee with the Norderelbe, are also at risk.

7.4 Outlook

The evaluation of the results, in particular the comparison with official maps and similar studies, has shown that the methodology used produced realistic results that enable an assessment of the flood risk of a compound event. Nevertheless, there is potential to refine the assessment.

One option here is to use smaller spatial units for a more detailed recording of rainfall events. As a study by Verworn Langenhagen & Kuchenbecker (n.d.) shows, precipitation patterns vary in different parts of Hamburg. An evaluation of precipitation records from various measuring stations in the city area, accompanied by a calculation of the amount of rainfall for the defined return period, would enable a more realistic modelling of flood risk.

A comparison of the univariate heavy rainfall map created with the official heavy rainfall hazard map of the city of Hamburg revealed some differences in flood risk. This can largely be attributed to the use of a more complex hydrodynamic model. For this study, a pure surface model was used, which determines the extent and depth of flooding based on topography and surface roughness. Coupled sewer network and surface models are capable of capturing flow behaviour on the surface and in the sewer system, as well as modelling interactions between the two models, such as water entering the sewer system from the surface via manholes (HSB, 2017). When using these models, a DEM with a higher spatial resolution, e.g. 1 m, is usually used, which enables accurate mapping of ditches and retention areas (BUKEA & RISA, 2024). Furthermore, hydrological loss approaches, such as infiltration and interception, can be integrated into the model (BUKEA & RISA, 2024). The use of such complex models enables greater accuracy in flood simulation but also comes with a high computational cost (Mondal et al., 2023). Despite this, they are increasingly being used for the analysis of univariate and bivariate flooding. For example, Fernández-Pato et al. (2020) simulate flooding caused by fluvial flooding in Glasgow, and Tang et al. (2025) use a coupled 1D-2D model for the analysis of compound coastal flooding in urban regions.

The study conducted shows the current flood risk of a compound event. For planning purposes, such as the dimensioning of sewer systems and flood protection facilities, it is also of central importance how the flood risk will develop in the future. The evaluation of the projections has shown that the frequency and intensity of heavy rainfall events will increase in Hamburg (KLIWA, 2019) and that the height of storm surges will increase with SLR (Klein et al., 2018). Therefore, the flood risk posed by compound events will also increase in the future (Bevacqua et al., 2019). In order to include the effects of climate change in the construction of design values, a series of projections on SLR and heavy rainfall development can be included in the analysis (Ghanbari et al., 2021). A non-stationary methodology is used to capture future changes in the probability structure and correlation of the variables. Unlike the methodology used in this study, the parameters of the probability distributions and the copula are not stationary but can change over time (Ghanbari et al., 2021). Various studies have adopted this methodology. For example, Wang et al. (2023) use a non-stationary analysis to determine the current and future probability of compound flooding from heavy rainfall and storm surges in Ho Chi Minh City. Their findings show that, when climate change is taken into account, the design values obtained using a non-stationary methodology for a 100-year compound event are

15–30% higher than those obtained using a stationary methodology. They also find that the probability of compound flooding will increase by over 50% by the year 2100 (Wang et al., 2023). Similarly, Ghanbari et al. (2021) find, using a non-stationary methodology, that the frequency of compound coastal-fluvial flooding in the south-eastern United States in 2050 will be two to three times higher than it is today.

8. Conclusion

The aim of this study was to quantify the flood risk posed by a compound flood from heavy rainfall and storm surge in Hamburg, Germany, and to characterise the divergence of separately occurring heavy rainfall and storm surge events with the same return period. This was intended to close the research gap regarding the lack of assessment of the flood risk of compound events in Hamburg. In the course of this, two research questions with associated hypotheses were answered.

The first hypothesis put forward in this paper addresses the research question: 'How can the statistical correlation between storm surges and heavy rainfall in Hamburg be characterised?' The hypothesis states that there is a significant positive correlation between the two factors. As a result, the probability and intensity of a compound event are higher than it would appear if the two factors were assumed to be independent. The correlation analysis conducted in this study found a non-significant correlation between the two variables, thereby rejecting the hypothesis. The reason for this lies in the seasonal separation of heavy rainfall and storm surge events.

The second hypothesis deals with the flood risk of univariate and bivariate events with a uniform return period of 100 years. The first research question posed in this regard is: 'Which areas of Hamburg are at risk from a compound flood caused by storm surge and heavy rainfall with a return period of 100 years?' The hypothesis states that areas adjacent to the Elbe and its tributaries, as well as low-lying areas, are generally at risk. The second research question examines the comparison between the univariate and bivariate events. The question is: 'What spatial divergences arise when comparing the flood risk of the compound and individual extreme events?'. The hypothesis in this case refers to the coastal backwater effect, which leads to a higher flood risk for the compound event compared to the univariate events. The findings confirm the hypotheses that were put forward. The evaluation of the maps that were created showed that the flood risk of a compound event is higher than that of the two univariate extreme events. The main reason for this is the backwater effect, which prevents the rainwater from draining into the Elbe, causing significant flooding in the low-lying areas of the city.

The results of this study therefore reinforce the appeal made in previous studies that the inclusion of compound events in flood risk management in vulnerable regions is essential to protect people and property from flooding. For Hamburg, it was found that existing flood protection structures are very effective in defending against storm surges. The primary flood driver is therefore heavy rainfall. To reduce the flood risk from univariate and, in particular, compound events in Hamburg, it is essential to reduce surface runoff from rainwater as much as possible. The implementation of the 'sponge city' concept presented in the context of heavy rainfall prevention can contribute to this. However, against the backdrop of climate change, which will lead to a higher frequency and intensity of univariate and compound extreme events in Hamburg, further measures may be necessary.

The results of this study can also be applied to other regions. The correlation analysis showed that there is no significant correlation between storm surge and heavy rainfall in Hamburg, which means that the probability of occurrence / magnitude of the variables for a defined return period is low. Nevertheless, a high flood risk was identified. As the literature review showed, this phenomenon could also occur in other regions where a low correlation is expected, such as in large parts of Europe. However, since there is a positive correlation in most regions of the world, it is to be expected that the flood risk posed by compound flooding from storm surges and heavy rainfall will be significantly higher there. This underlines the need for the analysis of compound flooding to continue to be a high priority in the future.

References

Agency of Roads, Bridges and Waters (LSBG) (2012): Sturmflutschutz in Hamburg. gestern – heute – morgen [Storm surge protection in Hamburg. Yesterday – today – tomorrow]. *Berichte des Landesbetriebes Straßen, Brücken und Gewässer Nr. 10 / 2012*.

Agency of Roads, Bridges and Waters (LSBG) (2022). *Beispielhafte Übertragung des extremen Regenereignisses im Ahrtal von Juli 2021 auf Hamburg* [Exemplary transfer of the extreme rainfall event in the Ahr Valley in July 2021 to Hamburg]. https://lsbg.hamburg.de/resource/blob/784532/51bcf7a4156e4adc0a5680da1f1d60c2/berichtnr-19-beispielhafte-uebertragung-des-extremen-regenereignisses-im-ahrtal-von-juli-2021-aufhamburg-data.pdf

Altenau, E. H., Pavelsky, T. M., Bates, P. D., & Neal, J. C. (2017). The effects of spatial resolution and dimensionality on modeling regional-scale hydraulics in a multichannel river. *Water Resources Research*, *53*(2), 1683-1701.

Bates, P. D., & De Roo, A. P. J. (2000). A simple raster-based model for flood inundation simulation. *Journal of hydrology*, *236*(1-2), 54-77.

Bates, P. D., Dawson, R. J., Hall, J. W., Horritt, M. S., Nicholls, R. J., Wicks, J., & Hassan, M. A. A. M. (2005). Simplified two-dimensional numerical modelling of coastal flooding and example applications. *Coastal Engineering*, *52*(9), 793-810.

Bates, P. D., Quinn, N., Sampson, C., Smith, A., Wing, O., Sosa, J., Savage, J., Olcese, G., Neal, J., Schumann, G., Giustarini, L., Coxon, G., Porter, J. R., Amodeo, M. F., Chu, Z., Lewis-Gruss, S., Freeman, N. B., Houser, T., Delgado, M., Hamidi, A., Bol liger, I., E. McCusker, K., Emanuel, K., Ferreira, C. M., Khalid, A., Haigh, I. D., Couasnon, A., E. Kopp, R., Hsiang, S., & Krajewski, W. F (2021). Combined modeling of US fluvial, pluvial, and coastal flood hazard under current and future climates. *Water Resources Research*, *57*(2), e2020WR028673.

Bates, P., Trigg, M., Neal, J., & Dabrowa, A. (2013). LISFLOOD-FP user manual. *Code release*, *5*(6).

Beirlant, J., Teugels, J. L., & Vynckier, P. (1996). *Practical analysis of extreme values*.

Ben-Zvi, A. (2009). Rainfall intensity–duration–frequency relationships derived from large partial duration series. *Journal of Hydrology*, *367*(1-2), 104-114.

Bernardara, P., Mazas, F., Kergadallan, X., & Hamm, L. (2014). A two-step framework for over-threshold modelling of environmental extremes. *Natural Hazards and Earth System Sciences*, *14*(3), 635-647.

Bevacqua, E., Maraun, D., Hobæk Haff, I., Widmann, M., & Vrac, M. (2017). Multivariate statistical modelling of compound events via pair-copula constructions: analysis of floods in Ravenna (Italy). *Hydrology and Earth System Sciences*, *21*(6), 2701-2723.

Bevacqua, E., Maraun, D., Vousdoukas, M. I., Voukouvalas, E., Vrac, M., Mentaschi, L., & Widmann, M. (2019). Higher probability of compound flooding from precipitation and storm surge in Europe under anthropogenic climate change. *Science advances*, *5*(9), eaaw5531.

Bezak, N., Brilly, M., & Šraj, M. (2014). Comparison between the peaks-over-threshold method and the annual maximum method for flood frequency analysis. *Hydrological Sciences Journal*, *59*(5), 959-977.

Bremen University (HSB) (2017). *Praxisleitfaden. Ermittlung von Überflutungsgefahren mit vereinfachten und detaillierten hydrodynamischen Modellen* [Practical guide. Determination of flood risks using simplified and detailed hydrodynamic models]. https://www.klivoportal.de/SharedDocs/Steckbriefe/DE/praxisleitfaden_ueberflutungs vorsorg e_hb/praxisleitfaden_ueberflutungsvorsorge_hb_steckbrief.html

Brockwell, P. J., & Davis, R. A. (2009). *Time series: theory and methods*. Springer science & business media.

Brunner, M. I., Seibert, J., & Favre, A. C. (2016). Bivariate return periods and their importance for flood peak and volume estimation. *Wiley Interdisciplinary Reviews: Water*, *3*(6), 819-833.

Bulti, D. T., & Abebe, B. G. (2020). A review of flood modeling methods for urban pluvial flood application. *Modeling earth systems and environment*, *6*(3), 1293-1302.

Burkey, J. (2025). *Mann-Kendall Tau-b with Sens's Method (enhanced)* [Matlab function]. Matlab File Exchange. https://de.mathworks.com/matlabcentral/fileexchange/11190-mannkendall-tau-b-with-sen-s-method-enhanced?s_tid=srchtitle

Camus, P., Haigh, I. D., Nasr, A., Wahl, T., Darby, S. E., & Nicholls, R. J. (2021). Regional analysis of multivariate compound flooding potential: sensitivity analysis and spatial patterns. *Natural Hazards and Earth System Sciences Discussions*, *2021*, 1-32.

Candela, A., & Aronica, G. T. (2017). Probabilistic flood hazard mapping using bivariate analysis based on copulas. *ASCE-ASME Journal of Risk and Uncertainty in Engineering Systems, Part A: Civil Engineering*, *3*(1), A4016002.

Centre for Research on the Epidemiology of Disasters (2023). *Disasters in Numbers.* https://files.emdat.be/reports/2023_EMDAT_report.pdf

Chang, C. P., Yang, Y. T., & Kuo, H. C. (2013). Large increasing trend of tropical cyclone rainfall in Taiwan and the roles of terrain. *Journal of Climate*, *26*(12), 4138-4147.

Chen, H., Xu, Z., Chen, J., Liu, Y., & Li, P. (2023). Joint risk analysis of extreme rainfall and high tide level based on extreme value theory in coastal area. *International Journal of Environmental Research and Public Health*, *20*(4), 3605.

Chen, L., & Guo, S. (2019). *Copulas and its application in hydrology and water resources* (pp. 13-38). Springer Singapore.

Chen, L., Guo, S., Yan, B., Liu, P., & Fang, B. (2010). A new seasonal design flood method based on bivariate joint distribution of flood magnitude and date of occurrence. *Hydrological Sciences Journal–Journal des Sciences Hydrologiques*, *55*(8), 1264-1280.

Chen, W. B., & Liu, W. C. (2014). Modeling flood inundation induced by river flow and storm surges over a river basin. *Water*, *6*(10), 3182-3199.

Chowdhury, A., & Kesserwani, G. (2024). LISFLOOD-FP 8.2: GPU-accelerated multiwavelet discontinuous Galerkin solver with dynamic resolution adaptivity for rapid, multiscale flood simulation. *Geoscientific Model Development Discussions*, *2024*, 1-42.

Climate Change and Consequences for Water Management (KLIWA) (2019). *Starkniederschläge. Entwicklungen in Vergangenheit und Zukunft* [Heavy rainfall. Past and future developments]. https://www.kliwa.de/_download/KLIWA-Kurzbericht_Starkregen.pdf

Coles, S. (2001). *An introduction to statistical modeling of extreme values.* Springer London. https://doi.org/10.1007/978-1-4471-3675-0

Coles, S., Heffernan, J., & Tawn, J. (1999). Dependence measures for extreme value analyses. *Extremes*, *2*(4), 339-365.

Copernicus (2025). *Climate Indicators. Sea level.* https://climate.copernicus.eu/climateindicators/sea-level

Copernicus Climate Change Service (2022). *Global sea level change time series from 1950 to 2050 derived from reanalysis and high resolution CMIP6 climate projections* [Data set]. https://doi.org/10.24381/cds.a6d42d60

Couasnon, A., Eilander, D., Muis, S., Veldkamp, T. I., Haigh, I. D., Wahl, T., Winsemius, H. C. & Ward, P. J. (2020). Measuring compound flood potential from river discharge and storm surge extremes at the global scale. *Natural Hazards and Earth System Sciences*, *20*(2), 489504.

Cunnane, C. (1979). A note on the Poisson assumption in partial duration series models. *Water Resources Research*, *15*(2), 489-494.

Dey, P. (2025). *Pettitt Change point test for univariate time series data* [Matlab function]. Matlab File Exchange. https://de.mathworks.com/matlabcentral/fileexchange/60973-pettittchange-point-test-for-univariate-time-series-data?s_tid=srchtitle

Dubois, K., Larsen, M. A. D., Drews, M., Nilsson, E., & Rutgersson, A. (2024). Influence of data source and copula statistics on estimates of compound flood extremes in a river mouth environment. *Natural Hazards and Earth System Sciences*, *24*(9), 3245-3265.

Emanuel, K. (2017). Assessing the present and future probability of Hurricane Harvey's rainfall. *Proceedings of the National Academy of Sciences*, *114*(48), 12681-12684.

Environment, Climate, Energy and Agriculture Authority (BUKEA) (n.d.a). *Hochwasserschutz in Hamburg heute* [Flood protection in Hamburg today]. https://www.hamburg.de/politik-und-verwaltung/behoerden/bukea/themen/wasser/hochwasser/hochwasserschutz-176712

Environment, Climate, Energy and Agriculture Authority (BUKEA) (n.d.b). *Was ist eigentlich… Küstenhochwasserschutz?* [What exactly is... coastal flood protection?].

https://www.moinzukunft.hamburg/was-bedeutet-klimaschutz-in-hamburg/das-macht-diestadt-hamburg/was-ist-eigentlich-kuestenhochwasserschutz-785144

Environment, Climate, Energy and Agriculture Authority (BUKEA) (n.d.c). *Regen neu denken* [Rethinking rain]. RISA. https://www.risa-hamburg.de/

Environment, Climate, Energy and Agriculture Authority (BUKEA) (2014). *Sturmflutgebiet von 1962* [Storm surge area of 1962] [Data set]. https://geoportal-hamburg.de/#
Environment, Climate, Energy and Agriculture Authority (BUKEA) (2015a). *Hintergrunddokument der Freien und Hansestadt Hamburg zum Hochwasserrisikomanagementplan der Flussgebietsgemeinschaft Elbe* [Background document from the Free and Hanseatic City of Hamburg on the flood risk management plan for the Elbe river basin district]. https://www.hamburg.de/resource/blob/176596/ea0f463056f57712ccd1c637753b6df9/d-3hintergrunddokument-hwrm-plan-data.pdf

Environment, Climate, Energy and Agriculture Authority (BUKEA) (2015b). *Information der Öffentlichkeit gemäß § 79 Wasserhaushaltsgesetz (WHG) über die Umsetzung der Hochwasserrisikomanagementrichtlinie (Richtlinie 2007/60/EG) in der Flussgebietsgemeinschaft Elbe* [Public information pursuant to Section 79 of the Water Resources Act (WHG) on the implementation of the Flood Risk Management Directive (Directive 2007/60/EC) in the Elbe River Basin District]. https://www.hamburg.de/resource/blob/176596/ea0f463056f57712ccd1c637753b6df9/d-3hintergrunddokument-hwrm-plan-data.pdf

Environment, Climate, Energy and Agriculture Authority (BUKEA) (2020). *Information der Öffentlichkeit gemäß § 79 WHG über die Umsetzung der Hochwasserrisikomanagement-Richtlinie für den deutschen Teil der Flussgebietseinheit Elbe – Aktualisierung der Hochwassergefahren- und Hochwasserrisikokarten gemäß § 74 WHG für die Freie und Hansestadt Hamburg* [Public information pursuant to Section 79 of the Federal Water Act (WHG) on the implementation of the Flood Risk Management Directive for the German part of the Elbe river basin district – Update of flood hazard and flood risk maps pursuant to Section 74 WHG for the Free and Hanseatic City of Hamburg]. https://www.hamburg.de/resource/blob/176554/299811be431727751531cb35a7217b60/d-hhbegleittext-gefahrenrisikokarten-jan2020-data.pdf

Environment, Climate, Energy and Agriculture Authority (BUKEA) (2021). *Hintergrunddokument der Freien und Hansestadt Hamburg zum Hochwasserrisikomanagementplan der Flussgebietsgemeinschaft Elbe für den Zeitraum von 2021 bis 2027* [Background document from the Free and Hanseatic City of Hamburg on the flood risk management plan of the Elbe River Basin Community for the period from 2021 to 2027]. https://www.hamburg.de/resource/blob/176566/e7214cc5487a9fdf64426e85fd59d7ea/d-3hintergrunddokument-hwrm-plan-2-data.pdf

Environment, Climate, Energy and Agriculture Authority (BUKEA) (2024a). *Richtiges Verhalten bei Sturmflut* [What to do in the event of a storm surge]. https://www.hafencity.com/_Resources/Persistent/1/f/a/3/1fa3d30a6c693bcdc33f4afc07c859f 8344e107d/2024-merkblatt-sturmfluten-hafencity-leichte-sprache.pdf

Environment, Climate, Energy and Agriculture Authority (BUKEA) (2024b). *Technisches Informationsblatt zur Starkregengefahrenkarte Hamburg* [Technical information sheet on the Heavy Rainfall Hazard Map for Hamburg]. https://www.hamburg.de/resource/blob/173730/5270f2cb96a1e41b5e45b64f84aa853e/dtechnischesinformationsblatt-srgk-data.pdf

Environment, Climate, Energy and Agriculture Autority (BUKEA) (2025a). *Themenblock 2 – Die Situation in Hamburg* [Topic 2 – The situation in Hamburg]. https://www.hamburg.de/politik-und-verwaltung/behoerden/bukea/872926-872926

Environment, Climate, Energy and Agriculture Autority (BUKEA) (2025b). *Landschaftsprogramm Hamburg – Änderungsübersicht* [Hamburg Landscape Programme – Overview of changes]. Geoportal Hamburg. https://geoportal-hamburg.de/?mdid=E91CB0516248-4AF4-A616-4B0962526CE2

Environment, Climate, Energy and Agriculture Autority (BUKEA) & RISA (2024). *Technisches Informationsblatt zur Starkregengefahrenkarte Hamburg* [Technical information sheet on the heavy rain hazard map for Hamburg]. https://www.hamburg.de/resource/blob/173730/5270f2cb96a1e41b5e45b64f84aa853e/dtechnischesinformationsblatt-srgk-data.pdf

Eslamian, S., & Eslamian, F. (Eds.). (2022). *Flood Handbook: Analysis and Modeling*. CRC Press.

Favre, A. C., El Adlouni, S., Perreault, L., Thiémonge, N., & Bobée, B. (2004). Multivariate hydrological frequency analysis using copulas. *Water resources research*, *40*(1).

Federal Emergency Management Agency (2016). *Guidance for Flood Risk Analysis and Mapping. Coastal flood frequency and extreme value analysis.* https://

www.fema.gov/sites/default/files/2020-02/Coastal_Flood_ Frequency_and_Extreme_Value_Analysis_Guidance_Nov _2016.pdf

Federal Maritime and Hydrographic Agency (2011). *Kurzberichte zu Sturmflutereignissen der Kategorie schwer und sehr schwer seit Mitte 2011 an der Nordseeküste* [Brief reports on severe and very severe storm surge events since mid-2011 on the North Sea coast]. https://www.schleswigholstein.de/DE/fachinhalte/H/hochwasserschutz/Downloads/kurzberichteNordseekueste.pdf?_ _blob=publicationFile&v=1

Federal Maritime and Hydrographic Agency (2018). *Kurzberichte zu Sturmflutereignissen der Kategorie schwer und sehr schwer seit Mitte 2018 an der schleswig-holsteinischen Nordseeküste und Tideelbe* [Brief reports on severe and very severe storm surge events since mid-2018on the North Sea coast of Schleswig-Holstein and the tidal Elbe]. https://www.schleswigholstein.de/DE/fachinhalte/H/hochwasserschutz/Downloads/schwereSturmflutenNordsee.pdf? __blob=publicationFile&v=2

Federal Statistical Office of Germany (2025). *Bevölkerungsentwicklung in Hamburg* [Population development in Hamburg]. Bund-Länder Demografie Portal. https://www.demografie-portal.de/DE/Fakten/bevoelkerungszahl-hamburg.html

Federal Waterways and Shipping Administration (WSV) (n.d.). *Download langfristiger Wasserstände (Rohdaten) ab dem 1.1.2000* [Download long-term water levels (raw data) from 1 January 2000 onwards] [Data set]. Retrieved September 2, 2025, from https://www.pegelonline.wsv.de/gast/stammdaten?pegelnr=5950090

Federal Waterways and Shipping Administration (WSV) (2022). *Topographie 2022* [Topography 2022] [Data set]. https://www.kuestendaten.de/Tideelbe/DE/Service/Kartenthemen/Kartenthemen_node.html

Fernández-Pato, J., García, R., & García-Navarro, P. (2020). A 1D-2D hydrodynamic model for sewer-overland coupled flow using GPU technology. In *River Flow 2020* (pp. 1940-1947). CRC Press.

Fickert, M. & Strotmann, T. (2007). Hydrodynamische Entwicklung der Tideelbe [Hydrodynamic development of the tidal Elbe]. *Coastal Reports (9),* 59-68.

Floris, M., D'Alpaos, A., Squarzoni, C., Genevois, R., & Marani, M. (2010). Recent changes in rainfall characteristics and their influence on thresholds for debris flow triggering in the Dolomitic area of Cortina d'Ampezzo, north-eastern Italian Alps. *Natural Hazards and Earth System Sciences*, *10*(3), 571-580.

Free and Hanseatic City of Hamburg, Ministry of Urban Development and Housing (2022). *Bodennutzung – Hamburg* [Land use – Hamburg] [Data set]. Esri Deutschland – Open Data Portal. https://opendata-esridech.hub.arcgis.com/datasets/esri-de-content::bodennutzunghamburg/about

Gallegos, H. A., Schubert, J. E., & Sanders, B. F. (2009). Two-dimensional, high-resolution modeling of urban dam-break flooding: A case study of Baldwin Hills, California. *Advances in water resources*, *32*(8), 1323-1335.

Ganguli, P., Paprotny, D., Hasan, M., Güntner, A., & Merz, B. (2020). Projected changes in compound flood hazard from riverine and coastal floods in northwestern Europe. *Earth's Future*, *8*(11), e2020EF001752.

Garner, A. J., Mann, M. E., Emanuel, K. A., Kopp, R. E., Lin, N., Alley, R. B., Horton, B. P., DeConto, R. M., Donnelly, J. P., & Pollard, D. (2017). Impact of climate change on New York City’s coastal flood hazard: Increasing flood heights from the preindustrial to 2300 CE. *Proceedings of the National Academy of Sciences*, *114*(45), 11861-11866.

Germany's National Meteorological Service (DWD) (n.d.a). *tageswerte RR 01975 19360101 20241231 hist* [daily values RR 01975 19360101 20241231 hist] [Data set]. https://opendata.dwd.de/climate_environment/CDC/observations_germany/climate/daily/mor e_precip/historical/

Germany's National Meteorological Service (DWD) (n.d.b). *stundenwerte RR 01975 19360101 20241231 hist* [hourly values RR 01975 19360101 20241231 hist] [Data set]. https://opendata.dwd.de/climate_environment/CDC/observations_germany/climate/hourly/pre cipitation/historical/

Germany's National Meteorological Service (DWD) (2021). *Klimareport Hamburg. Fakten bis zur Gegenwart – Erwartungen für die Zukunft* [Hamburg Climate Report. Facts to date – expectations for the future]. https://www.dwd.de/DE/leistungen/klimareports/klimareport_hh_2021_download.pdf?__blob =publicationFile&v=3

Germany's National Meteorological Service (DWD) (2024). *Datensatzbeschreibung – Tägliche Niederschlagsbeobachtungen für Deutschland* [Data set description – Daily precipitation observations for Germany]. https://opendata.dwd.de/climate_environment/CDC/observations_germany/climate/daily/mor e_precip/BESCHREIBUNG_obsgermany-climate-daily-more_precip_de.pdf

Ghanbari, M., Arabi, M., Kao, S. C., Obeysekera, J., & Sweet, W. (2021). Climate change and changes in compound coastal-riverine flooding hazard along the US coasts. *Earth's Future*, *9*(5), e2021EF002055.

Green, J., Haigh, I. D., Quinn, N., Neal, J., Wahl, T., Wood, M., Eilander, D., de Ruiter, M., Ward, P., & Camus, P. (2025). A comprehensive review of compound flooding literature with a focus on coastal and estuarine regions. *Natural Hazards and Earth System Sciences*, *25*(2), 747-816.

HafenCity Hamburg GmbH (n.d.). *Hafencity*. https://www.hafencity.com/en

Hafen Hamburg Marketing e.V. (2022). *Die Fahrrinne ist bereit für tiefergehende Schiffe* [The fairway is ready for deeper-draft vessels]. Hafen Hamburg. https://www.hafenhamburg.de/de/hamburger-hafen/fahrrinnenanpassung/

Haight, F. A. (1967). *Handbook of the Poisson distribution*.

Hamburg Ministry of Economics and Innovation (n.d.). *Standortprofil* [Location profile]. Metropolregion Hamburg. https://metropolregion.hamburg.de/wirtschaftwissenschaft/wirtschaftsstandort-12692

Hamburg Port Authortiy (HPA) (2019). *Gewässerkundliche Information. Gewässerkundliches Jahr 2019* [Hydrological information. Hydrological year 2019]. https://www.tideelbe.info/fileadmin/user_upload/Downloads/Berichte/Gewaesserkundliche_I nformation_2019.pdf

Hamburg Wasser (2020). *Hamburg schützt sich vor Starkregen* [Hamburg protects itself against heavy rainfall]. https://www.hamburgwasser.de/umwelt/vorsorge/starkregen#c764

Hamburg Wasser (2024). *Sturmflutsaison startet mit Probealarm* [Storm surge season begins with test alarm]. https://www.hamburgwasser.de/magazin/hochwasser

Hamburg Wasser (2025). *Hamburgs Sielnetz – geheime Unterwelt* [Hamburg's network of sewers – a secret underworld]. https://www.hamburgwasser.de/wasser/weg-deswassers/sielnetz

Hawcroft, M. K., Shaffrey, L. C., Hodges, K. I., & Dacre, H. F. (2012). How much Northern Hemisphere precipitation is associated with extratropical cyclones?. *Geophysical Research Letters*, *39*(24).

Hendry, A., Haigh, I. D., Nicholls, R. J., Winter, H., Neal, R., Wahl, T., Joly-Laugel, A., & Darby, S. E. (2019). Assessing the characteristics and drivers of compound flooding events around the UK coast. *Hydrology and Earth System Sciences*, *23*(7), 3117-3139.

Intergovernmental Panel on Climate Change (IPCC) (2021). The Physical Science Basis. Contribution of Working Group I to the Sixth Assessment Report of the Intergovernmental Panel on Climate Change. https://www.ipcc.ch/report/ar6/wg1/

Jahanbazi, M., & Egger, U. (2014). Application and comparison of two different dual drainage models to assess urban flooding. *Urban Water Journal*, *11*(7), 584-595.

Jalili Pirani, F., & Najafi, M. R. (2023). Characterizing compound flooding potential and the corresponding driving mechanisms across coastal environments. *Stochastic Environmental Research and Risk Assessment*, *37*(5), 1943-1961.

Jensen, J. (2019). *Kleine Dokumentation historischer Sturmfluten* [Brief documentation of historical storm surges]. Universität Siegen. https://www.bau.unisiegen.de/fwu/wb/publikationen/sturmflutarchiv/?lang=en%22

Khouakhi, A., Villarini, G., & Vecchi, G. A. (2017). Contribution of tropical cyclones to rainfall at the global scale. *Journal of Climate*, *30*(1), 359-372.

Kidson, R., & Richards, K. S. (2005). Flood frequency analysis: assumptions and alternatives. *Progress in Physical Geography*, *29*(3), 392-410.

Kim, B., Sanders, B. F., Schubert, J. E., & Famiglietti, J. S. (2014). Mesh type tradeoffs in 2D hydrodynamic modeling of flooding with a Godunov-based flow solver. *Advances in Water Resources*, *68*, 42-61.

Knottnerus, O. S. (2005). History of human settlement, cultural change and interference with the marine environment. *Helgoland Marine Research*, *59*(1), 2-8.

Koscielny-Bunde, E., Kantelhardt, J. W., Braun, P., Bunde, A., & Havlin, S. (2006). Longterm persistence and multifractality of river runoff records: Detrended fluctuation studies. *Journal of Hydrology*, *322*(1-4), 120-137.

Kottegoda, N. T. (1980). *Stochastic water resources technology*. Springer.

Kourtis, I. M., Bellos, V., & Tsihrintzis, V. A. (2017). Comparison of 1D-1D and 1D-2D urban flood models. In *Proceedings of the 15th International Conference on Environmental Science and Technology (CEST 2017), Rhodes, Greece* (Vol. 31).

Kumbier, K., Carvalho, R. C., Vafeidis, A. T., & Woodroffe, C. D. (2018). Investigating compound flooding in an estuary using hydrodynamic modelling: a case study from the Shoalhaven River, Australia. *Natural Hazards and Earth System Sciences*, *18*(2), 463-477.

Lai, Y., Li, J., Gu, X., Liu, C., & Chen, Y. D. (2021). Global compound floods from precipitation and storm surge: Hazards and the roles of cyclones. *Journal of Climate*, *34*(20), 8319-8339.

Lamb, H. H. (1995). *Climate, history and the modern world*. Routledge.

Lang, M., Ouarda, T. B., & Bobée, B. (1999). Towards operational guidelines for overthreshold modeling. *Journal of hydrology*, *225*(3-4), 103-117.

Laubitz-Bertram, A. (2012). *Hamburg – Sturmflut 1962* [Hamburg – Storm Surge 1962] [Map]. In P. Cremer (Ed.), *Heimat und Welt – Weltatlas + Geschichte* [Home and World – World Atlas + History] Westermann.

Lee, C., Hwang, S., Do, K., & Son, S. (2019). Increasing flood risk due to river runoff in the estuarine area during a storm landfall. *Estuarine, Coastal and Shelf Science*, *221*, 104-118.

Li, F., & Zheng, Q. (2016). Probabilistic modelling of flood events using the entropy copula. *Advances in water resources*, *97*, 233-240.

Li, W., Wang, C., Mo, J., Hou, S., Dang, X., Shi, H., & Gong, Y. (2025). Compound Flood Risk Assessment of Extreme Rainfall and High River Water Level. *Water (20734441)*, *17*(6).

Lian, J. J., Xu, K., & Ma, C. (2013). Joint impact of rainfall and tidal level on flood risk in a coastal city with a complex river network: a case study of Fuzhou City, China. *Hydrology and Earth System Sciences*, *17*(2), 679-689.

Link, T. (n.d.). *The history of aircraft construction in Hamburg*. Walther Blohm Stiftung. https://www.walther-blohm-stiftung.de/en/history

Lima, C. H., Lall, U., Troy, T. J., & Devineni, N. (2015). A climate informed model for nonstationary flood risk prediction: Application to Negro River at Manaus, Amazonia. *Journal of Hydrology*, *522*, 594-602.

Liu, Y., Zhang, W., & Cui, X. (2012). Flood emergency management using hydrodynamic modelling. *Procedia Engineering*, *28*, 750-753.

Liu, Z., Merwade, V., & Jafarzadegan, K. (2019). Investigating the role of model structure and surface roughness in generating flood inundation extents using one-and two-dimensional hydraulic models. *Journal of Flood Risk Management*, *12*(1), e12347.

Loganathan, G. V., Kuo, C. Y., & Yannaccone, J. (1987). Joint probability distribution of streamflows and tides in estuaries. *Hydrology Research*, *18*(4-5), 237-246.

Lowe, J. A., & Gregory, J. M. (2005). The effects of climate change on storm surges around the United Kingdom. *Philosophical Transactions of the Royal Society A: Mathematical, Physical and Engineering Sciences*, *363*(1831), 1313-1328.

Lucey, J. T., & Gallien, T. W. (2024). Quantifying compound flood event uncertainties in a wave and tidally dominated coastal region: The impacts of copula selection, sampling, record length, and precipitation gauge selection. *Journal of Flood Risk Management*, *17*(3), e12984.

Maity, R. (2018). *Statistical Methods in Hydrology and Hydroclimatology.* Springer Singapore.

Marcos, M., Jordà, G., Gomis, D., & Pérez, B. (2011). Changes in storm surges in southern Europe from a regional model under climate change scenarios. *Global and Planetary Change*, *77*(3-4), 116-128.

Marcos, M., Rohmer, J., Vousdoukas, M. I., Mentaschi, L., Le Cozannet, G., & Amores, A. (2019). Increased extreme coastal water levels due to the combined action of storm surges and wind waves. *Geophysical Research Letters*, *46*(8), 4356-4364.

Marcus, W. A., Roberts, K., Harvey, L., & Tackman, G. (1992). An evaluation of methods for estimating Manning's n in small mountain streams. *Mountain Research and Development*, 227-239.

Mathias, S. A. (2023). *Hydraulics, Hydrology and Environmental Engineering.* Springer.

Mazas, F., & Hamm, L. (2017). An event-based approach for extreme joint probabilities of waves and sea levels. *Coastal Engineering*, *122*, 44-59.

Milly, P. C. D., Wetherald, R. T., Dunne, K. A., & Delworth, T. L. (2002). Increasing risk of great floods in a changing climate. *Nature*, *415*(6871), 514-517.

Ming, X., Liang, Q., Dawson, R., Xia, X., & Hou, J. (2022). A quantitative multi-hazard risk assessment framework for compound flooding considering hazard inter-dependencies and interactions. *Journal of Hydrology*, *607*, 127477.

Ministry of Food, Agriculture and Forestry, State Office for Water Management, Schleswig-Holstein (1962). Die Sturmflut vom 16./17. Februar 1962 an der Schleswig-Holsteinischen Westküste [The storm surge of 16/17 February 1962 on the west coast of Schleswig-Holstein]. *Die Küste, 10* (1), 55-80. https://hdl.handle.net/20.500.11970/100781

Ministry of Urban Development and Housing (2025). *Stadt Umland Atlas Hamburg* [City and Surroundings Atlas Hamburg]. https://www.jovis.de/de/book/9783986122300

Mondal, K., Bandyopadhyay, S., & Karmakar, S. (2023). Framework for global sensitivity analysis in a complex 1D-2D coupled hydrodynamic model: Highlighting its importance on flood management over large data-scarce regions. *Journal of Environmental Management*, *332*, 117312.

Muis, S., Verlaan, M., Winsemius, H. C., Aerts, J. C., & Ward, P. J. (2016). A global reanalysis of storm surges and extreme sea levels. *Nature communications*, *7*(1), 11969.

Naghettini, M. (Ed.) (2017). *Fundamentals of statistical hydrology* (Vol. 1). Cham: Springer International Publishing.

Nkwunonwo, U. C., Whitworth, M., & Baily, B. J. S. A. (2020). A review of the current status of flood modelling for urban flood risk management in the developing countries. *Scientific African*, *7*, e00269.

North German Public Radio & TV (NDR) (2024). *Überschwemmte Straßen durch Unwetter in Hamburg* [Flooded streets due to severe weather in Hamburg] [Video]. https://www.ndr.de/nachrichten/hamburg/Ueberschwemmte-Strassen-durch-Unwetter-inHamburg,hamj148682.html

North German Public Radio & TV (NDR) (2025). *Sturmflut 1962: Als Hamburg im Wasser versank* [Storm surge of 1962: When Hamburg was submerged in water]. https://www.ndr.de/geschichte/chronologie/Die-Sturmflut-1962-Als-Hamburg-im-Wasserversank,grossesturmflut2.html

Nelsen, R. B. (2003, March). Properties and applications of copulas: A brief survey. In *Proceedings of the first brazilian conference on statistical modeling in insurance and finance* (pp. 10-28). Sao Paulo: University Press USP.

Ngongondo, C., Li, L., Gong, L., Xu, C. Y., & Alemaw, B. F. (2013). Flood frequency under changing climate in the upper Kafue River basin, southern Africa: a large scale hydrological model application. *Stochastic Environmental Research and Risk Assessment*, *27*(8), 18831898.

Nwogwu, N., Linhoss, A., Alarcon, V. J., Kelble, C. R., & Mickle, P. (2025). The Effect of Grid Resolution on Hydrodynamic Modeling. *Journal of Coastal Research*.

Önöz, B., & Bayazit, M. (2001). Effect of the occurrence process of the peaks over threshold on the flood estimates. *Journal of hydrology*, *244*(1-2), 86-96.

O'Loughlin, F. E., Neal, J., Schumann, G. J. P., Beighley, E., & Bates, P. D. (2020). A LISFLOOD-FP hydraulic model of the middle reach of the Congo. *Journal of hydrology*, *580*, 124203.

Paprotny, D., Vousdoukas, M. I., Morales-Nápoles, O., Jonkman, S. N., & Feyen, L. (2018). Compound flood potential in Europe. *Hydrology and Earth System Sciences Discussions*, *2018*, 1-34.

Pettitt, A. N. (1979). A non-parametric approach to the change-point problem. *Journal of the Royal Statistical Society: Series C (Applied Statistics)*, *28*(2), 126-135.

Pickands, J. (1975). Statistical inference using extreme order statistics. *the Annals of Statistics*, 119-131.

RainGain (2015) *Urban pluvial flood modelling: current theory and practice. review document related to work package 3—Action 13.* http://www.raingain.eu/sites/default/files/wp3_review_document.pdf

Rangari, V. A., Gonugunta, R., Umamahesh, N. V., Patel, A. K., & Bhatt, C. M. (2018). 1d-2d modeling of urban floods and risk map generation for the part of hyderabad city. *The International Archives of the Photogrammetry, Remote Sensing and Spatial Information Sciences*, *42*, 445-450.

River Basin Community Elbe (FGG Elbe) (2021). *Hochwasserrisikomanagementplan für den deutschen Teil der Flussgebietseinheit Elbe für den Zeitraum von 2021 bis 2027 gemäß § 75 WHG* [Flood risk management plan for the German part of the Elbe river basin district for the period from 2021 to 2027 in accordance with Section 75 of the Federal Water Act (WHG)]. https://www.fgg-elbe.de/hwrm-rl/hwrm-plan.html

River Basin Community Elbe (FGG Elbe) (2024). *Information der Öffentlichkeit über die Umsetzung der Hochwasserrisikomanagement-Richtlinie für den deutschen Teil der Flussgebietseinheit Elbe* [Public information on the implementation of the Flood Risk Management Directive for the German part of the Elbe river basin district]. https://www.fggelbe.de/files/Downloads/HWRM_RL/ber/vorl_bew/Broschuere_Bewertung_HWRisiko_2024.pdf

Royal Netherlands Meteorological Institute (KNMI) (2024). *KNMI national climate scenarios 2023 for the Netherlands.*

https://cdn.knmi.nl/system/data_center_publications/files/000/071/902/original/KNMI23_climate_scenarios_scientific_report_WR23-02.pdf?1710489430

Ruggiero, P., Komar, P. D., & Allan, J. C. (2010). Increasing wave heights and extreme value projections: The wave climate of the US Pacific Northwest. *Coastal Engineering*, *57*(5), 539552.

Rutgersson, A., Kjellström, E., Haapala, J., Stendel, M., Danilovich, I., Drews, M., Jylhä, K., Kujala, P., Larsén, X. G., Halsnæs, K., Lehtonen, I., Luomaranta, A., Nilsson, E., Olsson, T., Särkkä, J., Tuomi, L., & Wasmund, N. (2021). Natural hazards and extreme events in the Baltic Sea region. *Earth System Dynamics Discussions*, *2021*, 1-80.

Sadegh, M., Moftakhari, H., Gupta, H. V., Ragno, E., Mazdiyasni, O., Sanders, B., Matthew, R., & AghaKouchak, A. (2018). Multihazard scenarios for analysis of compound extreme events. *Geophysical Research Letters*, *45*(11), 5470-5480.

Sadegh, M., Ragno, E., & AghaKouchak, A. (2017). Multivariate C opula A nalysis T oolbox (MvCAT): describing dependence and underlying uncertainty using a B ayesian framework. *Water Resources Research*, *53*(6), 5166-5183.

Sadegh M., Ragno E., AghaKouchak A. (2018). *Multivariate Copula Analysis Toolbox (MvCAT)* [Matlab toolbox]. Matlab File Exchange. https://de.mathworks.com/matlabcentral/fileexchange/69217-multivariate-copula-analysistoolbox-mvcat?s_tid=srchtitle

Salas, J. D. (1993). Analysis and modelling of hydrological time series. *Handbook of hydrology*, *19*.

Salvadori, G., De Michele, C., & Durante, F. (2011). On the return period and design in a multivariate framework. *Hydrology and Earth System Sciences*, *15*(11), 3293-3305.

Salvadori, G., Durante, F., & De Michele, C. (2013). Multivariate return period calculation via survival functions. *Water Resources Research*, *49*(4), 2308-2311.

Schlauß, S., & Grottker, M. (2016). Coupling Process for 1D-2D Numerical Flash Flood Simulation: A Parameter Study of Involved Variables for Gullies and Manholes.

Schulte, M. (2015). *Anwendung von Copula-Modellen in der Hochwasserstatistik zur Planung technischer Rückhaltemaßnahmen* [Application of copula models in flood statistics for planning technical retention measures]. Lehrstuhl für Hydrologie, Wasserwirtschaft und Umwelttechnik, Ruhr-Univ.

Serinaldi, F., Bonaccorso, B., Cancelliere, A., & Grimaldi, S. (2009). Probabilistic characterization of drought properties through copulas. *Physics and Chemistry of the Earth, Parts a/B/C*, *34*(10-12), 596-605.

Shen, Y., & Jiang, C. (2023). A comprehensive review of watershed flood simulation model. *Natural Hazards*, *118*(2), 875-902.

Shustikova, I., Domeneghetti, A., Neal, J. C., Bates, P., & Castellarin, A. (2019). Comparing 2D capabilities of HEC-RAS and LISFLOOD-FP on complex topography. *Hydrological Sciences Journal*, *64*(14), 1769-1782.

Sklar, A. (1973). Random variables, joint distribution functions, and copulas. *Kybernetika*, *9*(6), 449-460.

State Agency for Roads, Bridges and Waterways (2020). *Deichinformationen Hamburg* [Dyke information Hamburg] [Data set]. https://geoportal-hamburg.de/#

State Office for Geoinformation and Cadastre Lower Saxony (2025). *Digitales Geländemodell (DGM1)* [Digital elevation model (DGM1)] [Data set]. https://ni-harvestprod.geocat.live/catalogue/srv/ger/catalog.search#/metadata/740e33da-3310-4173-bae1d30c31124b3a

State Office for Geoinformation and Surveying of the City of Hamburg (1962). *Karte von Hamburg und Umgebung. Sturmflut-Katastrophe am 16. / 17. Februar 1962* [Map of Hamburg and surrounding area. Storm surge disaster on 16/17 February 1962] [Map]. https://www.rettet-die-elbe.de/1kapitel/karte_1962_komplett_leg.jpg

State Office for Geoinformation and Surveying of the City of Hamburg (2022). *Digitales Höhenmodell Hamburg DGM 1* [Digital elevation model of Hamburg DGM 1] [Data set]. https://geoportal-hamburg.de

State Office for Surveying and Geoinformation Schleswig-Holstein (2023). *ATKIS-DGM* [Data set]. https://www.schleswig-holstein.de/DE/landesregierung/ministerienbehoerden/LVERMGEOSH/Service/servic eGeobasisdaten/geodatenService_Geobasisdaten_ DGM?nn=b7e3eb10-4e7a-4dd0-8caf-a8911c06430a

Storch, von H., Meinke, I., & Claußen, M. (2017). *Hamburger Klimabericht–Wissen über Klima, Klimawandel und Auswirkungen in Hamburg und Norddeutschland* [Hamburg Climate Report – Knowledge about climate, climate change and its effects in Hamburg and northern Germany]. Springer Nature.

Strahler, A. N., & Chow, V. T. (1964). Handbook of applied hydrology. *Quantitative geomorphology of drainage basins and channel networks*, 39-76.

Svensson, C., & Jones, D. A. (2004). Dependence between sea surge, river flow and precipitation in south and west Britain. *Hydrology and Earth System Sciences*, *8*(5), 973-992.

Tang, B., Nederhoff, K., & Gallien, T. W. (2025). Quantifying compound coastal flooding effects in urban regions using a tightly coupled 1D–2D model explicitly resolving flood defense infrastructure. *Coastal Engineering*, *199*, 104728.

Tawn, J. A., Vassie, J. M., & Gumbel, E. J. (1989). Extreme sea levels: the joint probabilities method revisited and revised. *Proceedings of the Institution of Civil Engineers*, *87*(3), 429442.

Trigo, R. M., Ramos, C., Pereira, S. S., Ramos, A. M., Zêzere, J. L., & Liberato, M. L. (2016). The deadliest storm of the 20th century striking Portugal: Flood impacts and atmospheric circulation. *Journal of Hydrology*, *541*, 597-610.

Tu, X., Du, Y., Singh, V. P., & Chen, X. (2018). Joint distribution of design precipitation and tide and impact of sampling in a coastal area. *International Journal of Climatology*, *38*, e290e302.

United States Geological Survey (n.d.). *Total Water Level and Coastal Change Forecast Viewer*. Retrieved October 24, 2025, from https://www.usgs.gov/data/total-water-level-andcoastal-change-forecast-viewerhttps://www.usgs.gov/data/total-water-level-and-coastalchange-forecast-viewer

Van der Sande, C. J., De Jong, S. M., & De Roo, A. P. J. (2003). A segmentation and classification approach of IKONOS-2 imagery for land cover mapping to assist flood risk and flood damage assessment. *International Journal of applied earth observation and geoinformation*, *4*(3), 217-229.

Verworn Langenhagen, H. R., & Kuchenbecker, A. (n.d.). *Regenreihen für Hamburg 2020* [Rain series for Hamburg 2020]. Hamburg Wasser. https://www.hamburgwasser.de/fileadmin/Redakteur/Downloads/divs/HW_Bemessungsregen _2020.pdf

Vogel, R. M., Yaindl, C., & Walter, M. (2011). Nonstationarity: flood magnification and recurrence reduction factors in the United States 1. *JAWRA Journal of the American Water Resources Association*, *47*(3), 464-474.

Vousdoukas, M. I., Voukouvalas, E., Annunziato, A., Giardino, A., & Feyen, L. (2016). Projections of extreme storm surge levels along Europe. *Climate Dynamics*, *47*(9), 31713190.

Wahl, T., Jain, S., Bender, J., Meyers, S. D., & Luther, M. E. (2015). Increasing risk of compound flooding from storm surge and rainfall for major US cities. *Nature Climate Change*, *5*(12), 1093-1097.

Wahl, T., Mudersbach, C., & Jensen, J. (2012). Assessing the hydrodynamic boundary conditions for risk analyses in coastal areas: a multivariate statistical approach based on Copula functions. *Natural Hazards and Earth System Sciences*, *12*(2), 495-510.

Walsh, K. J., McBride, J. L., Klotzbach, P. J., Balachandran, S., Camargo, S. J., Holland, G., Knutson, T. R., Kossin, J. P., Lee, T., Sobel, A., & Sugi, M. (2016). Tropical cyclones and climate change. *Wiley Interdisciplinary Reviews: Climate Change*, *7*(1), 65-89.

Walton Jr, T. L. (2000). Distributions for storm surge extremes. *Ocean Engineering*, *27*(12), 1279-1293.

Wang, H., Xuan, Y., Tran, T. V. T., Couasnon, A., Scussolini, P., Luu, L. N., Nguyen, H. Q., & Reeve, D. E. (2023). Changes in seasonal compound floods in Vietnam revealed by a time-varying dependence structure of extreme rainfall and high surge. *Coastal Engineering*, *183*, 104330.

Ward, P. J., Couasnon, A., Eilander, D., Haigh, I. D., Hendry, A., Muis, S., Veldkamp, T. I. E., Winsemius, H. C., & Wahl, T. (2018). Dependence between high sea-level and high river discharge increases flood hazard in global deltas and estuaries. *Environmental Research Letters*, *13*(8), 084012.

Weisse, R., von Storch, H., Niemeyer, H. D., & Knaack, H. (2012). Changing North Sea storm surge climate: An increasing hazard?. *Ocean & coastal management*, *68*, 58-68.

Willems, P. (2000). Compound intensity/duration/frequency-relationships of extreme precipitation for two seasons and two storm types. *Journal of Hydrology*, *233*(1-4), 189-205.

Wing, O. E., Quinn, N., Bates, P. D., Neal, J. C., Smith, A. M., Sampson, C. C., Coxon, G., Yamazaki, D., Sutanudjaja, E. H., & Alfieri, L. (2020). Toward global stochastic river flood modeling. *Water Resources Research*, *56*(8), e2020WR027692.

Xiao Y, Guo SL, Liu P, Fang B (2008). A new design flood hydrograph method based on bivariate joint distribution. In: Chen XH, Chen YD, Xia J, Zhang H (eds). *Hydrological sciences for managing water resources in the asian developing world*, IAHS Press, IAHS Publications 319, Wallingford, pp 75–82

Xiao, Y., Guo, S., Liu, P., Yan, B., & Chen, L. (2009). Design flood hydrograph based on multicharacteristic synthesis index method. *Journal of Hydrologic Engineering*, *14*(12), 13591364.

Xu, H., Ragno, E., Jonkman, S. N., Wang, J., Bricker, J. D., Tian, Z., & Sun, L. (2024). Combining statistical and hydrodynamic models to assess compound flood hazards from rainfall and storm surge: a case study of Shanghai. *Hydrology and Earth System Sciences*, *28*(16), 3919-3930.

Xu, H., Ragno, E., Tan, J., Antonini, A., Bricker, J. D., Jonkman, S. N., Liu, Q., & Wang, J. (2023). Perspectives on compound flooding in Chinese estuary regions. *International Journal of Disaster Risk Science*, *14*(2), 269-279.

Xu, H., Xu, K., Lian, J., & Ma, C. (2019). Compound effects of rainfall and storm tides on coastal flooding risk. *Stochastic Environmental Research and Risk Assessment*, *33*(7), 12491261.

Xu, H., Xu, K., Wang, T., & Xue, W. (2022). Investigating flood risks of rainfall and storm tides affected by the parameter estimation coupling bivariate statistics and hydrodynamic models in the coastal city. *International journal of environmental research and public health*, *19*(19), 12592.

Yan, K., Muis, S., Aleksandrova, N., Gwee, R., Veenstra, J., Dullaart, J., Aerts, J., Duong, T., & Ranasinghe, R. (2024). *Global sea level change time series from 1950 to 2050 derived from reanalysis and high resolution CMIP6 climate projections: Product User Guide*. ECMWF. https://confluence.ecmwf.int/display/CKB/Global+sea+level+change+time+series+from+1950+to+2050+derived+from+reanalysis+and+high+resolution+CMIP6+climate+projections%3 A+Product+User+Guide

Zellou, B., & Rahali, H. (2019). Assessment of the joint impact of extreme rainfall and storm surge on the risk of flooding in a coastal area. *Journal of Hydrology*, *569*, 647-665.

Zhang, W., Villarini, G., Vecchi, G. A., & Smith, J. A. (2018). Urbanization exacerbated the rainfall and flooding caused by hurricane Harvey in Houston. *Nature*, *563*(7731), 384-388.

Zhong, M., Xiao, L., Li, X., Mei, Y., Jiang, T., Song, L., & Chen, X. (2024). A study on compound flood prediction and inundation simulation under future scenarios in a coastal city. *Journal of Hydrology*, *628*, 130475.

Zhong, M., Wang, J., Jiang, T., Huang, Z., Chen, X., & Hong, Y. (2020). Using the apriori algorithm and Copula function for the bivariate analysis of flash flood risk. *Water*, *12*(8), 2223.

Zhou, C. R., Chen, Y. F., Gu, S. H., Huang, Q., Yuan, J. C., & Yu, S. N. (2016, August). A new threshold selection method for peak over for nonstationary time series. In *IOP Conference Series: Earth and Environmental Science* (Vol. 39, No. 1, p. 012071). IOP Publishing.

Zhu, Z., Zhang, W., & Zhu, W. (2024). Compound impact of storm surge and flood characteristics in coastal area based on copula. *Water*, *16*(2), 270.

Appendix

Table A1 - Pairs of extreme rainfall and associated maximum TWL of the same day used for the bivariate analysis.

Date	Rainfall [mm]	TWL [cm]	Date	Rainfall [mm]	TWL [cm]
01-Aug-2000	35.8	184	09-Sep-2013	22.6	197
27-Jun-2001	24.1	186	12-Oct-2013	24.1	114
23-Aug-2001	22.4	194	04-Nov-2013	27.3	280
07-Sep-2001	24.0	229	08-Dec-2013	20.6	267
18-Sep-2001	30.6	228	04-Apr-2014	20.3	145
11-Feb-2002	30.3	261	08-Jul-2014	28.0	157
28-Jun-2002	29.6	301	22-Dec-2014	36.1	343
17-Jul-2002	45.7	216	13-Sep-2015	25.8	176
21-Jul-2002	35.7	187	15-Nov-2015	33.5	258
01-Aug-2002	36.6	176	21-Feb-2016	24.1	266
26-Oct-2002	26.0	297	24-Jun-2016	26.1	221
16-Nov-2002	20.5	192	22-Jul-2016	35.9	206
29-Aug-2003	23.4	194	03-Jan-2017	25.1	276
06-Feb-2004	21	201	19-Mar-2017	23.5	227
09-Jun-2004	20.3	199	19-May-2017	37.1	220
20-Jul-2004	21.1	181	03-Jun-2017	22.9	187
21-Sep-2004	38.6	342	22-Jun-2017	20.6	173
20-Jul-2005	36.4	241	30-Jun-2017	28.1	242
29-Jul-2005	36.6	184	05-Oct-2017	23.4	309
14-Aug-2006	35.4	225	03-Jan-2018	22.2	297
18-Jan-2007	24.8	324	21-Jun-2018	20.4	267
16-Jun-2007	28.6	203	27-Aug-2019	39.4	157
21-Jun-2007	30.6	195	29-Sep-2019	31.1	218
26-Jun-2007	43.4	314	15-Oct-2019	21.2	209
22-Jul-2007	34.8	183	29-Jan-2020	29.5	264
29-Oct-2007	20.8	214	09-Jul-2020	24.7	195
21-Jan-2008	24.7	221	23-Dec-2020	25.1	190
29-Feb-2008	20.2	194	30-Jun-2021	22.7	226
04-Jul-2008	37.8	240	06-Feb-2022	21.0	314
22-Aug-2008	32.3	203	08-Sep-2022	23.2	169

16-Oct-2008	32.3	257	22-Jun-2023	28.8	217
23-Mar-2009	25.3	282	31-Jul-2023	43.1	203
01-Nov-2009	22.4	162	20-Oct-2023	21.9	26
10-Dec-2009	35.4	201	23-Dec-2023	22.4	301
26-Mar-2010	23.7	180	02-Jan-2024	30.8	215
30-Mar-2010	20.8	205	22-May-2024	28.4	183
04-Nov-2010	36.0	252	27-May-2024	30.5	206
05-Feb-2011	30.4	391	27-Jun-2024	33.3	214
02-Jul-2011	26.1	244	01-Jul-2024	22.4	200
13-Jul-2011	24.2	159	27-Jul-2024	23.9	220
05-Dec-2011	22.0	251	14-Aug-2024	22.8	188
24-Jun-2012	23.4	197	04-Sep-2024	21.9	203
29-Jul-2012	24.5	166	08-Sep-2024	24.9	205
21-May-2013	47.1	180	09-Oct-2024	29.0	196
19-Jun-2013	28.2	193	27-Nov-2024	26.1	196

Series from Lund University

Department of Physical Geography and Ecosystem Science

Master Thesis in Geographical Information Science

1. *Anthony Lawther:* The application of GIS-based binary logistic regression for slope failure susceptibility mapping in the Western Grampian Mountains, Scotland (2008).
2. *Rickard Hansen:* Daily mobility in Grenoble Metropolitan Region, France. Applied GIS methods in time geographical research (2008).
3. *Emil Bayramov:* Environmental monitoring of bio-restoration activities using GIS and Remote Sensing (2009).
4. *Rafael Villarreal Pacheco:* Applications of Geographic Information Systems as an analytical and visualization tool for mass real estate valuation: a case study of Fontibon District, Bogota, Columbia (2009).
5. *Siri Oestreich Waage:* a case study of route solving for oversized transport: The use of GIS functionalities in transport of transformers, as part of maintaining a reliable power infrastructure (2010).
6. *Edgar Pimiento:* Shallow landslide susceptibility – Modelling and validation (2010).
7. *Martina Schäfer:* Near real-time mapping of floodwater mosquito breeding sites using aerial photographs (2010).
8. *August Pieter van Waarden-Nagel:* Land use evaluation to assess the outcome of the programme of rehabilitation measures for the river Rhine in the Netherlands (2010).
9. *Samira Muhammad:* Development and implementation of air quality data mart for Ontario, Canada: A case study of air quality in Ontario using OLAP tool. (2010).
10. *Fredros Oketch Okumu*: Using remotely sensed data to explore spatial and temporal relationships between photosynthetic productivity of vegetation and malaria transmission intensities in selected parts of Africa (2011).
11. *Svajunas Plunge:* Advanced decision support methods for solving diffuse water pollution problems (2011).

12. *Jonathan Higgins:* Monitoring urban growth in greater Lagos: A case study using GIS to monitor the urban growth of Lagos 1990 - 2008 and produce future growth prospects for the city (2011).

13. *Mårten Karlberg:* Mobile Map Client API: Design and Implementation for Android (2011).

14. *Jeanette McBride:* Mapping Chicago area urban tree canopy using color infrared imagery (2011).

15. *Andrew Farina:* Exploring the relationship between land surface temperature and vegetation abundance for urban heat island mitigation in Seville, Spain (2011).

16. *David Kanyari*: Nairobi City Journey Planner: An online and a Mobile Application (2011).

17. *Laura V. Drews:* Multi-criteria GIS analysis for siting of small wind power plants - A case study from Berlin (2012).

18. *Qaisar Nadeem:* Best living neighborhood in the city - A GIS based multi criteria evaluation of ArRiyadh City (2012).

19. *Ahmed Mohamed El Saeid Mustafa:* Development of a photo voltaic building rooftop integration analysis tool for GIS for Dokki District, Cairo, Egypt (2012).

20. *Daniel Patrick Taylor*: Eastern Oyster Aquaculture: Estuarine Remediation via Site Suitability and Spatially Explicit Carrying Capacity Modeling in Virginia's Chesapeake Bay (2013).

21. *Angeleta Oveta Wilson:* A Participatory GIS approach to *unearthing* Manchester's Cultural Heritage '*gold mine'* (2013).

22. *Ola Svensson:* Visibility and Tholos Tombs in the Messenian Landscape: A Comparative Case Study of the Pylian Hinterlands and the Soulima Valley (2013).

23. *Monika Ogden:* Land use impact on water quality in two river systems in South Africa (2013).

24. *Stefan Rova:* A GIS based approach assessing phosphorus load impact on Lake Flaten in Salem, Sweden (2013).

25. *Yann Buhot:* Analysis of the history of landscape changes over a period of 200 years. How can we predict past landscape pattern scenario and the impact on habitat diversity? (2013).

26. *Christina Fotiou:* Evaluating habitat suitability and spectral heterogeneity models to predict weed species presence (2014).

27. *Inese Linuza:* Accuracy Assessment in Glacier Change Analysis (2014).

28. *Agnieszka Griffin:* Domestic energy consumption and social living standards: a GIS analysis within the Greater London Authority area (2014).

29. *Brynja Guðmundsdóttir:* Detection of potential arable land with remote sensing and GIS - A Case Study for Kjósarhreppur (2014).

30. *Oleksandr Nekrasov:* Processing of MODIS Vegetation Indices for analysis of agricultural droughts in the southern Ukraine between the years 2000-2012 (2014).

31. *Sarah Tressel:* Recommendations for a polar Earth science portal in the context of Arctic Spatial Data Infrastructure (2014).

32. *Caroline Gevaert:* Combining Hyperspectral UAV and Multispectral Formosat-2 Imagery for Precision Agriculture Applications (2014).

33. *Salem Jamal-Uddeen:* Using GeoTools to implement the multi-criteria evaluation analysis - weighted linear combination model (2014).

34. *Samanah Seyedi-Shandiz:* Schematic representation of geographical railway network at the Swedish Transport Administration (2014).

35. *Kazi Masel Ullah:* Urban Land-use planning using Geographical Information System and analytical hierarchy process: case study Dhaka City (2014).

36. *Alexia Chang-Wailing Spitteler:* Development of a web application based on MCDA and GIS for the decision support of river and floodplain rehabilitation projects (2014).

37. *Alessandro De Martino:* Geographic accessibility analysis and evaluation of potential changes to the public transportation system in the City of Milan (2014).

38. *Alireza Mollasalehi:* GIS Based Modelling for Fuel Reduction Using Controlled Burn in Australia. Case Study: Logan City, QLD (2015).

39. *Negin A. Sanati:* Chronic Kidney Disease Mortality in Costa Rica; Geographical Distribution, Spatial Analysis and Non-traditional Risk Factors (2015).

40. *Karen McIntyre:* Benthic mapping of the Bluefields Bay fish sanctuary, Jamaica (2015).

41. *Kees van Duijvendijk:* Feasibility of a low-cost weather sensor network for agricultural purposes: A preliminary assessment (2015).

42. *Sebastian Andersson Hylander:* Evaluation of cultural ecosystem services using GIS (2015).

43. *Deborah Bowyer:* Measuring Urban Growth, Urban Form and Accessibility as Indicators of Urban Sprawl in Hamilton, New Zealand (2015).

44. *Stefan Arvidsson:* Relationship between tree species composition and phenology extracted from satellite data in Swedish forests (2015).

45. *Damián Giménez Cruz*: GIS-based optimal localisation of beekeeping in rural Kenya (2016).

46. *Alejandra Narváez Vallejo:* Can the introduction of the topographic indices in LPJ-GUESS improve the spatial representation of environmental variables? (2016).

47. *Anna Lundgren:* Development of a method for mapping the highest coastline in Sweden using breaklines extracted from high resolution digital elevation models (2016).

48. *Oluwatomi Esther Adejoro:* Does location also matter? A spatial analysis of social achievements of young South Australians (2016).

49. *Hristo Dobrev Tomov:* Automated temporal NDVI analysis over the Middle East for the period 1982 - 2010 (2016).

50. *Vincent Muller:* Impact of Security Context on Mobile Clinic Activities A GIS Multi Criteria Evaluation based on an MSF Humanitarian Mission in Cameroon (2016).

51. *Gezahagn Negash Seboka:* Spatial Assessment of NDVI as an Indicator of Desertification in Ethiopia using Remote Sensing and GIS (2016).

52. *Holly Buhler:* Evaluation of Interfacility Medical Transport Journey Times in Southeastern British Columbia. (2016).

53. *Lars Ole Grottenberg*: Assessing the ability to share spatial data between emergency management organisations in the High North (2016).

54. *Sean Grant:* The Right Tree in the Right Place: Using GIS to Maximize the Net Benefits from Urban Forests (2016).

55. *Irshad Jamal:* Multi-Criteria GIS Analysis for School Site Selection in Gorno-Badakhshan Autonomous Oblast, Tajikistan (2016).

56. *Fulgencio Sanmartín:* Wisdom-volkano: A novel tool based on open GIS and time-series visualization to analyse and share volcanic data (2016).

57. *Nezha Acil:* Remote sensing-based monitoring of snow cover dynamics and its influence on vegetation growth in the Middle Atlas Mountains (2016).

58. *Julia Hjalmarsson:* A Weighty Issue: Estimation of Fire Size with Geographically Weighted Logistic Regression (2016).

59. *Mathewos Tamiru Amato:* Using multi-criteria evaluation and GIS for chronic food and nutrition insecurity indicators analysis in Ethiopia (2016).

60. *Karim Alaa El Din Mohamed Soliman El Attar:* Bicycling Suitability in Downtown, Cairo, Egypt (2016).

61. *Gilbert Akol Echelai:* Asset Management: Integrating GIS as a Decision Support Tool in Meter Management in National Water and Sewerage Corporation (2016).

62. *Terje Slinning:* Analytic comparison of multibeam echo soundings (2016).

63. *Gréta Hlín Sveinsdóttir:* GIS-based MCDA for decision support: A framework for wind farm siting in Iceland (2017).

64. *Jonas Sjögren:* Consequences of a flood in Kristianstad, Sweden: A GIS-based analysis of impacts on important societal functions (2017).

65. *Nadine Raska:* 3D geologic subsurface modelling within the Mackenzie Plain, Northwest Territories, Canada (2017).

66. *Panagiotis Symeonidis*: Study of spatial and temporal variation of atmospheric optical parameters and their relation with PM 2.5 concentration over Europe using GIS technologies (2017).

67. *Michaela Bobeck:* A GIS-based Multi-Criteria Decision Analysis of Wind Farm Site Suitability in New South Wales, Australia, from a Sustainable Development Perspective (2017).

68. *Raghdaa Eissa*: Developing a GIS Model for the Assessment of Outdoor Recreational Facilities in New Cities Case Study: Tenth of Ramadan City, Egypt (2017).

69. *Zahra Khais Shahid*: Biofuel plantations and isoprene emissions in Svea and Götaland (2017).

70. *Mirza Amir Liaquat Baig*: Using geographical information systems in epidemiology: Mapping and analyzing occurrence of diarrhea in urban - residential area of Islamabad, Pakistan (2017).

71. *Joakim Jörwall*: Quantitative model of Present and Future well-being in the EU-28: A spatial Multi-Criteria Evaluation of socioeconomic and climatic comfort factors (2017).

72. *Elin Haettner*: Energy Poverty in the Dublin Region: Modelling Geographies of Risk (2017).

73. *Harry Eriksson*: Geochemistry of stream plants and its statistical relations to soil- and bedrock geology, slope directions and till geochemistry. A GIS-analysis of small catchments in northern Sweden (2017).

74. *Daniel Gardevärn:* PPGIS and Public meetings – An evaluation of public participation methods for urban planning (2017).

75. *Kim Friberg:* Sensitivity Analysis and Calibration of Multi Energy Balance Land Surface Model Parameters (2017).

76. *Viktor Svanerud:* Taking the bus to the park? A study of accessibility to green areas in Gothenburg through different modes of transport (2017).

77. *Lisa-Gaye Greene*: Deadly Designs: The Impact of Road Design on Road Crash Patterns along Jamaica's North Coast Highway (2017).

78. *Katarina Jemec Parker*: Spatial and temporal analysis of fecal indicator bacteria concentrations in beach water in San Diego, California (2017).

79. *Angela Kabiru*: An Exploratory Study of Middle Stone Age and Later Stone Age Site Locations in Kenya's Central Rift Valley Using Landscape Analysis: A GIS Approach (2017).

80. *Kristean Björkmann*: Subjective Well-Being and Environment: A GIS-Based Analysis (2018).

81. *Williams Erhunmonmen Ojo*: Measuring spatial accessibility to healthcare for people living with HIV-AIDS in southern Nigeria (2018).

82. *Daniel Assefa*: Developing Data Extraction and Dynamic Data Visualization (Styling) Modules for Web GIS Risk Assessment System (WGRAS). (2018).

83. *Adela Nistora*: Inundation scenarios in a changing climate: assessing potential impacts of sea-level rise on the coast of South-East England (2018).

84. *Marc Seliger*: Thirsty landscapes - Investigating growing irrigation water consumption and potential conservation measures within Utah's largest master-planned community: Daybreak (2018).

85. *Luka Jovičić*: Spatial Data Harmonisation in Regional Context in Accordance with INSPIRE Implementing Rules (2018).

86. *Christina Kourdounouli*: Analysis of Urban Ecosystem Condition Indicators for the Large Urban Zones and City Cores in EU (2018).

87. *Jeremy Azzopardi*: Effect of distance measures and feature representations on distance-based accessibility measures (2018).

88. *Patrick Kabatha*: An open source web GIS tool for analysis and visualization of elephant GPS telemetry data, alongside environmental and anthropogenic variables (2018).

89. *Richard Alphonce Giliba*: Effects of Climate Change on Potential Geographical Distribution of Prunus africana (African cherry) in the Eastern Arc Mountain Forests of Tanzania (2018).

90. *Eiður Kristinn Eiðsson*: Transformation and linking of authoritative multi-scale geodata for the Semantic Web: A case study of Swedish national building data sets (2018).

91. *Niamh Harty*: HOP!: a PGIS and citizen science approach to monitoring the condition of upland paths (2018).

92. *José Estuardo Jara Alvear*: Solar photovoltaic potential to complement hydropower in Ecuador: A GIS-based framework of analysis (2018).

93. *Brendan O'Neill*: Multicriteria Site Suitability for Algal Biofuel Production Facilities (2018).

94. *Roman Spataru*: Spatial-temporal GIS analysis in public health – a case study of polio disease (2018).

95. *Alicja Miodońska*: Assessing evolution of ice caps in Suðurland, Iceland, in years 1986 - 2014, using multispectral satellite imagery (2019).

96. *Dennis Lindell Schettini*: A Spatial Analysis of Homicide Crime's Distribution and Association with Deprivation in Stockholm Between 2010-2017 (2019).

97. *Damiano Vesentini*: The Po Delta Biosphere Reserve: Management challenges and priorities deriving from anthropogenic pressure and sea level rise (2019).

98. *Emilie Arnesten*: Impacts of future sea level rise and high water on roads, railways and environmental objects: a GIS analysis of the potential effects of increasing sea levels and highest projected high water in Scania, Sweden (2019).

99. *Syed Muhammad Amir Raza*: Comparison of geospatial support in RDF stores: Evaluation for ICOS Carbon Portal metadata (2019).

100. *Hemin Tofiq*: Investigating the accuracy of Digital Elevation Models from UAV images in areas with low contrast: A sandy beach as a case study (2019).

101. *Evangelos Vafeiadis*: Exploring the distribution of accessibility by public transport using spatial analysis. A case study for retail concentrations and public hospitals in Athens (2019).

102. *Milan Sekulic*: Multi-Criteria GIS modelling for optimal alignment of roadway by-passes in the Tlokweng Planning Area, Botswana (2019).

103. *Ingrid Piirisaar*: A multi-criteria GIS analysis for siting of utility-scale photovoltaic solar plants in county Kilkenny, Ireland (2019).

104. *Nigel Fox*: Plant phenology and climate change: possible effect on the onset of various wild plant species' first flowering day in the UK (2019).

105. *Gunnar Hesch*: Linking conflict events and cropland development in Afghanistan, 2001 to 2011, using MODIS land cover data and Uppsala Conflict Data Programme (2019).

106. *Elijah Njoku*: Analysis of spatial-temporal pattern of Land Surface Temperature (LST) due to NDVI and elevation in Ilorin, Nigeria (2019).

107. *Katalin Bunyevácz*: Development of a GIS methodology to evaluate informal urban green areas for inclusion in a community governance program (2019).

108. *Paul dos Santos*: Automating synthetic trip data generation for an agent-based simulation of urban mobility (2019).

109. *Robert O' Dwyer*: Land cover changes in Southern Sweden from the mid-Holocene to present day: Insights for ecosystem service assessments (2019).

110. *Daniel Klingmyr*: Global scale patterns and trends in tropospheric NO2 concentrations (2019).

111. *Marwa Farouk Elkabbany*: Sea Level Rise Vulnerability Assessment for Abu Dhabi, United Arab Emirates (2019).

112. *Jip Jan van Zoonen*: Aspects of Error Quantification and Evaluation in Digital Elevation Models for Glacier Surfaces (2020).

113. *Georgios Efthymiou*: The use of bicycles in a mid-sized city – benefits and obstacles identified using a questionnaire and GIS (2020).

114. *Haruna Olayiwola Jimoh*: Assessment of Urban Sprawl in MOWE/IBAFO Axis of Ogun State using GIS Capabilities (2020).

115. *Nikolaos Barmpas Zachariadis*: Development of an iOS, Augmented Reality for disaster management (2020).

116. *Ida Storm*: ICOS Atmospheric Stations: Spatial Characterization of CO2 Footprint Areas and Evaluating the Uncertainties of Modelled CO2 Concentrations (2020).

117. *Alon Zuta*: Evaluation of water stress mapping methods in vineyards using airborne thermal imaging (2020).

118. *Marcus Eriksson*: Evaluating structural landscape development in the municipality Upplands-Bro, using landscape metrics indices (2020).

119. *Ane Rahbek Vierø*: Connectivity for Cyclists? A Network Analysis of Copenhagen's Bike Lanes (2020).

120. *Cecilia Baggini*: Changes in habitat suitability for three declining Anatidae species in saltmarshes on the Mersey estuary, North-West England (2020).

121. *Bakrad Balabanian*: Transportation and Its Effect on Student Performance (2020).

122. *Ali Al Farid*: Knowledge and Data Driven Approaches for Hydrocarbon Microseepage Characterizations: An Application of Satellite Remote Sensing (2020).

123. *Bartlomiej Kolodziejczyk*: Distribution Modelling of Gene Drive-Modified Mosquitoes and Their Effects on Wild Populations (2020).

124. *Alexis Cazorla*: Decreasing organic nitrogen concentrations in European water bodies - links to organic carbon trends and land cover (2020).

125. *Kharid Mwakoba*: Remote sensing analysis of land cover/use conditions of community-based wildlife conservation areas in Tanzania (2021).

126. *Chinatsu Endo*: Remote Sensing Based Pre-Season Yellow Rust Early Warning in Oromia, Ethiopia (2021).

127. *Berit Mohr*: Using remote sensing and land abandonment as a proxy for long-term human out-migration. A Case Study: Al-Hassakeh Governorate, Syria (2021).

128. *Kanchana Nirmali Bandaranayake*: Considering future precipitation in delineation locations for water storage systems - Case study Sri Lanka (2021).

129. *Emma Bylund*: Dynamics of net primary production and food availability in the aftermath of the 2004 and 2007 desert locust outbreaks in Niger and Yemen (2021).

130. *Shawn Pace*: Urban infrastructure inundation risk from permanent sea-level rise scenarios in London (UK), Bangkok (Thailand) and Mumbai (India): A comparative analysis (2021).

131. *Oskar Evert Johansson*: The hydrodynamic impacts of Estuarine Oyster reefs, and the application of drone technology to this study (2021).

132. *Pritam Kumarsingh*: A Case Study to develop and test GIS/SDSS methods to assess the production capacity of a Cocoa Site in Trinidad and Tobago (2021).

133. *Muhammad Imran Khan*: Property Tax Mapping and Assessment using GIS (2021).

134. *Domna Kanari*: Mining geosocial data from Flickr to explore tourism patterns: The case study of Athens (2021).

135. *Mona Tykesson Klubien*: Livestock-MRSA in Danish pig farms (2021).

136. *Ove Njøten*: Comparing radar satellites. Use of Sentinel-1 leads to an increase in oil spill alerts in Norwegian waters (2021).

137. *Panagiotis Patrinos*: Change of heating fuel consumption patterns produced by the economic crisis in Greece (2021).

138. *Lukasz Langowski*: Assessing the suitability of using Sentinel-1A SAR multi-temporal imagery to detect fallow periods between rice crops (2021).

139. *Jonas Tillman*: Perception accuracy and user acceptance of legend designs for opacity data mapping in GIS (2022).

140. *Gabriela Olekszyk*: ALS (Airborne LIDAR) accuracy: Can potential low data quality of ground points be modelled/detected? Case study of 2016 LIDAR capture over Auckland, New Zealand (2022).

141. *Luke Aspland*: Weights of Evidence Predictive Modelling in Archaeology (2022).

142. *Luís Fareleira Gomes*: The influence of climate, population density, tree species and land cover on fire pattern in mainland Portugal (2022).

143. *Andreas Eriksson*: Mapping Fire Salamander (Salamandra salamandra) Habitat Suitability in Baden-Württemberg with Multi-Temporal Sentinel-1 and Sentinel-2 Imagery (2022).

144. *Lisbet Hougaard Baklid*: Geographical expansion rate of a brown bear population in Fennoscandia and the factors explaining the directional variations (2022).

145. *Victoria Persson*: Mussels in deep water with climate change: Spatial distribution of mussel (Mytilus galloprovincialis) growth offshore in the French Mediterranean with respect to climate change scenario RCP 8.5 Long Term and Integrated Multi-Trophic Aquaculture (IMTA) using Dynamic Energy Budget (DEB) modelling (2022).

146. *Benjamin Bernard Fabien Gérard Borgeais*: Implementing a multi-criteria GIS analysis and predictive modelling to locate Upper Palaeolithic decorated caves in the Périgord noir, France (2022).

147. *Bernat Dorado-Guerrero*: Assessing the impact of post-fire restoration interventions using spectral vegetation indices: A case study in El Bruc, Spain (2022).

148. *Ignatius Gabriel Aloysius Maria Perera*: The Influence of Natural Radon Occurrence on the Severity of the COVID-19 Pandemic in Germany: A Spatial Analysis (2022).

149. *Mark Overton*: An Analysis of Spatially-enabled Mobile Decision Support Systems in a Collaborative Decision-Making Environment (2022).

150. *Viggo Lunde*: Analysing methods for visualizing time-series datasets in open-source web mapping (2022).

151. *Johan Viscarra Hansson*: Distribution Analysis of Impatiens glandulifera in Kronoberg County and a Pest Risk Map for Alvesta Municipality (2022).

152. *Vincenzo Poppiti*: GIS and Tourism: Developing strategies for new touristic flows after the Covid-19 pandemic (2022).

153. *Henrik Hagelin*: Wildfire growth modelling in Sweden - A suitability assessment of available data (2023).

154. *Gabriel Romeo Ferriols Pavico*: Where there is road, there is fire (influence): An exploratory study on the influence of roads in the spatial patterns of Swedish wildfires of 2018 (2023).

155. *Colin Robert Potter*: Using a GIS to enable an economic, land use and energy output comparison between small wind powered turbines and large-scale wind farms: the case of Oslo, Norway (2023).

156. *Krystyna Muszel*: Impact of Sea Surface Temperature and Salinity on Phytoplankton blooms phenology in the North Sea (2023).

157. *Tobias Rydlinge*: Urban tree canopy mapping - an open source deep learning approach (2023).

158. *Albert Wellendorf*: Multi-scale Bark Beetle Predictions Using Machine Learning (2023).

159. *Manolis Papadakis*: Use of Satellite Remote Sensing for Detecting Archaeological Features: An Example from Ancient Corinth, Greece (2023).

160. *Konstantinos Sourlamtas*: Developing a Geographical Information System for a water and sewer network, for monitoring, identification and leak repair - Case study: Municipal Water Company of Naoussa, Greece (2023).

161. *Xiaoming Wang*: Identification of restoration hotspots in landscape-scale green infrastructure planning based on model-predicted connectivity forest (2023).

162. *Sarah Sienaert*: Usability of Sentinel-1 C-band VV and VH SAR data for the detection of flooded oil palm (2023).

163. *Katarina Ekeroot*: Uncovering the spatial relationships between Covid-19 vaccine coverage and local politics in Sweden (2023).

164. *Nikolaos Kouskoulis*: Exploring patterns in risk factors for bark beetle attack during outbreaks triggered by drought stress with harvester data on attacked trees: A case study in Southeastern Sweden (2023).

165. *Jonas Almén*: Geographic polarization and clustering of partisan voting: A local-level analysis of Stockholm Municipality (2023).

166. *Sara Sharon Jones*: Tree species impact on Forest Fire Spread Susceptibility in Sweden (2023).

167. *Takura Matswetu*: Towards a Geographic Information Systems and Data-Driven Integration Management. Studying holistic integration through spatial accessibility of services in Tampere, Finland. (2023).

168. *Duncan Jones*: Investigating the influence of the tidal regime on harbour porpoise *Phocoena phocoena* distribution in Mount's Bay, Cornwall (2023).

169. *Jason Craig Joubert*: A comparison of remote sensed semi-arid grassland vegetation anomalies detected using MODIS and Sentinel-3, with anomalies in ground-based eddy covariance flux measurements (2023).

170. *Anastasia Sarelli*: Land cover classification using machine-learning techniques applied to fused multi-modal satellite imagery and time series data (2024).

171. *Athanasios Senteles*: Integrating Local Knowledge into the Spatial Analysis of Wind Power: The case study of Northern Tzoumerka, Greece (2024).

172. *Rebecca Borg:* Using GIS and satellite data to assess access of green area for children living in growing cities (2024).

173. *Panagiotis–Dimitrios Tsachageas*: Multicriteria Evaluation in Real Estate Land-use Suitability Analysis: The case of Volos, Greece (2024).

174. *Hugo Nilsson*: Inferring lane-level topology of signalised intersections from aerial imagery and OpenStreetMap using deep learning (2024).

175. *Pavlos Alexantonakis*: Estimating lake water volume fluctuations using Sentinel-2 and ICESat-2 remote sensing data (2024).

176. *Karl-Martin Wigen*: Physical barriers and where to find them (2024).

177. *Martin Storsnes*: Temporal RX-algorithm performance on Sentinel-2 images (2024).

178. *Saulė Gabrielė Petraitytė*: The Relation Between Covid-19 Vaccination and Voting Trends in Lithuania: A Spatial Analysis (2024).

179. *Pedro Martinez Duran*: Olive yield forecasting from remote sensing and climate datasets in the Jaen province (Spain) (2024).

180. *Josefine Kynde Hämberg*: Proximity to Urban Green Spaces for Older Adults in Specific Housings - a Case Study of Malmö, Sweden (2024).

181. *Max Bengtsson*: A Site Selection of An Energy Island in the North Sea: Optimal Location in an Ecological and an Economic Scenario Using a Multicriteria Decision Analysis (MCDA) (2024).

182. *Anna Börmann*: Assessing Great Britain as a relocation site for the threatened Iberian Lynx in a changing climate (2024).

183. *Josephine Roosli*: Flood Risk Assessment for the Kävlinge River for Present and Future Climate Scenarios using HEC-RAS Rain-on-Grid (2024).

184. *Seán Flanagan*: Spatiotemporal dynamics of E-scooter sharing ridership and their associations with the built environment: A Swedish comparative study (2024).

185. *Wouter Vorsters*: Assessing the Impact of Combined Sewer Overflow on the Habitat of Lampetra planeri: A Case Study in Flanders, Belgium (2025).

186. *Kathleen Macdonald*: Cetacean strandings on the Scottish coast: coastal accessibility factors lead to underreporting (2025).

187. *Athanasios Emmanouil Mourampetzis*: Navigating the Shadows: A Comparative Analysis of SAR and Optical Imagery for Detecting (Dark) Vessels (2025).

188. *Nizam-ud-Din*: Spatial Land Records System using Geospatial Techniques: a case study of a Mid-Sized Village in Pakistan (2025).

189. *Nedim Nasic Kjellgren*: Linked Geodata: Improving Rooftop Photovoltaic Production Estimates through BIM-GIS Integration using Semantic Web Technologies (2025).

190. *Vedrana Pretkovic*: Spatio-temporal vegetation changes in the Pacific-Chocó region of Colombia during the conflict and post-conflict periods (2025).

191. *Evelina Bengtsson*: A Socioeconomic Dimension of Crime: A Spatial Study of Firearm-related Violence in Malmö (2025).

192. *Martynas Bielinis*: Application of C-band Radar Interferometry for Dune Monitoring in the Curonian Spit (2025).

193. *Paulina Magdalena Rieke*: Case study of the benefits of BIM and GIS solutions used on a live infrastructure project (2025).

194. *Alina Schärer*: Evaluating the Impact of Urban Green Spaces and Vegetation Characteristics on Land Surface Temperature Across Swiss Cities Using Machine Learning (2025).

195. *Paul Stewart:* Where is wild in Glasgow's Southside? A test of the applicability of relative wildness mapping to suburban Scotland (2025).

196. *Georgios Fylakis:* Spatiotemporal analysis of the integration between shared e-scooters and public transport: Case studies in Oslo and Stockholm (2025).

197. *Andreas Klasson*: Generating 3D building models according to Swedish building specification using footprints and airborne laser scanning (2025).

198. *Agaton Järemo Lawin*: The spread of Japanese knotweed in Scania: Invasion suitability prediction using species distribution modelling (2025).

199. *Jesse Stewart:* Contextualizing the Geographic Influence on Infantry Manoeuvrability in a Historical Battlefield Using GIS: A Case Study of the Canadian Corps in the Second Battle of Passchendaele, First World War (2025).

200. *Oskar Vejkdal Thorsberg*: Automatic geometry extraction in digital building permits: A case study using BIM and NS Building (2025).

201. *Spyridon Gerafentis*: Impact of the COVID-19 "Lockdown" on Air Quality in Athens (2025).

202. *Symeon Andriotis*: Political Violence in Athens, Greece (2008-2024): A Machine Learning Approach for Predictive Modelling of Spatial Risk Patterns (2025).

203. *Simon Westman*: Detecting Structurally Old Scots Pine: A Crown-Metric Approach Using National ALS and LIFT Enrichment (2026).

204. *Freja Randeris Kristoffersen*: Satellite-Derived Bathymetry of Danish Coastal Waters Using Machine Learning with Sentinel-2 and ICESat-2 data (2026).

205. *Markus Honkanen*: Securitas Per Scientiam: GIS-MCDA of Civil Defence Shelter Distribution Efficiency in the Helsinki Capital Region (2026).

206. *Amanda Carolina Santos Motta*: Visualization Tools for Simulation Results Based on 3D City Models: An Urban Planner-Focused Study (2026).

207. *Gintars Krumins*: Mapping forest felling activities in Latvia from Sentinel-2 satellite imagery using machine learning (2026).

208. *Jenny Berntsson*: Using Multi-criteria GIS analysis in nature conservation planning in Lilla Edet municipality (2026).

209. *Sebastian Daland*: Flood impacts on road accessibility and buildings in Gothenburg during a 100-year rainfall event (2026).

210. *Polyxeni Karapanagiotidou*: GIS-based Multi-Criteria Decision Analysis (MCDA) framework for Flood Risk Assessment in the Thermi Basin (2026).

211. *Nour Abdulmagid A. Bensaid*: Urban Expansion and its Relation to the Urban Heat Island Effect: A Case Study of Tripoli, Libya (2026).

212. *Iris Krohn*: Compound Extreme Events in Hamburg, Germany: A Flood Risk Assessment (2026).